BIOACTIVE GLYCOPEPTIDE NANOFIBERS FOR TISSUE REGENERATION APPLICATIONS

A THESIS SUBMITTED TO

THE GRADUATE SCHOOL OF ENGINEERING AND SCIENCE

OF BILKENT UNIVERSITY

IN PARTIAL FULFILLMENT OF THE REQUIREMENTS FOR

THE DEGREE OF

MASTER OF SCIENCE

IN

MATERIALS SCIENCE AND NANOTECHNOLOGY

By

ÖZÜM ŞEHNAZ ÇALIŞKAN

May 2016

BIOACTIVE GLYCOPEPTIDE NANOFIBERS FOR TISSUE REGENERATION APPLICATIONS

By Özüm Şehnaz Çalışkan
May 2016

We certify that we have read this thesis and that in our opinion it is fully adequate, in scope and in quality, as a thesis for the degree of Master of Science.

Mustafa Özgür Güler (Advisor)

Ayşe Begüm Tekinay (Co-Advisor)

Hüseyin Özkan

Tarık Baytekin

Approved for the Graduate School of Engineering and Science:

Levent Onural
Director of the Graduate School

ABSTRACT

BIOACTIVE GLYCOPEPTIDE NANOFIBERS FOR TISSUE REGENERATION APPLICATIONS

Özüm Şehnaz Çalışkan

M.S.in Materials Science and Nanotechnology

Advisor: Mustafa Özgür Güler

Co-Advisor: Ayse Begüm Tekinay

May, 2016

Natural extracellular matrix (ECM) is rich in glycopeptides and glycosaminoglycans, which function in controlling cellular processes. In this thesis, glycopeptide molecules that mimic natural glycopeptides and glycosaminoglycans were designed and synthesized and it was demonstrated that they induce directed differentiation of mesenchymal stem cells into chondrogenic and adipogenic lineages.

In the first part of the study, hyaluronic acid (HA)-mimicking glycopeptide amphiphile molecules were synthesized to induce chondrogenic differentiation of mesenchymal stem cells (MSC). HA is the most abundant glycosaminoglycan (GAG) found in hyaline cartilage ECM. Peptide amphiphiles were synthesized by solid phase peptide synthesis method and used to form self-assembled bioactive glycopeptide nanofibers which mimic fibrous morphology of the ECM. Scanning electron microscopy (SEM), transmission electron microscopy (TEM), and circular

dichroism (CD) were used for morphology and secondary structure analyses of the obtained nanofibers. It was demonstrated that glycopeptide amphiphiles create fibrous structure formed by nanofibers. Morphological changes, GAG production (Safranin-O staining and DMMB analysis), and chondrogenic gene marker expressions (qRT-PCR) of MSCs cultured on HA-mimetic nanofibers were analyzed. It was shown that HA-mimetic glycopeptide nanofibers induce early differentiation of MSCs into hyaline like chondrocytes.

In the second part of the study, it was demonstrated that minor changes on glycopeptide backbone can create specific glycopeptides which induce differentiation of MSCs into brown adipocytes. Brown fat adipocytes do not store chemical energy as fat but dissipates it as heat and so they have emerged as promising anti-obesity agents. Lipid droplet accumulation (Oil Red-O staining) and adipogenic gene marker expression analyses (qRT-PCR) showed that the new glycopeptide nanofiber scaffold is a specific inducer of differentiation of MSCs into brown fat adipocytes.

Keywords: Peptide amphiphile, peptide nanofiber, glycosaminoglycan, glycopeptide, mesenchymal stem cell, extracellular matrix, hyaluronic acid, mesenchymal stem cell differentiation, cartilage tissue, tissue regeneration, brown fat tissue, adipogenesis.

ÖZET

BİYOAKTİF GLİKOPEPTİT NANOFİBERLERİN DOKU REJENERASYONU UYGULAMALARI

Özüm Şehnaz Çalışkan

Malzeme Bilimi ve Nanoteknoloji, Yüksek Lisans

Tez Danışmanı: Mustafa Özgür Güler

Tez Eşdanışmanı: Ayşe Begüm Tekinay

Mayıs, 2016

Doğal hücreler arası matris (HAM), hücresel olayları kontrol eden glikopeptit ve glikozaminoglikanlar bakımından zengin bir yapıdır. Bu tez çalışmasında, doğal glikopeptitleri ve glikozaminoglikanları taklit eden ve mezenkimal kök hücrelerin (MKH) kıkırdak ve yağ hücrelerine farklılaşmasını tetikleyen glikopeptit moleküller tasarlanmış ve sentezlenmiştir.

Çalışmanın ilk bölümünde, hyaluronik asidi (HA) taklit eden glikopeptit amfifil molekülleri MKH'lerin kıkırdak hücre hattına farklılaşmasını tetiklemek amacıyla sentezlenmiştir. HA, camsı kıkırdak HAM'inde en fazla miktarda bulunan glikozaminoglikandır. Peptit amfifil molekülleri katı fazlı peptit sentezi yöntemi ile sentezlenmiş ve HAM'in fibröz yapısını taklit etmek amacıyla kendiliğinden bir araya gelen biyoaktif glikopeptit nanofiberler oluşturulması için kullanılmışlardır.

Taramalı ve geçirimli elektron mikroskopisi ve dairesel dikorizm yöntemleri ile elde edilen nanofiberlerin ikincil yapıları ve morfolojileri incelenmiş, glikopeptit amfifillerin nanofiberlerden oluşan boşluklu fibröz bir yapı oluşturduğu gösterilmiştir. HA'yı taklit eden nanofiberler üzerinde kültürlenen MKH'lerin morfolojik değişimleri, GAG üretim miktarları (Safranin-O boyaması ve DMMB analizi) ve kondrojenik gen işaretleyicilerinin ifade seviyeleri (gerçek zamanlı RT-PZR) analiz edilmiştir. Analizler sonucunda HA-taklidi glikopeptit nanofiberlerin MKH'lerin camsı kıkırdak hücrelere farklılaşmasını sağladığı ve bunu erken dönemde başlattığı gösterilmiştir.

Çalışmanın ikinci kısmında, glikopeptit omurgasında yapılan kimyasal değişimler sayesinde MKH'lerin kahverengi yağ hücrelerine dönüşümü gösterilmiştir. Kahverengi yağ hücreleri kimyasal enerjiyi yağ olarak depolamaz; bunun yerine ısı olarak harcarlar. Bu sayede umut vaat eden anti-obezite ajanları olarak kabul edilmektedirler. Lipit damla birikimi (Oil-Red O boyası) ve adipojenik gen işaretleyicilerinin ifade seviyelerinin incelenmesi (gerçek zamanlı RT-PZR) ile elde ettiğimiz sonuçlar, bu glikopeptitnanofiber iskelenin MKH'lerin kahverengi yağ hücrelerine dönüşmesinin spesifik tetikleyicisi olduğunu göstermiştir.

Anahtar Sözcükler: Peptit amfifil, peptit nanofiberler, glikozaminoglikan, glikopeptit, mezenkimal kök hücre, hücrelerarası iskele, hyaluronik asit, mezenkimal kök hücre farklılaşması, kıkırdak doku, doku rejenerasyonu, kahverengi yağ dokusu, adipojenez.

Acknowledgement

Time I spent at UNAM has been one of the important periods of my life. I felt this time course scientifically and personally developed me. I would like to express my appreciations to all people who contribute this process either by their experiences, knowledge, help or their mental and emotional support.

I would like to express the deepest gratitude to my advisor Prof. Mustafa Özgür Güler and to my co-advisor Prof. Ayşe Begüm Tekinay who are the leading roles of this period. They gained me different scientific perspectives, let me be part of their research groups, and patiently followed my maturation and completion of this work. Their immense knowledge, encouragement and guidance are invaluable.

I would like to thank our old post-doc Dr. Ashif Shaikh for sharing his knowledge, valuable collaboration and for supplying me GlcNAc-PA. I would like to express my sincere appreciations to Dr. Seher Üstün Yaylacı, who taught me *in vitro* experiments for her valuable supports. I want to express my special thanks to our cartilage sub-group members Çağla Eren, İbrahim Çelik, Özge Uysal, and separately to Elif Arslan who is old-hand member of our group for sharing her experienced knowledge. We shared lots of knowledge, experiences and help as cartilage group. I would like to express my special thanks to Dr. Gözde Uzunallı. She taught, supervised and helped me a lot although she was also new in her chondrogenesis studies.

I learnt something from every people that I communicated through this period but I owe more special thanks to some of them who shared a lot their valuable time

with me and contributed to this study. I express my sincere appreciation to Melike Sever for her kind help for qRT-PCR experiments and analyses. I owe her a lot. I am grateful to Meryem Hatip for going through all TEM images for selection and her kind support. I appreciate Merve Şen for her help in primer design. I would like to express my special thanks to Gökhan Günay and Seren Hamsici, who also make this master period enjoyable, for their help in FACS analyses and friendship. I would also thank to our new post-doc Bhavna Rajasekaran for her kind help about confocal microscopy. I also acknowledge Yasin Tümtaş and Öncay Yaşa, whom I learnt experimental details about adipogenesis study for their help and legating their materials to me.

I owe very special thanks to two people; Zeynep Orhan and Nurcan Haştar, for their excellent collaborations in projects that we took part together. This thesis study would not be completed without their help; their efforts are invaluable. I would like to express my most sincere, deepest gratitude to them.

I would like to give my special thanks to Göksu Çınar, Egemen Deniz Eren, and Hatice Kübra Kara for their warm friendship, and I would also like to acknowledge my old and present lab and office members Gülistan Tansık, M. Aref Khalily, Dr. Ruslan Garifullah, Gülcihan Gülseren, Nuray Gündüz, Berna Şentürk, Dr. Rashad Mammadov, Dr. Büşra Mammadov, Melis Göktaş, Dr. Özlem Erol, Dr. Hakan Ceylan, Oya İlke Şentürk, Begüm Kocatürk, Dr. Aslı Çelebioğlu, Zeynep Aytaç, Yelda Ertaş, Dr. Fatma Kayacı, Dr. Okan Öner Ekiz, Seylan Ayan, Sude Selin Su Yirmibeşoğlu, Hepi Hari Susapto, İ. Ceren Garip, Dilek Sezer, İkra Gizem Yıldız, Elif Ergül, Aygül Zengin, Mevhibe Geçer, Mustafa Beter, Canelif Yılmaz, Idil Uyan, Fatih Yergöz, Şehmus Tohumeken, Oğuz Tuncay, Ahmet Emin Topal, Alper Devrim

Özkan and Göksemin Şengül for creating a peaceful, warm and so an excellent working environment.

And Melis Şardan Ekiz, a new PhD, a wise supervisor, a good collaborator and a dear friend; she deserves the sincerest gratitude. I am really grateful for her help, the PAs that she supplied me and for her emotional support.

My special thanks are to Zeynep Erdoğan, whom I learnt a lot and to Mustafa Güler, for their technical helps. I would also like to thank our janitorial laborers for providing us a clean environment and doing it in a cheerful way. I especially thank to Suna Abla and Hatice Abla for spreading their happiness with their good-humor.

I would like to thank the National Nanotechnology Research Center (UNAM) and Bilkent University for providing pleasant facilities and latest equipments, and to thank The Scientific and Technological Research Council of Turkey (TÜBİTAK BIDEB 2210-C, 213M406, 113T045) for partial financial support.

I would like to express my appreciations to MBG department of Bilkent University and to İhsan Gürsel for letting me use their departmental and private centrifuges.

I am grateful to my old and gold friends Betül Savaş, Selen Güzel, Seda Karakaş, Özge Taşdan, Nazlı Sezek and Gülşah Zorgör who had always been there for me. I also convey my thanks to my dear undergraduate departmental friends Gizem Güneş, Ayça Yörükoğlu and Burcu Nur Keçeli who are thousands of miles away but pursuing a similar career for their warm friendship. They are the ones who can understand the feelings of a graduate student.

I would like to thank my whole family; from grandmothers to aunts they wish me the best. I would like to give my sincere gratitude to my new family, the Çalışkans, for their warm and peaceful support and encouragement.

I would like to express my gratitude to my mother, my father and my little sister separately. My mother who always believes in me, whom I know will always be there for me unconditionally, my father who was being with me during his short winter break by coming Ankara, cooking and carrying the dinner for me and being with me here while I performing experiments, and my little sister who is my emotional support in Ankara, who is always humorous just the way she is, they gave their best encouragements and supports me in the way I am. Their presence in my life is priceless.

His support, encouragement and help to complete my thesis are invaluable but I want to give my deepest, most amative thanks to Okan Çalışkan, my beloved one, for the hearty laughter that we had, for his excellent perception which can always intuit my feelings, and for the miles that we took separately but to reach each other.

Contents

List of Figures

List of Tables

List of Abbreviations

ECM	**:**	Extracellular Matrix
PA	**:**	Peptide Amphiphile
GAG	**:**	Glycosaminoglycan
DIEA	**:**	*N*,*N*-diisopropylethylamine
TFA	**:**	Trifluoroacetic Acid
TIS	**:**	Triisoproplysilane
DMF	**:**	Dimethylformamide
DCM	**:**	Dichloromethane
LC-MS	**:**	Liquid Chromatography Mass Spectroscopy
HPLC	**:**	High Pressure Liquid Chromatography
CD	**:**	Circular Dichroism
SEM	**:**	Scanning Electron Microscopy
TEM	**:**	Transmission Electron Microscopy
FBS	**:**	Fetal Bovine Serum
DMEM	**:**	Dulbecco's Modified Eagle Medium
DMMB	**:**	Dimethylmethylene Blue
OD	**:**	Optical Density
PS	**:**	Penicillin/Streptomycin
BrdU	**:**	Bromodeoxyuridine
rMSC	**:**	Rat Mesenchymal Stem Cell
GAPDH	**:**	Glyceraldehyde 3-phosphate dehydrogenase
Co1 I	**:**	Collagen 1

Col II	**:**	Collagen 2
Sox9	**:**	Transcription Factor SOX-9
ADIPOQ	**:**	Adiponectin
FABP4	**:**	Fatty Acid Binding Protein 4
UCP1	**:**	Uncoupled Protein 1
qRT-PCR	**:**	Quantitative Real-Time Polymerase Chain Reaction

CHAPTER 1

INTRODUCTION

1.1 A brief introduction to tissue regeneration

Tissue failure or loss has been a major health problem throughout the history of humanity.[1] It adversely affects the patient's life quality and even most severe losses may cause deaths. Therefore, there has been a huge effort to address tissue loss problems since old human history. Drug treatment can be applied for the least severe cases[2], however more severe cases require different treatment options. The other treatment options include artificial prostheses, surgical repair, mechanical device replacements and any type of transplantations (auto-, allo-, and xenograft).[2,3] However, artificial prostheses or surgical repair do not meet the needs of a fully functional tissue or organ replacement. Transplantation then emerges as a best option, but it has certain drawbacks and limitations. Autografts are the best option for replacement, however, its excision creates another surgical site in the patient and it cannot satisfy the need if the required tissue size is large. The other option, allografts, can create immune response by the patient. In addition to this, to find an appropriate allograft donor is a really big challenge.[1] According to current data supplied by the Ministry of Health of the Republic of Turkey, more than 28.000 patients are on transplant wait list in Turkey.[4] Xenogafts, cross-species transplantation, offer an unlimited supply of organs but they have similar constraints with allograft transplantation. Besides, it is less likely that tissues or organs from different species match with humans.[5] Then, mechanical devices emerge to answer the needs, but they are currently very limited in terms of variety.

Tissue regeneration by biomaterials, or tissue engineering, is emerging as a potential alternative and complementary solution. Tissue engineering can be defined as fabricating new and functional tissues by use of living cells, a matrix or scaffold

which guide the cells to proliferate, differentiate and to communicate with other cells for tissue development.[2] Tissue engineering is an inter- and multidisciplinary field that combines cells, biomaterials and biological signals.[6] These cells, the biomaterials and the interactions between the cells and biomaterials are the fundamentals of tissue engineering. Biomaterials are generally used as scaffolds. Scaffolds provide the structural support for cell attachment and subsequent tissue development.[7] Scaffolds have to mimic the natural structure of tissue of interest. Physical, chemical and rheological structure of a scaffold is very important for tissue formation as it affects the cellular behaviors like differentiation, adhesion and proliferation.[7] Applied cyclic load, electrical signals and extension/contraction of scaffold are the other factors that change the differentiation profile of the cells.[8] These scaffolds can either be used to grow tissue in *in vitro* conditions[9] or be applied *in vivo* to support the body to regenerate the tissue.[10] As different tissues have different properties, there is a variety of scaffold types developed for different application purposes. Degradable, non-degradable, synthetic, natural, synthetic-natural hybrid, inert or bioactive scaffolds are noted in literature.[11,12,13,14,15,16] The unchanging parameter for all type of scaffolds is cyto- or tissue compatibility.

Cell types have enormous influence on the formation of functional tissue type of interest. Progenitor-type cells or stem cells are used for tissue engineering and regeneration. Embryonic stem or embryonic germ line cells are non-differentiated cells and are able to differentiate into any type of cells.[6] For this reason, they attract much attention for tissue engineering purposes. Stem cells also exist in adults; however, they are not able to differentiate into all kinds of cells into body. The tissue origin of the adult stem cells determines their differentiation capability and the

lineages that stem cells differentiate into.[17] Therefore it is important to choose appropriate origin of stem cells depending on the type of tissue that is aimed to regenerate.

Growth factors have a huge impact to differentiate cells towards certain types. Growth factors are specific proteins that are secreted by paracrine or autocrine manner and play key roles in cellular behavior like proliferation and differentiation.[6] Therefore growth factors, proteins and hormones that are involved in formation of tissue of interest have to be clearly identified and appropriate cocktail of the factors should be supplied to the environment for tissue regeneration and engineering.[18]

There are certain challenges about tissue engineering. First of all, behaviors of cells in normal development, factors that control differentiation, proliferation and communication between cells should be learned in detail in order to mimic and stimulate these behaviors in engineering process. Second, limited source of stem cells or limited number of progenitor-type cells are other challenges. Another challenge is the limitations over methods for scaffold fabrication. All these fields require more studies to understand and better address the needs of tissue engineering field.

1.2 Tissue Types

Human body is composed of different and complex types of tissues and organs. Each tissue has its own physical, physiological and mechanical characteristics. For tissue engineering and regeneration purposes, these characteristics have to be known in order to design appropriate scaffolds, choose the correct cell type and to create optimum environment by chemical factors. In this section, two different types of tissues are introduced briefly: cartilage and adipose tissue. These are the tissue types

into which differentiation of mesenchymal stem cells is induced by peptide amphiphile scaffolds in this thesis study.

1.2.1 Cartilage Tissue

Cartilage is a type of connective tissue with a dense but elastic structure. It is not rigid as bone tissue but also not elastic as muscle tissue, which are other types of connective tissues. Cartilage is found in the body where there is need for some structural support but also elasticity in a certain range due to its unique rheological properties. Cartilage functions as shock absorber, gives some support to body and creates friction free surfaces especially between the articular surfaces of bones.[19] Its most important characteristic is that it lacks of blood vessels and nerves.[20] Water (~75%), collagen (~20%) and proteoglycans (~5%) are the main constituents of cartilage.[20] The ratios can change depending on the type of cartilage, age of the person and healthy structure of the cartilage.

Cartilage has four basic components: perichondrium, chondroblasts, chondrocytes and matrix. Perichondrium is an exception because fibrous and articular hyaline cartilages do not have perichondrium.[21] Perichondrium is a vascularized connective tissue sheet that is rich in collagens (collagen I especially) and surrounds cartilage like a capsule.[22] As perichondrium is the only vascularized part of the cartilage, it is at the same time the only source of the nourishment for cartilage. Nutrients diffuse from the capillaries that reside in perichondrium into the matrix.[21] Cartilage thickness should be in a certain range as increased thickness hardens the diffusion of nutrients. Perichondrium is also the part where growth and repair of cartilage occurs.[21] It consists of an outer fibrous layer and an inner chondrogenic layer.[23] The

outer layer contains fibroblasts that secrete collagenous fibers. Inner layers host the chondroblasts and some undifferentiated mesenchymal cells. Chondroblasts differentiate from MSCs that reside in the perichondrium and are progenitors, or immature forms of chondrocytes.[24] They secrete type II collagen and other components of the extracellular matrix.[25] As they continue ECM production, they are entrapped by the ECM inside small spaces called lacunae.[23] Inside lacunae, chondroblasts mature and turn into chondrocytes, which are the only cells found in healthy cartilage tissue. Chondrocytes are specialized cells that synthesize and maintain matrix infrastructure.[26] Matrix is composed of fibers, either elastic or collagenous, and ground substance which is a gel-like substance surrounding the cells.[22] Ground substance contains combinations of proteins and sugars, glycosaminoglycans (GAGs), most notably hyaluronic acid, proteoglycans and glycopeptides. These glycoproteins help anchor chondrocytes to matrix, maintain tissue integrity and mediate transmembrane signaling.[27] Glycoproteins perform these tasks via their multiple binding sites to the receptors on chondrocyte surfaces.[21] Presence of GAGs and proteoglycans make the matrix basophilic. Due to high negative charges that GAGs and proteoglycans have, they attract positive molecules and repel negative molecules and this increases ion concentration in the matrix. Increased ion concentration increases osmolarity of the cartilage and thereby high amount of water is attracted.[22] Thus, GAGs and proteoglycans hold high amount of water indirectly by the increased osmolarity (Gibbs-Donnan effect) and directly via intermolecular hydrogen bonds.[21,28]

There are three types of cartilage; hyaline, elastic and fibrocartilage.[27] The classification is done depending on the density and type of fibers presented in its

composition. Therefore, they slightly differ from each other and they have very similar histology, but their localization in the body is different.[27] Hyaline cartilage localizes in tracheal rings, sterna margins of ribs and in the articular surfaces of joints where the bones meet with each other. Hyaline cartilage that is located in the articular surfaces may also be called as articular cartilage.[29] Hyaline means transparent, glassy substance and as the name suggests, hyaline cartilage has a transparent appearance.[30] It is the most abundant type of cartilage in the body. Chondrocytes constitute 1-1.5% volume of the hyaline cartilage.[31] Water is the prominent component of articular hyaline cartilage. 80% of the superficial zone and 65% of the deep zone of articular hyaline cartilage matrix is composed of water.[31] Resilience against load, which is a critical biomechanical function of articular hyaline cartilage, is attributed to this high amount of water.[21] Major classes of proteoglycans found in hyaline cartilage are aggrecans[32], large aggregating proteoglycans, and small proteoglycans like decorin and fibromodulin. Hyaluronic acid is the GAG that acts as central chain of proteoglycans. The principal component of the framework of hyaline cartilage is collagen type II, which forms the 90-95% of it.[29] The matrix contains abundant amounts of collagen type II as thin fibrils and they provide tensile strength. Elastic cartilage cannot be differentiated from hyaline cartilage in histological staining, unless elastin fibers are stained.[27] Matrix and perichondrium of elastic cartilage contains thick bundles of elastic fibers.[21] It is found in ears, epiglottis and eustacian tube and it is not calcified with increasing age. Fibrocartilage is found in inter-vertebral disc. Collagen type I layers interrupting the matrix is the distinct feature of fibrocartilage.[23] Another important characteristic

about fibrocartilage is that it does not have perichondrium, like articular hyaline cartilage.

1.2.2 Adipose Tissue

Adipose tissue, also known as body fat, is a fibrous loose connective tissue that is primarily composed of adipocytes.[33] Apart from mature adipocytes, which form approximately one-third of fat tissue, a combination of mesenchymal stem cells (MSCs), T regulatory cells, endothelial precursor cells, macrophages and preadipocytes in various stages of development form the remaining two-third of the fat tissue.[34] Adipose tissue is primarily located in subcutaneous layer between muscle and dermis, particularly in the abdominal region of the body.[35,36] However, the selective localization of adipose tissue may differ between men and women.[37] Additionally, it surrounds the vital organs like heart and kidney.[35] Due to its particular locations and tissue structure, adipose tissue acts as a cushion against a physical collision and insulator for heat loss.[35,37] As an insulator, it passively assists in body temperature regulation.[35] Apart from them, primary function of adipose tissue is accepted as storage of excess energy in the body until the recent decades. Discovery of complement factor D (today most commonly known as adipsin, which is an endocrine factor) in 1987 and subsequent identification of leptin (another circulating endocrine hormone) in 1994 introduced adipose tissue as an endocrine organ.[33,38] Adipose tissue is now known to be involved in a variety of biological processes including energy metabolism, neuroendocrine function, and immune function.[33] There are two distinct types of adipose tissue: white adipose tissue (WAT) and brown adipose tissue (BAT).[39] They differ from each other both

histologically and metabolically. WAT is the energy storage reservoir of the body and has endocrine functions; BAT on the other hand is the site of nonshievering thermogenesis.[39] White adipocytes are monolocular, they have one and large lipid droplets and nucleus is located near the membrane. In contrast, brown adipocytes are unilocular, have abundant mitochondria and characteristic protein called UCP1.[39] There is a third type of adipocytes which is called beige fat cell.[40] They highly resemble white adipocytes with extremely low basal expression of UCP1, however, upon induction by different elements such as cold exposure, beige adipocytes turnover their metabolism into brown fat like metabolism, highly elevate UCP1 expression and get involved in heat production.[41] Beige cells derive from different embryonic precursors and express different genes from brown fat cells. Thus, beige cells are introduced as a third distinct type of fat cell.[42]

1.3 Glycosaminoglycans (GAGs): Chemistry, Functions, Regenerative Potentials, and Applications

Glycosaminoglycans (GAGs) are a group of extracellular matrix (ECM) polysaccharides which are unbranched and are involved in numerous biological activities.[43] They are important as molecular co-receptors in cell–cell interactions via their ability to interact with ECM proteins and peptide growth factors.[44] GAGs have vital roles in the binding and activation of growth factors in cell signal transduction required for biological development such as cell adhesion, migration, growth and differentiation.[45]

GAGs are unique in terms of their repeating disaccharide units.[43] The reason behind name given as GAG is that one of the two sugars in the repeating disaccharide is always an amino sugar (N-acetylglucosamine or N-acetylgalactosamine). Except hyaluronic acid, the amino sugar of all GAGs is sulfated.[43,46] Due to the presence of sulfate or carboxyl groups on most of their sugars, GAGs are highly negatively charged. For this reason, they can be accepted as the most anionic molecules produced by animal cells.[47]

GAGs can be grouped into four categories according to their sugars, the type of linkage between the sugars, and the number and location of sulfate groups. GAG types are hyaluronic acid, chondroitin sulfate and dermatan sulfate, heparan sulfate, and keratin sulfate.[47] Repeating dissacharide monomers of GAGs can slightly vary in terms of type and also position of the sulfate groups. Most common forms of dissacharide units of GAGs are given in Table 1.1.

Table 1.1 GAGs and their repeating dissacharide units

Glycosaminoglycans	**Repeating dissacharide**
Hyaluronan	D-Glucuronic acid and N-acetylglucosamine
Chondroitin sulfate	D-Glucuronic acid and N-acetylgalactosamine
Dermatan sulfate	D-Glucuronic acid/L-iduronic acid and N-acetylgalactosamine
Heparan sulfate	D-Glucuronic acid/L-iduronic acid and D-glucosamine
Keratan sulfate	D-Galactose and N-acetylglucosamine

1.3.1 Chemical and functional properties of glycosaminoglycans

Apart from HA, GAG chains are usually covalently linked to a protein which is called core protein and form proteoglycans. Generally the properties of the GAGs tend to dominate the biophysical and biochemical characters of the entire molecule. GAGs are highly polyanionic molecules, therefore, in aqueous solution they attract bivalent cations such as Ca^{2+} and Na^{2+}.[48] This creates a high hydrodynamic volume combined with low compressibility.[48] GAGs with these properties take a role as a size-selective barrier in which only small molecules can freely diffuse, restricting the bioavailability of larger molecules.[48] In this way GAGs modulate water and extracellular cation homeostasis. GAGs are the major organic components of the extracellular matrix.[48] As an ECM component, GAGs modulate the attraction and migration of precursor cells, and their subsequent differentiation.[44,49] They also attract and regulate the action of proteins that are essential for tissue regeneration. GAGs also act as scaffolds that can modulate the function of diverse proteins, including cytokines, chemokines, growth factors, enzymes, and adhesion molecules.[43,50] Due to these interactions, GAGs regulate cellular processes such as adhesion, migration, proliferation, and differentiation of various cell types.[51] When processed into collagen scaffolds, they also modulate the structure of the collagen matrix. Their composition changes during the remodeling process such as bone formation, wound healing or scaring.[48] It is known that GAGs in the skin and bone undergo quantitative and qualitative changes upon aging and UV radiation.[48]

The degree of sulfation and polymer length is important to determine the precise action of glycosaminoglycans.[52] It has been shown that sulfation degree of GAGs changes their functional properties. In a recent study, native GAGs (HA and CS),

highly sulfated HA and CS and GAG free control were compared in different aspects.[53] This study revealed that sulfation causes the loss of the proliferative activity of MSCs by about 40%, while it almost completely suppresses necrosis and apoptosis.[53] Increased sulfation also modulates MSC differentiation. MSCs cultured in osteogenic medium show increased osteogenic marker gene expression when treated with sulfated GAGs compared to native GAGs. Mineral deposition of MSCs that are treated with sulfated GAGs also increased compared to native GAGs, which is an important marker of osteogenic differentiation[53]. In another study, it is shown that desulfation and/or shortening of heparin results in loss of its binding ability to heparin binding proteins.[48]

1.3.2 GAG types: a more detailed explanation

GAGs are classified into six different groups: chondroitin sulfate (CS), dermatan sulfate (DS), heparan sulfate (HS), heparin, keratin sulfate (KS), and hyaluronic acid.[54] This classification is done based on their uronic acid composition, amino sugar composition, linkage between amino sugar and uronic acid, chain length of the dissacharide polymer, presence or absence of sulfate groups and their position of attachment to the sugar, nature of the core protein to which they are attached and their tissue distribution.[55] CS disaccharide units are arranged in alternating unbranched sequences that can bear sulfate ester substituents in a variety of positions. Variations in molecular weight, chain length and the position of sulfate substitution can be observed depending on the species, which renders sequence heterogeneity.[56] CS chains have important functions in central nervous system development, wound repair, infection, growth factor signaling, morphogenesis and

cell division, in addition to their conventional structural roles.[56] It is also the most abundant GAG in the body with its presence in tendons, ligament, aorta and cartilage.[54] It binds to proteins, like aggrecan, to form large aggregates of proteoglycans.[54]

Dermatan sulfate (DS) is also known as chondroitin sulfate B. DS is first isolated from the skin.[57] DS is defined as a chondroitin sulfate if GalNAc is present in the structure. The presence of iduronic acid (IdoA) in DS distinguishes it from chondroitin sulfates-A and -C and bridges it to heparin and heparin sulfate.[58] DS is a key biological response modifier. It is a stabilizer of cofactor and/or co-receptor for growth factors, cytokines and chemokines. It regulates enzyme activity.[59] DS acts as signaling molecules in response to cellular damage, such as wounding, infection, and tumorigenesis.[58] Besides, it is a target for bacterial, viral and parasitic virulence factors for attachment, invasion and immune system evasion.[56]

Heparin and heparan sulfate (HS) terms can sometimes be confusing. There is not a certain definition or criteria that distinguish between heparan sulfate and heparin. Both molecules are sulfated but heparin is more extensively so, and that provides higher electronegativity.[60] Another structural difference between these two molecules is that HS includes a greater proportion of GlcA, whereas heparin contains more IdoA.[60] While heparin is only synthesized by connective tissue mast cells, HS is found on cell surfaces or in the extracellular matrix of all mammalian organs and tissues in the form of proteoglycans.[61] The initial product in their biosynthesis is a non-sulfated polymer and this polymer then enzymatically transformed into complex sulfated derivatives.[62] While heparin is used as an anticoagulant in the clinic, HS exists at the cell surface and ECM.[63] As HS is found at the cell surface, it binds to a

variety of protein ligands and regulates a wide variety of biological activities, including developmental processes, angiogenesis, blood coagulation and tumor metastasis.[63–65]

Keratan sulfate (KS) is an atypical GAG type. It is the most heterogeneous GAG type,[54] is the only one that does not contain uronic acid.[62] The family that it represents does not have acidic residues alternating in the basic unit structure with an N-acetylated amino-sugar.[56] It is highly expressed in cornea, bones and brain.[59] Corneal transparency is dependent on the amount of KS.[66]

HA, also called hyaluronan, is the sole GAG that does not form proteoglycan and is not sulfated.[54] It is synthesized in the cytoplasm at the plasma membrane and is delivered into the extracellular space without post-modification.[67] HA is a major component of the ECM of the skin, joints, eye, and cartilage.[68] Due to high degree of polymerization capability, HA molecules can compose large molecules that reach up to several million daltons in weight which exceeds other GAGs in length.[67] There are different types of HA-binding proteins that are called hyaladherins.[69] Among them, CD44 and CD168 are distinct HA cell surface receptors. CD168 triggers motility by controlling focal adhesion kinase, and activation of mitogen-activated protein kinases.[48] CD44 is the main receptor for HA and it modulates macrophage fusion, migration, and polarization of cells, and serves as co-receptor and organizer of the actin skeleton.[69,70]

HA has extraordinarily wide-ranging biological functions depending on the size despite its uniform and simple primary structure. For example in cartilage, HA is an important structural element of the matrix.[71,72] It creates an aggregation centre for aggrecan which is a large chondroitin sulfate proteoglycan that retains its

macromolecular assembly in the matrix due to specific HA–protein interactions.[73,56] The presence of negatively charged HA in cartilage ECM helps retain high water content and this creates a lubricant ECM that reduce friction between bones which also protects bones by absorbing dumping pressure. They also take role as space-filling, antiangiogenic and immunosuppressive materials.[56]

1.3.3 Roles of GAGs in biology

Glycosaminoglycans are seen in ECM of all the connective tissues. They modulate cell adhesion and motility. Many cell adhesion promoting components in ECM or on cell surfaces bind GAGs and support adhesion. GAGs and proteoglycans act as co-receptors for integrins and are involved in transducing signals.[74] Bioactivity of GAGs is related to the interaction of their negatively charged groups to the positively charged amino groups of proteins. It is hypothesized that these charged functional groups have vital role in the formation of proteoglycans, thus, they are important for biochemical processing/signaling related to cell functionality and survival.[45]

GAGs also take role in immunity. It is reported that CS creates an anti-inflammatory environment by downregulating the expression of MMPs, IL-1β, TNFα, COX-2, and NOS2 as a result of blocking the NF-κB signaling pathway.[48] HS has been shown to regulate leukocyte development and migration, immune activation, and inflammatory processes.[75] HA takes a role in the recruitment processes of leukocytes to the inflammation site through its interaction with CD44.[76] HA protects the healthy form of skin acting as scavenger for free radicals, that can be form upon exposure to UV light, which may result in oxidative stress on cell.[56] HA regulates osteoclast precursor mobility and may act as a diffusion barrier for enzymes from the resorption

area. It is suggested that HA may take a role in osteoclast attachment and resorption via CD44.[48] The main GAG type in bone tissue is chondroitin-4-sulfate while HA, DS and chondroitin-6-sulfate can be seen in less amounts in bone. Expression of these molecules enhances osteogenic differentiation of mesenchymal stem cells (MSCs).[77] Glycosaminoglycans modulate the attraction of bone precursor cells including the actions of proteins essential for bone regeneration.[45]

The epidermis and dermis, which are different layers of skin, contain various types of GAGs. Although they make up only 0.1–0.3% of the total skin weight, GAGs define skin volume and elasticity due to their large water-retaining capability.[78] When it comes to wound healing, the quantity and qualitative composition of GAGs differ in healthy skin and scar tissue.[48] In fact, this difference is one of the reasons of scar formation rather than complete healing. The fibroblasts in scar tissue, produce more HA, and more C4S (chondroitin-4-sulfate), but less DS than fibroblasts in healthy skin.[48] It is also known that *de novo* synthesis of GAGs is increased temporarily during the proliferation phase of wound healing. In addition to that persisting high HA levels in granulation tissue are related to scarless healing.[48]

GAGs are also studied in cancer biology due to their functional properties related to adhesion, motility and signal transduction. Tumor cells must adhere to extracellular matrix (ECM) proteins and molecules on other cells in order to invade and metastasize. Integrins, the receptors that are responsible for cell-to-ECM interactions are therefore important in tumor cell invasion and metastasis.[79] GAGs have a modulating role for integrin binding and this is one of the reaction types that makes them important molecules in cancer studies. There are several examples that show GAGs-cancer relation. In one example, α4β1 integrin-mediated melanoma cell

adhesion is stopped by removal of cell surface chondroitin sulfate glycosaminoglycan (CSGAG).[74]

As mentioned above GAGs have diverse biological functions and this makes them a shining candidate for regenerative purposes. Currently, collagen–GAG composites are developed for a wide range of applications in tissue engineering of bone and skin.[48] GAGs also can be used as anticoagulation agents. Heparin and heparin like GAGs are used to inactivate coagulation proteases and blood anticoagulation.[80] In another study, regeneration potential of GAGs on spinal cord injuries was studied. In this work, chondroitin sulfate with two sulfate groups showed excellent motor recovery *in vivo* assay, improved axonal growth *in vitro*, and neuroprotection against the NMDA induced neuronal cell death. Besides, it was observed that GAGs do not inhibit axonal growth.[81] The importance of GAGs in neural tissue regeneration is also revealed by studying healthy and crush-injury models of sciatic nerve *in vivo*. In this study, GAGs are recovered from supernatant and pellets of tissue homogenates and assayed for different GAG types. The study shows that GAG profile in supernatant and pellets differ among injury model and healthy tissue. In addition, GAG amount is two times higher in healthy samples. This indicates the need to modulate the glycosaminoglycan expression pattern in adult neural tissue regeneration after post-traumatic period.[82]

GAGs have several important roles in tissue healing and remodeling. HA accelerates healing processes of dermal wounds.[68] It is shown that hyaluronic acid modulates the inflammation at short term but also at later stages of tendon or ligament healing, also it involves in collagen fibril aggregation and development.[83] It improves the healing quality of the injured tissues by increasing cell migration and proliferation in the

internal parts of the injured tendon and ligaments and by reducing peritendinous adhesion over the tendon and ligament surface as it decreases cell proliferation. HA is also used as chondroprotective and its effects are shown *in vitro* and *in vivo*.[68] In addition, HA is used as space-filling matrix of the eye in ophthalmology applications.[68]

GAGs can also be used in vascular tissue regeneration. Vascular endothelial cells are the cells found in vascular tissue and they synthesize collagen IV and elastin during angiogenesis. In one study, it was shown that collagen IV and elastin deposition in matrix is increased and their mRNA expression is upregulated when endothelial cells are cultured in matrix that incorporated HA and HA+HS combination.[84]

In another study, GAGs were shown to modulate differentiation of MSCs. It was shown that hMSCs (mesenchymal stem cells isolated from human bone marrow) selectively differentiate into bone when they are cultured on GAG containing tissue culture plates. Except from chondroitin-4-sulfate, all tested GAG types which were DS, chondroitin-6-sulfate, heparin and HA, increase osteoblast differentiation related genes expression.[77] To sum up, GAGs of extracellular matrix played a significant role in regulating osteoblast differentiation and could be exploited in the biomimetic approach of fabricating or functionalizing scaffolds.[77] Depending on the type of GAG that is used, MSCs were also directed into chondrogenic differentiation by changing the mechanical and morphological properties of the scaffold that they were incorporated in. In the study that compares effects of CS and HA incorporated collagen based scaffolds on MSC differentiation, it was shown that HA scaffold promotes cartilage differentiation. While expression of chondrogenic related gene markers such as Sox-9 and collagen II increased significantly, HA scaffold also

provided greater levels of MSC infiltration in comparison to the CS scaffolds which is characteristic for cartilage tissue.[85] Conversely, gene expression studies, scaffold morphology and mechanical characterizations revealed that scaffold incorporated with CS induce osteogenic differentiation. Therefore, this study also points out that GAG type determines differentiation fate of the MSCs.

1.3.4 GAG-protein interactions

GAGs are generally believed to exert their biological activities through the localization, stabilization, activation or inactivation of interacting proteins.[80] GAG-receptor and GAG-protein interactions are important as these interactions modulate various biological signals. High molecular weight HA (HMW-HA) inhibits osteoclast differentiation via Toll-like receptor (TLR)-4 by interfering with colony stimulating factor (M-CSF) signaling. In the inflammatory phase, GAG binding of chemo-attractants such as IL-8 and TGF-β provides the ECM with cues directing the migration of neutrophils and macrophages, towards the wounded tissue. HA runs most of its reaction upon binding CD44, which is the main receptor for HA.[48] The most studied GAG-protein interactions involves HS and growth factors, especially fibroblastic growth factor.[61] DS is also shown to bind to hepatocyte growth factor.[58] Heparin forms complexes with thrombin and protease inhibitors, and inhibits coagulation.[61] There are different factors that affect GAG-protein binding. One of them is presence of internal ion pairing in place of counter-ions. For example Na^+ on GAGs and Cl^- on the proteins influence GAG-protein interactions. High energy binding sites and the entropy of the environment are other factors that affect interaction[80]. Amino acid sequence also affects the binding behavior. There are

certain amino acids that particularly bind to GAGs when they are found in peptide sequence. Peptides including high amounts of arginine and lysine bind to GAGs with greatest affinity.[54] Peptides with high affinity for heparan sulfate are also enriched in other polar amino acids including serine. Asparagine residues are commonly found in heparin binding site.[80] For heparan sulfate binding, peptides are enriched in glutamine residues. Tyrosine residues are also enriched in known heparin binding regions.[80] These specific preferences are believed to stem from differences in abundance of chemical interactions like hydrophobic and hydrophilic interactions.

1.4 Peptide Amphiphiles

Peptide amphiphiles are molecules that combine structural features of amphiphiles and with functions of peptides that can be biologically active. They consist of two main blocks: an alkyl tail connected to a peptide block. Alkyl tail is the part that gives the structure lipophilicity. Therefore, PAs can also be called as lipopeptides, or amphiphilic peptides.[86,87]

A typical PA design includes four key regions.[88] First region is the hydrophobic domain, which is generally composed of an alkyl tail and gives lipophilicity to the molecule. Second region is located adjacent to the alkyl tail and is composed of a short peptide sequence capable of forming intermolecular hydrogen bonding and β-sheet secondary structure. Third region is designed to enhance water solubility of the PA molecules by providing charges to the molecule. This part is composed of either basic or acidic amino acids. Another function of this region is to make PA molecule assembly controllable by charge, pH, salts and ions. The last part is used to present

bioactive signals which may be an epitope to interact with cell receptors, a segment that binds proteins or biomolecules, or a pharmacological agent. This typical design of PAs can change depending on the application purpose. For example, PAs that are designed to functionalize liposomes include proline residues instead of β-sheet forming amino acids in order to trigger micelle structure formation.[89]

PAs are self-assembling molecules in aqueous conditions. Forces that drive self-assembly include hydrophobic interactions of the alkyl tails, hydrogen bonding among the middle peptide segments, and electrostatic repulsions between the charged amino acids.[88] Amphiphilicity is the main triggering factor for the self-assembly of PA molecules.[86] Assembly of PAs can also be triggered by ions and pH change. Upon self-assembly, PAs can form diverse nanostructures. These structures can have α-helical, and parallel or anti-parallel β-sheet secondary structures. Nanofibers, nanotubes, tape-like structure and cylindrical micelles are among the more sophisticated structures that can be obtained by self-assembly PAs.[90–93]

PAs are biocompatible, biodegradable, and can be easily controlled to form different shapes. Another most important feature of PAs is their high density epitope presenting properties. As they intrinsically self assemble, they present bioactive epitope groups to the environment with a much higher density compared to single bioactive peptide molecules. These features make PAs versatile tools as self-assembled building blocks. PAs can be used as delivery agents for drugs and miRNAs, as MRI contrast agents, antimicrobial agents, incorporated into energy applications, used *in vitro* to control cell fate and *in vivo* to induce or suppress (depending on the purpose) angiogenesis and to trigger tissue regeneration.[10,11,89,94–97]

CHAPTER 2

EXPERIMENTAL

2.1 Materials

[4-[-(2',4'-dimethoxyphenyl) Fmoc-aminomethyl]phenoxy] acetamidonorleucyl-MBHA resin (Rink amide MBHA resin), Fmoc-Glu(OtBu)-Wang resin, 2-(1H Benzotriazol-1-yl)-1,1,3,3-tetramethyluronium hexafluoro-phosphate (HBTU), 9-Fluorenylmethoxycarbonyl (Fmoc) and tert-butoxycarbonyl (Boc) protected amino acids were purchased from NovaBiochem, ABCR and Sigma-Aldrich. Fmoc-Ser[-Glc$(OAc)_4$]-OH was purchased from AAPPTec. N,N-diisopropylethylamine (DIEA) and lauric acid were purchased from Merck. Piperidine, acetic anhydride, dichloromethane (DCM), dimethylformamide (DMF), trifluoroacetic acid (TFA) and triisoproplysilane (TIS) were obtained from Sigma-Aldrich. All other chemicals and materials were purchased from Invitrogen, Fisher, Merck, Alfa Aesar, and SigmaAldrich. Deionized water (ddH_2O) used in experiments had a resistance of 18.2 MΩ.cm (Millipore Milli-Q). All chemicals and materials were used as provided. For cell culture experiments, Dulbeccos Modified Eagle Medium (DMEM), Penicillin/Streptomycin (PS) antibiotic mix and Fetal Bovine Serum (FBS) were purchased from Gibco, Life Technologies. LIVE/DEAD Viability/Cytotoxicity Kit was purchased from Invitrogen. Cell Proliferation ELISA, BrdU (colorimetric) kit was purchased from Roche. Safranin-O and Oil Red-O were obtained from Sigma-Aldrich.

2.2 α-N-Acetyglucosamine Carboxylic Acid Synthesis

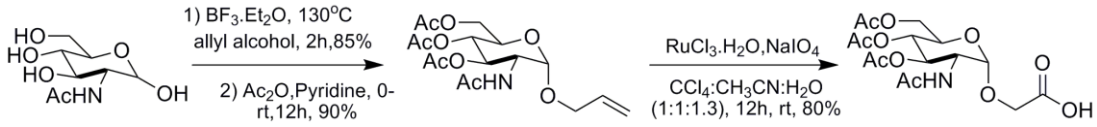

Figure 2.1 Synthesis of 2-Acetamido 2-deoxy-a-D-glucopyranose 3,4,6 triacetate carboxylic acid derivative. Carboxylic acid functionality appended to N-acetyl-glucosamine.

2.2.1 Synthesis of Allyl-N-Acetyl-α-D-Glucopyronoside-3,4,6 Triacetate

0.2 mL of $BF_3.Et_2O$ was added to a solution of 2 g *N*-acetyl-glucosamine in 50 mL allyl alcohol and reaction mixture was refluxed at 130 °C for 2 h. After complete conversion allyl alcohol was removed on rotary evaporator to get crude allyl-N-acetyl-α-D-glucopyranoside. The crude product was purified by dissolving in 20 mL ethanol and then adding diethyl ether. Desired compound separates as a white solid. White solid compound was dissolved in 20 mL dry pyridine, acetic anhydride at 0 °C was added and then stirred at room temperature for 12 h. After the completion of reaction, pyridine was removed on rotary evaporator. Then crude material was dissolved in ethyl acetate and washed with dil. HCl, brine and water. Organic layer was dried on anhydrous Na_2SO_4 and column purified to get desired compound after evaporating organic solvent. 1H NMR 5.88 (1H, m), 5.72 (1H, J=9.54Hz, d), 5.27 (3H, m), 5.12 (1H, J=9.54, t), 4.88 (1H, J=3.51Hz, d), 4.35 (1H, m), 4.23 (1H, J=12.30 & 4.52Hz, q), 4.18 (1H, m), 4.09 (1H, m), 4.02 (1H,m), 3.96 (1H,m), 2.09 (3H,s), 2.02 (3H,s), 2.01 (3H,s), 1.95 (3H,s).

2.2.2 Synthesis of N-Acetyl-α-D-Glucopyronoside-3,4,6 Triacetate Carboxylic Acid

Into the stirred solution of allyl-N-acetyl-α-D-glucopyronoside-3,4,6 triacetate, dissolved in 23 mL CCl_4, 23 mL CH_3CN and 30 mL H_2O at 0°C, $NaIO_4$ and $RuCl_3.H_2O$ was added. The reaction mixture was stirred for 12-16 h and after completion was checked by thin layer chromatography (TLC), reaction mixture was evaporated on rotary evaporator to get crude carboxylic acid derivative which was directly used for coupling on solid phase. 8Hz; 4.12-4.27 (m, 6H); 3.98 (d, J=15.0Hz, 1H), 3.54-3.79 (m, 9H), 3.20-3.50 (m, 26H), 3.10-3.17 (m, 5H), 2.10-2.25 (m, 5H), 1.93-2.01 (m, 4H), 1.86 (s, 3H), 1.55-1.81 (m,3H), 1.40-1.49 (m, 5H), 1.20-1.30 (m, 25H), 0.8-0.9 (m, 18H).

2.3 Synthesis, Identification and Purification of Peptide Amphiphile Molecules

2.3.1 Synthesis of Peptide Amphiphile Molecules

Peptide amphiphile molecules were synthesized by standard SPPS (solid phase peptide synthesis) method. Peptide amphiphiles, except E-PA, were constructed on MBHA Rink Amide resin, and E-PA [Lauryl-VVAGE] was constructed on Wang resin pre-loaded with Fmoc-Glu(OtBu). The resins were swelled in DCM for 30 min. Following resin swelling, DCM solvent was exchanged to DMF, in which all remaining reactions were carried out. All amino acid couplings, except Fmoc-Ser[-$Glc(OAc)_4$]-OH, were performed with 2 equivalents of Fmoc protected amino acid, 1.95 equivalents of HBTU and 3 equivalents of N,N-diisopropylethylamine (DIEA)

in DMF. Coupling duration was at least 3 h but varied depending on the type of amino acid that is coupled. Fmoc-Ser[Glc(OAc)$_4$]-OH coupling was performed with 1.2 equivalents of amino acid, 1.1 equivalents of HBTU and 1.8 equivalents of N,N-diisopropylethylamine (DIEA) in DMF. Equivalences are based on the resin that was used for construction.

Fmoc deprotections were performed with 20% piperidine/dimethylformamide (DMF) solution for 20 min. After each coupling reaction, resin was treated with 10% acetic anhydride in DMF for 30 min to block any remaining free amino groups. Before each succeeding event, washing was performed by DMF, DCM, and DMF three times each, respectively. Cleavage of the peptides from resin was carried out with a mixture of triuoroacetic acid (TFA) : triisoproplysilane (TIS) : water in the ratio of 95 : 2.5 : 2.5 for 2 h. Excess TFA was removed by rotary evaporation. The remaining viscous peptide solution was treated with ice-cold diethyl ether overnight at -20 °C. Ether decantation was performed after centrifugation at 4 °C, 8000 rpm for 15 min. After complete evaporation of diethyl ether via air drying, the resulting pellet was dissolved in ddH_2O, sonicated for 30 min, freeze-dried at -80 °C, and lyophilized. Deacetylation of Glc-PA [Lauryl-VVAGKS[β-*D*-Glc(OAc)$_4$)-Am] was carried out in solution phase. Acetyl protecting groups on glucose of Glc-PA [Lauryl-VVAGKS(β-*D*-Glc)-Am] were removed in NaOMe in methanol solution. The reaction was carried out at room temperature, in argon atmosphere, for 3-4 h by stirring. The reaction was quenched at acidic condition which is created by a few drops of acetic acid. Solution was removed by rotary evaporator and obtained product was dissolved in ddH_2O and freeze-dried. The PAs were stored at -20 °C.

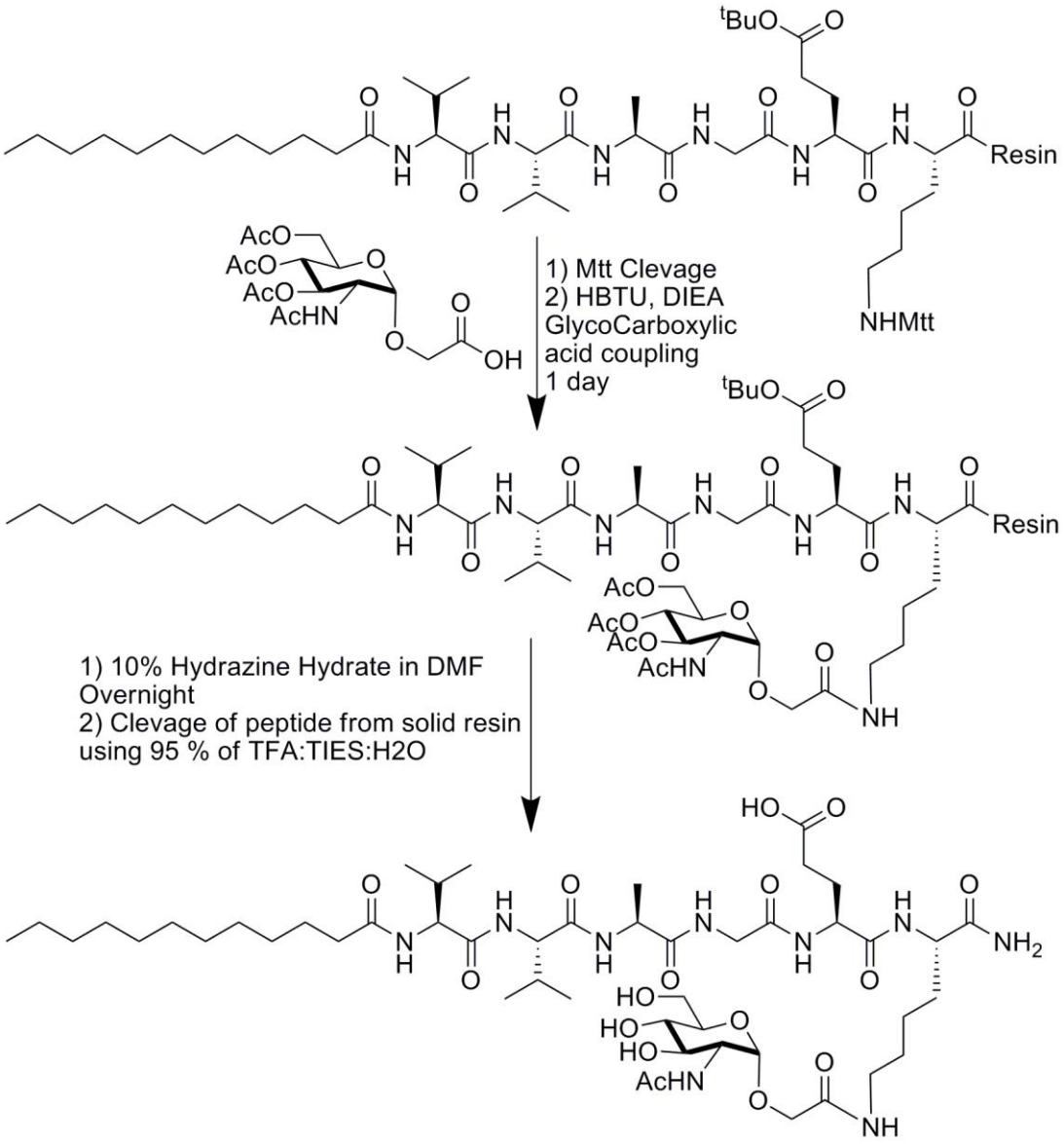

Figure 2.2 Schematic representation of the sequential synthesis of amphiphilic glycopeptide. N-acetyl-α-D-glucopyronoside-3,4,6 triacetate carboxylic acid was attached to the PA backbone from the side chain of lysine.

2.3.2 Characterization of Peptide Amphiphile Molecules

The synthesized peptide was characterized by liquid chromatography mass spectrometry (LC-MS) on an Agilent 6530 Q-TOF mass spectrometer equipped with ESI source and reverse phase analytical high performance liquid chromatography. Basic conditions and acidic conditions were used to identify negatively charged and positively charged PA molecules, respectively. For basic conditions, Zorbax Extend-C18 (4.6 x 50 mm) column and water/acetonitrile gradient with 0.1% volume of NH_4OH were used. For acidic conditions, Zorbax 300 SB-C8 (4.6 x100 mm) column and water/acetonitrile gradient with 0.1% volume of formic acid were used.

2.3.3 Purification of Peptide Amphiphile Molecules

An Agilent 1200 preparative reverse-phase HPLC system was used for purification of PA molecules. As stationary phase, a Luna 5u C8 (2) (21.20 x 100 mm) column for acidic conditions and a Gemni 5u C18 (21.20 x 100 mm) column for basic conditions were used to purify positively charged and negatively charged PA molecules, respectively. As mobile phase, water/acetonitrile gradient with 0.1% volume of NH_4OH for basic conditions and water/acetonitrile gradient with 0.1% volume of TFA for acidic conditions were used.

2.4 Formation of Peptide Amphiphile Nanostructures, Spectroscopy and Morphological Characterizations

2.4.1 Formation of Self-Assembled PA Nanostructures

To induce nanofiber formation, PA solutions were prepared from the solid form of the PAs by dissolving in ddH_2O. GlcNAc-PA [Lauryl-VVAGK(GlcNAc)-Am], Glc-PA (or other name K-Glc-PA) [Lauryl-VVAGKS(β-*D*-Glc)-Am], E-Glc-PA [Lauryl-VVAGES(β-*D*-Glc)- Am] and K-PA [Lauryl-VVAGK- Am] solutions were prepared at 1 mM concentration, E-PA [Lauryl-VVAGE] was prepared at 0.5 mM concentration and then PA solutions were sonicated for 15 min and sterilized under UV for 15 min. PA nanostructures were formed on well plates by mixing counter charged PAs with equal volume. Final net charges of PA mixtures were obtained as zero. Hyalgan® was 1:25 diluted in ddH_2O to arrange molarity as approximately 1 mM. Diluted Hyalgan® was mixed with 1 mM K-PA at 1:1 volume ratio. Coated plates were incubated at standard conditions for half an hour to allow homogeneous mixing of PA molecules. After the incubation, plates were left under laminar flow for overnight to dry peptide gel. Prior to cell seeding, plates were sterilized by UV radiation for 30 min.

2.4.2 Circular Dichorism

Secondary structures of the PA molecules were characterized by J-815 Jasco circular dichroism spectrophotometer in the far ultra-violet region. PA solutions were prepared and nanofiber formations were conducted as explained in the “Formation of Self-Assembled PA Nanostructures” part. PA solutions and peptide gel were

incubated for 15 min prior to measurement in order to allow self-assembly formation and diluted 1:3 with ddH_2O. CD spectrum was measured from 300 to 190 nm, with 100 nm/min scanning speed, 0.1 data pitch, 1 nm bandwidth, 4 s D.I.T. and measurements were performed with three accumulations. Selectivity was selected as standard. Measurements were performed in quartz cuvettes with 1 mm path length. The results were obtained as molar elipticity and converted into the unit of $deg.cm^2.dmol^{-1}$ using the formula given below:

$$[\theta] = \frac{100\ x\ \Omega}{(C\ x\ 0.l)}$$

where Ω is the obtained value, C is the concentration in molar, and 0.l is the cell path length in centimeters.

2.4.3 Scanning Electron Microscopy Imaging

For SEM imaging, peptide hydrogels were prepared on cleaned silica wafers, by mixing 10 mM PA solutions at 1:1 ratio, except combinations including E-PA. PAs that were combined with E-PA were mixed at 2:1 ratio, where E-PA was the 1 equivalent. Obtained gels were incubated for 20 min at room temperature to allow gelation and then dehydrated. Dehydration was performed in 20, 40, 60, 80, and 100% ethanol solutions, sequentially. Dehydrated gels were dried with a Tourismis Autosamdri-815B critical-point-drier to preserve the network structure. The dried samples were covered with Au/Pd at 5 nm thickness and visualized under high vacuum with a FEI Quanta 200 FEG scanning electron microscope equipped with ETD detector.

2.4.4 Transmission Electron Microscopy Imaging

TEM samples were prepared on a 200-mesh cupper TEM grid. Nanostructures were formed as explained above and these solutions were 10 times diluted. 30 μL from the solutions were dropped on a parafilm which is hydrophobic surface and the grid was placed onto droplet. After 5 min incubation, grid was taken, excess PA solution was removed and the grid was stained with 2 wt% uranyl-acetate for 3 min. Immediately after 3 min, uranyl-acetate was removed, the grid was rinsed with ddH_2O and left to air drying. TEM images were acquired with FEI Tecnai G2 F30 TEM at 300 kV.

2.5 Cell Culture and Maintenance

Rat mesenchymal stem cells (rMSCs) (Invitrogen) were cultured as monolayer cultures in DMEM medium supplemented with 10% FBS and 1% penicillin-streptomyocin in tissue culture plates at standard conditions (at 37 °C under 5% CO_2). Cells were seeded at 3000-5000 cells/cm^2 and passaged at 80% confluency by Trypsin-EDTA (0.025%). The culture medium was replaced every 3-4 days. In all experiments, cells between passage 6-9 were used. All cell culture reagents were purchased from Invitrogen.

2.6 Cell viability, Adhesion and Proliferation Analyses

2.6.1 Viability Assay: MTT assay

Viability of rMSCs seeded on nanofiber networks were quantified by MTT assay (Sigma, Cat no: TOX-1). In order to perform MTT assay, cells at a density of 1.2 x 10^4 cells/cm^2 were seeded on PA coated wells and on bare wells as a control in

maintenance medium. Then, plates were incubated at standard conditions for 12 h. After incubation period, medium was replaced with phenol red free medium containing (3-(4,5-dimethylthiazol-2-yl)-2,5 diphenyltetrazolium bromide (MTT) reagent and cells were incubated for 4 h at standard cell culture conditions. Following the incubation period, plates were removed from the incubator and resulting formazan crystals, formed by viable cells through cleavage of tetrazolium ring, was dissolved in MTT Solubilization Solution [M-8910] as indicated in the procedure. Spectroscopic measurement was performed at a wavelength of 570 nm and obtained results were converted into % viability against bare surface.

2.6.2 Cell Adhesion

Adhesion profile of rMSCs on PA coated and on bare surfaces were analyzed after 4 h incubation. To perform adhesion test, growth medium of the flask was replaced with adhesion medium which is serum free low glucose phenol red including DMEM, supplemented with 3 wt% BSA and 0.05 wt% cycloheximide, and cells were incubated for 1 h at standard cell culture conditions. In order to detach cells from the flask surface trypsin was added and incubated just for 30 sec. Later 0.6 x 10^4 cells per cm^2 were seeded on PA coated wells and on bare wells and incubated at standard conditions for 5 h. After 5 h, media was removed by aspiration, the wells were washed with PBS and cells were stained with 2 μM Calcein AM (Invitrogen) in PBS for 40 min. Stained cells were imaged by an inverted fluorescent microscope and counted by using ImageJ software. The experiment was carried out on a 96-well plate.

2.6.3 Cell Proliferation

Proliferation of cells was determined by Cell Proliferation ELISA, BrdU (colorimetric) (Roche) according to the manufacturer's protocol. 96-well plate was used for the proliferation assay. In brief, 1.2 x 10^4 cells per cm^2 were seeded on PA coated wells and on bare wells and incubated for 48 h at standard conditions. After 48 h, medium was replaced with 10 μM BrdU containing medium and cells were incubated at standard conditions for additional 4 h. Cells were then fixed and stained by using labeled antibody against BrdU. Cells were washed three times with PBS, and substrate solution was added. After 20 min, color development was measured at a wavelength of 370 nm by using microplate reader (Molecular Devices Spectramax M5) and subtracted from reference wavelength (492 nm) values.

2.7 Cell Differentiation Analyses

2.7.1 Sulfated Glycosaminoglycan Production Analyses

2.7.1.1 Safranin-O Staining

Glycosaminoglycan accumulation was visualized by Safranin-O staining. In order to perform Safranin-O staining, rMSCs were seeded on PA coated wells of 96 well plates and bare wells as a control in maintenance medium. Cells were seeded at a density of 1.2 x 10^4 cells/cm^2 and then plates were incubated at standard cell culture conditions. At the indicated time points, medium was discarded by aspiration and cells were washed with 1X PBS and fixed with 10% formalin (in PBS) for 15 min at RT. The cells were blocked with 1% BSA/PBS (w/v) for 30 min at RT after a washing step, in order to eliminate non-specific binding of dye. Thereafter cells were treated with 0.1% (w/v) Safranin-O in 1% (v/v) acetic acid for 5 min at RT.

Immediately after 5 min, dye was removed by aspiration and the wells were extensively washed with 0.1% (v/v) acetic acid in PBS to remove unbound dyes. That last washing step with 0.1% (v/v) acetic acid in PBS was repeated 3 times, each for 5 min on a shaker. After third wash, washing solution was replaced with ddH_2O and the stained cells were imaged by an inverted light microscope.

2.7.1.2 Dimethyl Methylene Blue Assay

Quantification of the accumulated sulfated glycosaminoglycans was performed by dimethylmethylene blue (DMMB) assay. For the DMMB assay, 48 well plates were coated with 200 µL peptide solution in total as described, and 1.2 x 10^4 cells per cm^2 were seeded. In order to perform DMMB assay, culture medium was removed by aspiration, wells were washed once with PBS, and 200 µL of papain digestion buffer (100 mM sodium phosphate buffer/ 10 mM Na_2EDTA/ 10 mM L-cysteine/ 0.125 mg/mL papain) per well was put. Cells were scraped with pipette in papain digestion buffer. The samples were collected in 1.5 mL eppendorf tubes and incubated overnight at 65 °C. Tubes were centrifuged at 2000 rpm for 5 min and supernatants were taken in a new tube and used for following measurements. DNA amount per construct was determined by using Qubit dsDNA quantification kit (Invitrogen) according to the manufacturer's instructions. Before each Qubit sample preparation sample tubes were vortexed for 3-5 sec. Gradually increasing concentrations of chondroitin-4-sulfate standards (from 0 to 35 µg/ mL) were used to generate a standard curve for the DMMB assay. In order to determine s-GAG amount, samples from the same supernatants and C4S standards were aliquoted into 96 well plates with a volume of 40 µL. 125 µL DMMB dye (16 mg/L 1,9-dimethylmethylene blue, 40 mM glycine, 40 mM NaCl, 9.5 mM HCl, pH 3.0) was added on 40 µL of the

papain digested samples and of standard solutions. Optical densities (ODs) of the mixtures were measured at a wavelength of 525 nm by using microplate reader (Molecular Devices Spectramax M5). The sulfated glycosaminoglycan content was normalized to total dsDNA.

2.7.2 Oil Red O Staining

Oil Red-O assay was performed in order to evaluate deposition of triglycerides and lipids. Nanofiber formation on 96-well plate was done as explained. Cells were seeded at a 1.2 x 10^4 cells per cm^2 density and incubated at standard conditions till the indicated experiment time points. At the indicated time points, medium was discarded by aspiration, cells were washed with 1X PBS and fixed in 10% formalin in 1X PBS. After 10 min, fixation solution was refreshed and the cells were incubated for an additional 1 h at room temperature. Later, wells were washed with ddH_2O and incubated in 60% isopropanol for 5 min at room temperature. After 5 min, isopropanol was discarded and plate was left open to air dry. When the wells were completely dried, 100 mL Oil Red working solution per well was added and incubated for 10 min by gently shaking on a shaker. Unbound dyes were washed with ddH_2O 4 times. Finally, ddH_2O was added on wells and images were acquired under an inverted light microscope.

2.7.3 Real-Time Gene Expression Analysis

Gene expression profiles of differentiating rMSCs were assessed by quantitative Real Time PCR (qRT-PCR) analyses. For total RNA extraction, cells were seeded at a 1.2 x 10^4 cells per cm^2 density on PA coated and bare well surfaces. For RNA extraction,

cells were grown on 24-well plate. Total RNAs of cells were extracted by using TRIzol (Invitrogen) according to the manufacturer's instructions. Concentration and purity of isolated RNAs were measured by Nanodrop 2000 (Thermoscientific). All samples were diluted to 50 ng/μL concentration prior to their use in qRT-PCR. Conversion of RNAs to cDNA and amplification of cDNAs were performed by using SuperScript III Platinum SYBR Green one-step qRT-PCR Kit (Invitrogen) according to the manufacturer's protocol. Reaction conditions were briefly as follows: 55 °C for 5 min, 95 °C for 5 min, 40 cycles of 95 °C for 15 s, X °C (where X is the annealing temperature of the primers, see Table 2.1) for 30 sec, and 40 °C for 1 min, followed by a melting curve analysis in order to confirm product specificity. The reaction efficiencies for each primer were determined by plotting a standard curve with 10-fold dilutions of the total RNA. Primer sequences and annealing temperatures for each gene are given in Table 2.1. Primary gene expression levels were normalized to GAPDH (a house-keeping gene) and comparative Ct method (Pfaffl method) was used to analyze results.

2.8 Statistical Analyses

All quantitative values are represented as means ± standard error of the mean (SEM). All experiments were performed with at least three replicates. One-way ANOVA with Bonferroni's multiple comparison post-test was used for statistical analysis and a p value of less than 0.05 was considered statistically significant, unless noted otherwise.

Table 2.1 Primer sequences and annealing temperatures of the genes used for qRT-PCR analyses.

Gene Name (Abbreviation)	**Primer Sequence: Forward/Reverse**	**Annealing Temperature (°C)**
Adiponectin **(ADIPOQ)**	5'-AAGGGAGACGCAGGTGTTCTTGG-3' 5'-ATGGGAACATTGGGGACAGTGAC-3'	58.0
Aggrecan **(ACAN)**	5′-GGTCACTGTTACCGCCACTT-3′ 5′-CCCCTTCGATAGTCCTGTCA-3′	58.0
Collagen 1 **(COL1)**	5'-GAATATGTATCACCAGACGCAGA-3' 5'-GGACATCTGGGAAGCAAAGT-3'	59.5
Collagen 2 **(COL2)**	5′-CGAGGTGACAAAGGAGAAGC-3′ 5'-TCCCGGTCTTCATGGGACTA-3'	55.0
Fatty Acid Binding Protein 4 **(FABP4)**	5'-CCCAGATGACAGGAAAGTGAAGAGC-3' 5'-CTTTCATGACACATTCCACCACCAG-3'	59.0
Glyceraldehyde-3-phosphate dehydrogenase **(GAPDH)**	5′- GTGCCAGCCTCGTCTCATA-3′ 5′- AACTTGCCGTGGGTAGAGTC-3′	57
Transcription Factor SOX-9 **(SOX9)**	5′-CCACCCCGATTACAAGTACC-3′ 5'-CAGCCACCTGGGACTCTAA-3'	61.5
Uncoupling Protein 1 **(UCP1)**	5′-CCAGTGTAGCGGGGTTTGAT-3′ 5′-GAGAGAAACGCCTGCCTCTT-3′	62.2

CHAPTER 3

GLYCOPEPTIDE NANOFIBERS FOR CELL DIFFERENTIATION INTO HYALINE CHONDROCYTES

3.1 INTRODUCTION

Cartilage is a flexible avascular tissue that has limited regeneration capacity. Cartilage has unique mechanical properties. It is the load bearing, cushioning part of the body. Water composes the highest volume of cartilage (~80%) and cartilage creates a friction-free environment at the articular parts of the bones. Chondrocytes, which are specialized cells that compose cartilage, produce large amounts of extracellular matrix (ECM) mainly made up of collagen fibers and aggrecan proteoglycans. Hyaluronic acid (HA), which is a non-sulfated glycosaminoglycan (GAG), is an important component of articular cartilage. Aggrecan and HA complex form negatively charged aggregates, hold extensive amount of water and so contribute to mechanical properties of the cartilage. HA in the ECM has a role in cell adhesion, proliferation and movement. Articular cartilage covers the bony surface of joints. Its function is to provide a low friction surface enabling the joint to withstand weight bearing through the range of motion needed to perform daily activities as well as athletic endeavors. Articular cartilage enables the knee to tolerate shear forces and absorb shock and loads up to 20 times the body's weight. Articular cartilage defects impact daily activities of the patients negatively. In this chapter, our motivation is to create cartilage mimicking ECM by using glycoconjugated peptide nanostructures in order to induce differentiation of mesenchymal stem cells (MSCs) into cartilage cells, especially having hyaline type cartilage features, and to obtain a biocompatible material that can be used for regeneration of articular cartilage defects. In this study, amphiphilic glycopeptides were successfully synthesized and characterized. Morphological and chemical analysis of the peptide networks were carried out. Differentiation experiments revealed that HA mimetic glycopeptide nanonetworks

trigger better and faster chondrogenic differentiation compared to positive control (Hyalgan®/peptide nanonetwork) and negative controls (bare tissue culture plate surface and non-bioactive PA combinations) even in the absence of chondrogenic medium.

3.2 RESULTS

3.2.1 Synthesis and Characterization of α-N-acetylglucosamine Allyl Glycoside

α-N-acetylglucosamine allyl glycoside was synthesized in order to develop hyaluronic acid mimetic PA network. It forms the GlcNAc mimetic part of the system. α-N-acetylglucosamine allyl glycoside was synthesized in two steps. Chemical identifications of the compounds were carried out by NMR and mass spectrometry (Figure 3.1-3.4). Obtained α-N-acetylglucosamine allyl glycoside was directly coupled to the side chain of lysine solid support using standard amide coupling and characterized by H-NMR (Figure 3.3).

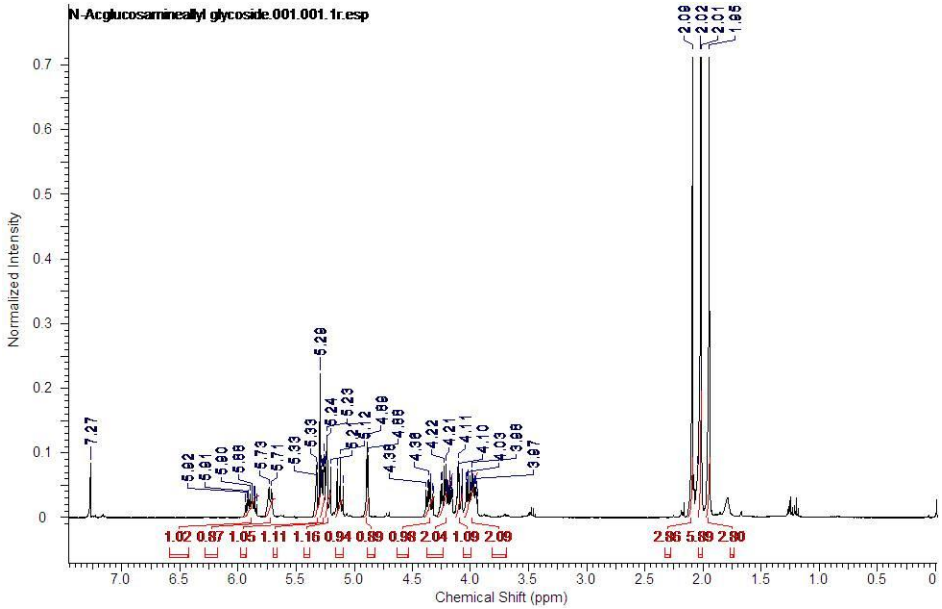

Figure 3.1 ^{1}H-NMR spectra of Allyl-N-Acetyl-α-D-Glucopyronoside-3,4,6 triacetate. Peaks show the successful synthesis of the compound.

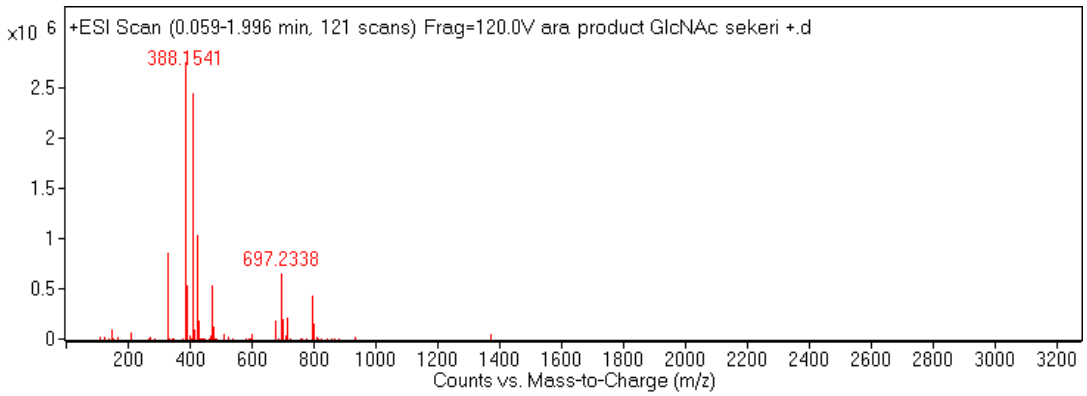

Figure 3.2 Mass spectrum of Allyl-N-Acetyl-α-D-Glucopyronoside-3,4,6 triacetate. Experimental m/z $[M+H]^+$ = 388.1541, $[M+Na]^+$ = 410.1358 $[(M+K)]^+$ = 426.1103, $[(M+H)*2]^+$ = 697.2338, calculated m/z $[M+H]^+$ = 388.15.

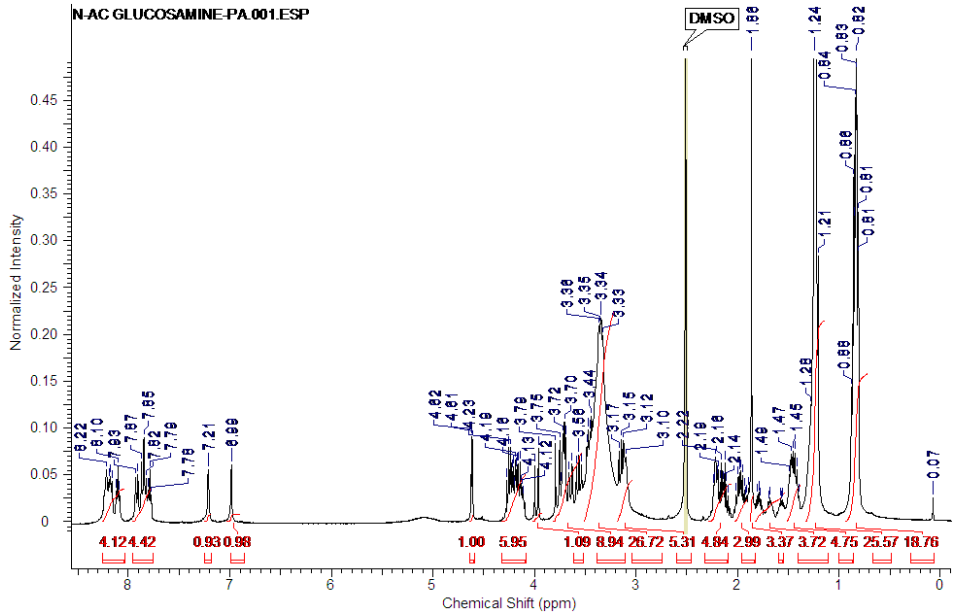

Figure 3.3 ^{1}H-NMR spectra of N-Acetylglucosamine-E-PA. N-Acetyl-α-D-Glucopyronoside-3,4,6 triacetate carboxylic acid coupled to the Lauryl-VVAGEK-Am backbone from the side chain of lysine.

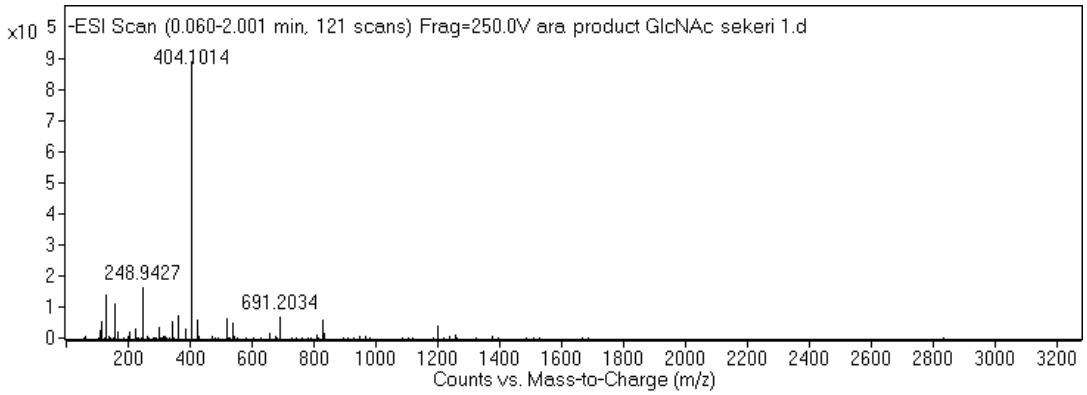

Figure 3.4 Mass spectrum of N-Acetyl-α-D-Glucopyronoside-3,4,6 triacetate carboxylic acid. Experimental m/z $[M-H]^-$ = 404.1014, calculated m/z $[M-H]^-$ = 404.13.

3.2.2 Synthesis and Characterization of Peptide Amphiphile Molecules

In this study, four different peptide amphiphile molecules were designed (Figure 3.5). Amino acid sequences, theoretical molecular weights and theoretical net charges of the PA molecules at neutral pH are given in Table 3.1. PA molecules were synthesized by solid phase peptide synthesis method, purified by preparative HPLC and characterized by LC-MS. Purity of PA molecules were investigated LC-MS spectroscopy. Experimental molecular masses of the PA molecules determined by MS spectroscopy were 654.4975 ($[M+H]^+$) for K-PA, 903.5758 ($[M+H]^+$) for Glc-PA, 1042.4484 ($[M-H]^-$) for GlcNAc-PA, and 654.2844 ($[M-H]^-$) for E-PA. Theoretical masses of the designed PA molecules were matched with these experimental results. This match proved the synthesis success. Prep-HPLC purification was performed for all PA molecules independent from their purity as they are used in cell culture studies. After prep-HPLC purification of the PAs, a second round LC-MS was performed to check the final purity of PA molecules (Figure 3.6-3.10). All PA molecules have more than 94% final purity.

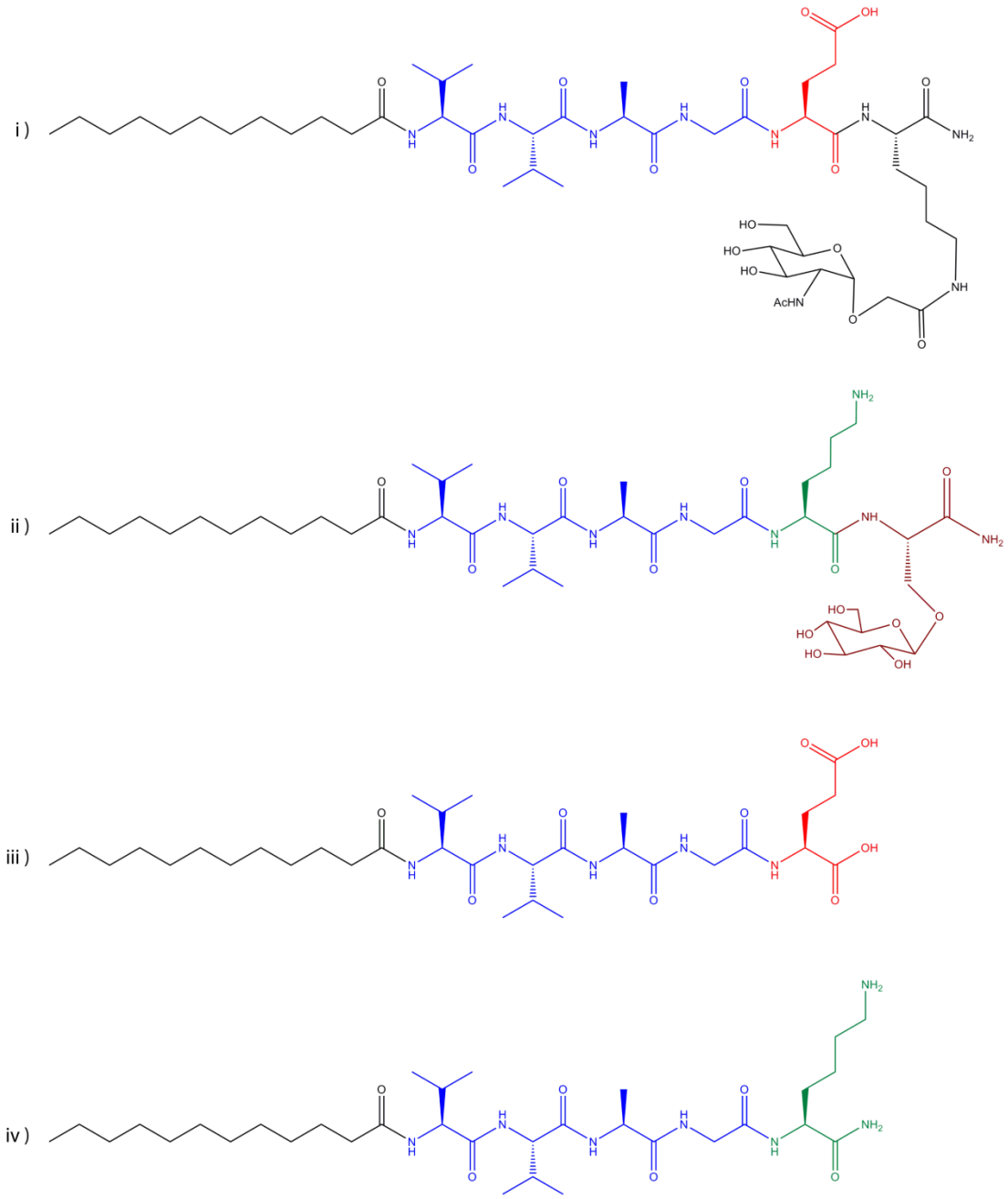

Figure 3.5 Chemical structures of the peptide amphiphiles. GlcNAc-PA (i), Glc-PA (ii), E-PA (iii), and K-PA (iv). Color codes of the structures indicate alkyl tail (black), β-sheet forming units (blue), positively charged amino acids (green), and negatively charged amino acids (red).

Table 3.1 Sequences, molecular weights and theoretical overall charges of the peptide amphiphiles at neutral pH.

Peptide Amphiphile	Sequence	Molecular Weight	Net Charge
GlcNAc-PA	Lauryl -VVAGEK(GlcNAc**)**-Am	1043.61	-1
Glc-PA	Lauryl-VVAGKS**(**β-*D*-Glc**)**-Am	902.57	+1
E-PA	Lauryl-VVAGE	655.42	-2
K-PA	Lauryl-VVAGK-Am	653.48	+1

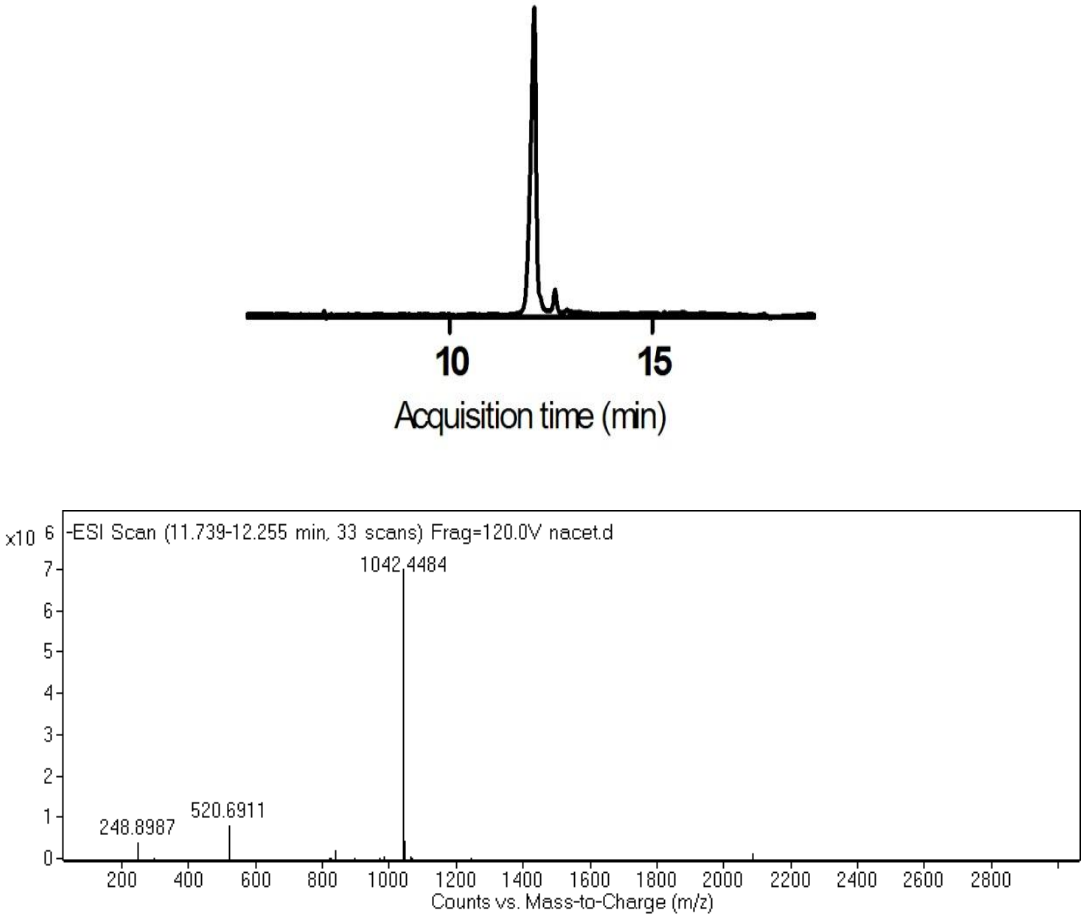

Figure 3.6 Liquid chromatography-mass spectrometry (LC-MS) analysis of GlcNAc-PA. The purity of the crude product was analyzed according to the optical density at 220 nm. Experimental m/z $[M-H]^-$ = 1042.4484, $[(M-H)/2]^-$ = 520.6911, calculated m/z $[M-H]^-$ = 1042.61.

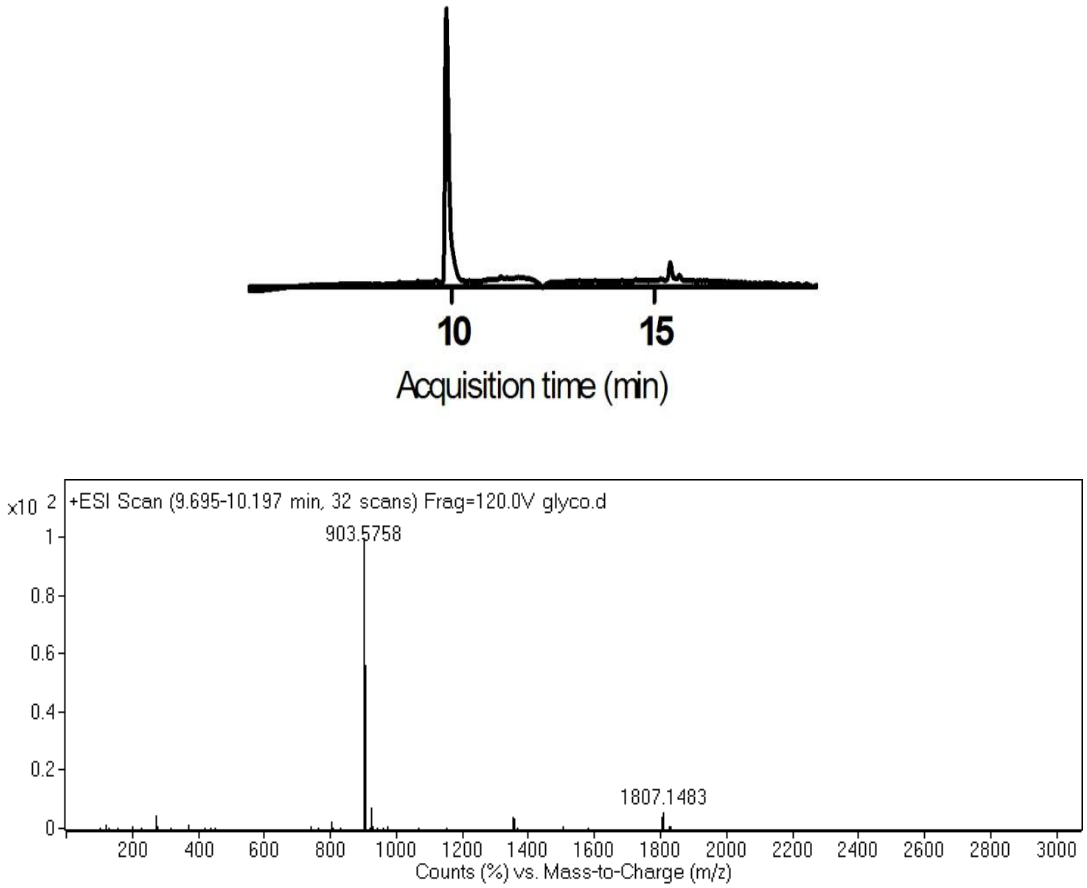

Figure 3.7 Liquid chromatography-mass spectrometry (LC-MS) analysis of Glc-PA. The purity of the crude product was analyzed according to the optical density at 220 nm. Experimental m/z $[M+H]^+$ = 903.5758, $[(M+H)*2]^+$ = 1807.1483, calculated m/z $[M+H]^+$ = 903.57.

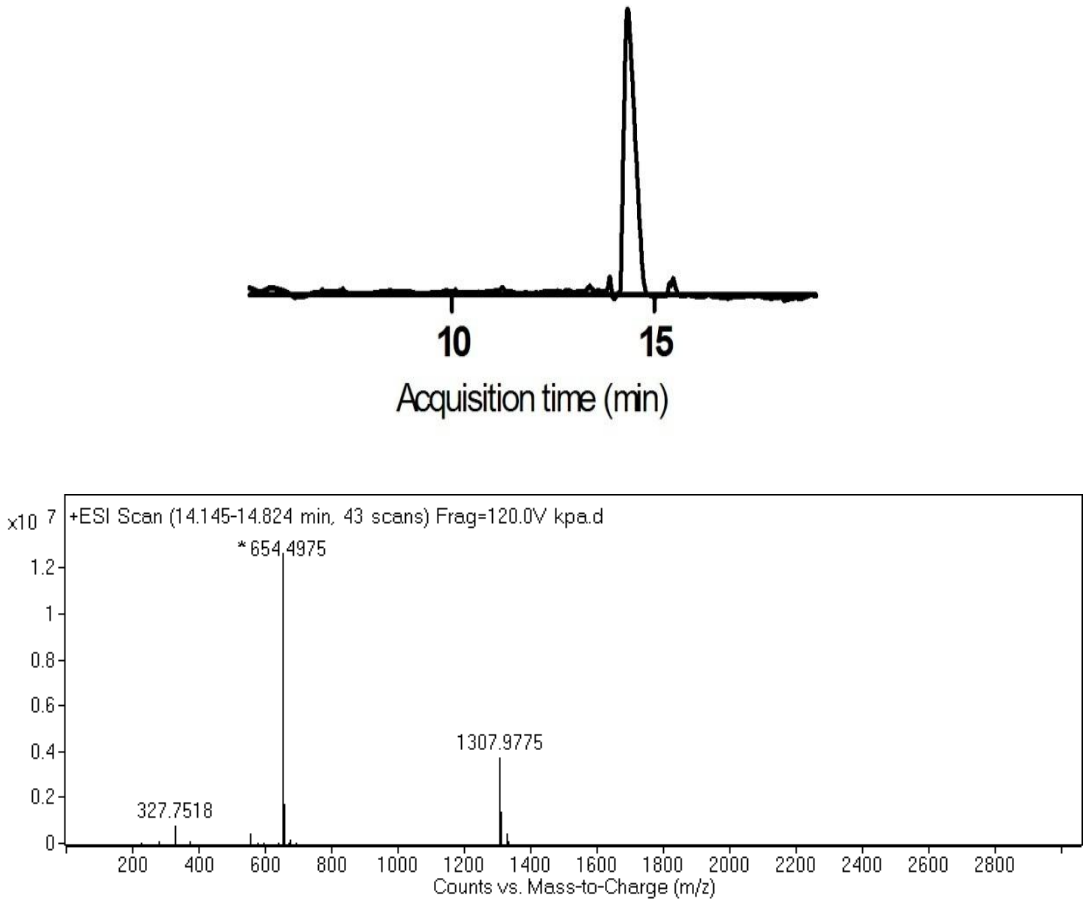

Figure 3.8 Liquid chromatography-mass spectrometry (LC-MS) analysis of K-PA. The purity of the crude product was analyzed according to the optical density at 220 nm. Experimental m/z $[M+H]^+$ = 654.4975, $[(M+H)*2]^+$ = 1307.9775, $[(M+H)/2]2^+$ = 327.7518, calculated m/z $[M+H]^+$ =654.48.

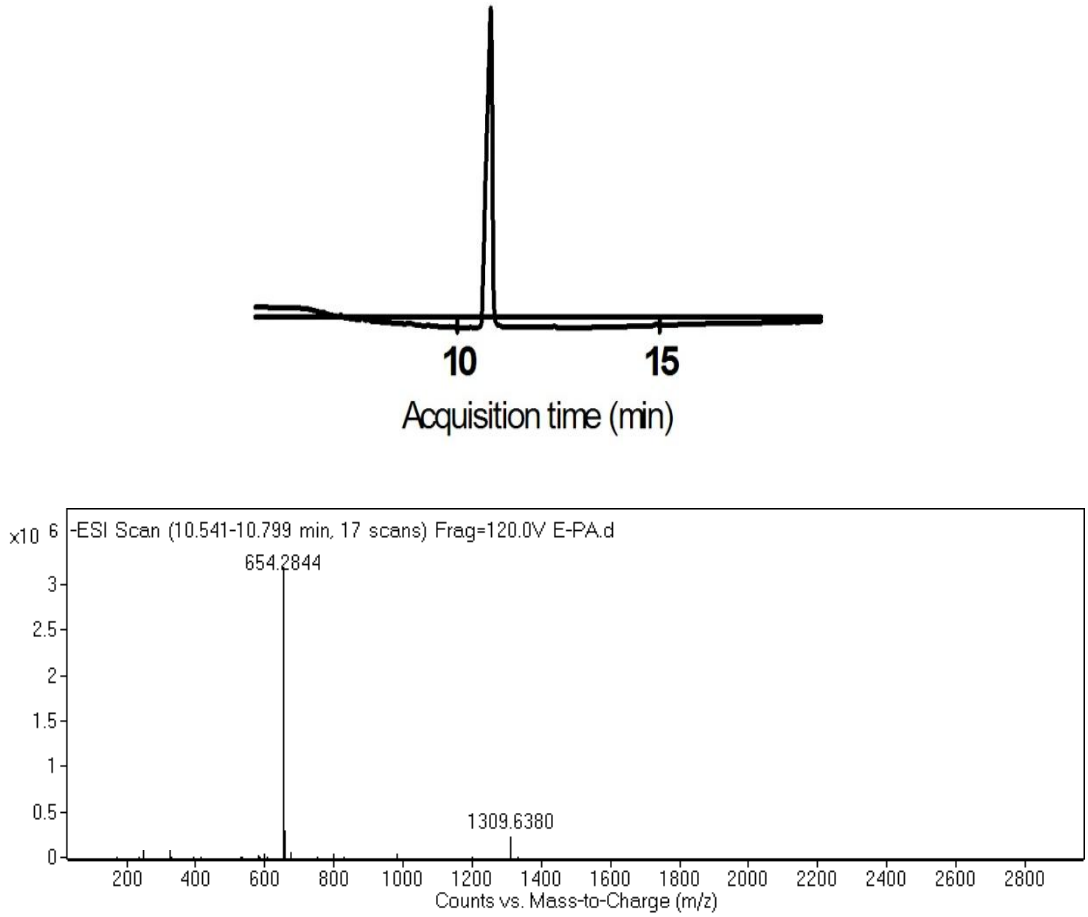

Figure 3.9 Liquid chromatography-mass spectrometry (LC-MS) analysis of E-PA. The purity of the crude product was analyzed according to the optical density at 220 nm. Experimental m/z $[M-H]^-$ = 654.2844, $[(M-H)*2]^-$ = 1309.6380, calculated m/z $[M-H]^-$ = 654.42.

3.2.3 PA Nanofiber Formation

Peptide amphiphiles are versatile tools due to their intrinsic self-assembly and high density epitope presenting properties. In this study, Glc-PA (Lauryl-VVAGKS(β-*D*-Glc)-Am) and GlcNAc-PA (Lauryl-VVAGEK(GlcNAc)-Am) are designed to mimic glucoronic acid and N-acetylglucosamine part of hyaluronic acid disaccharide units,

respectively. Positively charged K-PA (Lauryl-VVAGK-Am) and negatively charged E-PA (Lauryl-VVAGE) peptide amphiphiles were designed as non-sugar bearing control PA molecules. Peptide amphiphile nanofiber scaffolds were generated through self-assembly mediated by electrostatic interactions among charged amino acids and hydrophobic collapse of the alkyl tails, and intermolecular hydrogen bonding of hydrophobic amino acids in β-sheet driving units at physiological pH.[88] Hyalgan® is a commercially available knee-injection polymer and it is used to relief patient's pains that stem from chondro-degenerated knee.[98] Hyalgan® is used as positive control in this study. As it is highly anionic, it was treated as if it is negatively charged PA and in order to form nanofibers was mixed with K-PA.

Five different nanofiber network systems were formed. GlcNAc-PA/Glc-PA network generates hyaluronic acid mimetic scaffold. This combination is aimed to mimic the hyaluronic acid in a more coherent way than other combinations. GlcNAc-PA/K-PA and Glc-PA/E-PA networks were designed to investigate the response of MSCs to single sugar units. Hyalgan®/K-PA was used to compare effectiveness of our exclusive PA systems with a hybrid system that is formed by commercially available product and a peptide amphiphile. K-PA/E-PA nanofiber network was generated as non-sugar bearing scaffold, which is a negative control of PA network. Bare surface, which is tissue culture plate that does not contain any scaffolds, was included in the study as negative control to compare MSC response to any kind of PA scaffolds.

3.2.4 Characterizations of PA Nanofibers

Biophysical and morphological characterizations of PA molecule mixtures were performed with circular dichroism (CD), scanning electron microscopy (SEM) and transmission electron microscopy (TEM).

3.2.4.1 Secondary structure analysis

The secondary structure of single PA molecules and co-assembled PA molecule systems were characterized by CD spectroscopy (Figure 3.10-3.11). All combinations of PA molecules predominantly demonstrated β-sheet secondary structure as revealed with chiral absorbance minima around 220 nm and maxima around 200 nm.[99] Single PA molecules at neutral pH showed disordered conformation with a chiral absorbance except from GlcNAc-PA molecule. GlcNAc-PA molecule had CD peaks that demonstrate β-sheet structure, possibly due to the hydroxyl groups of the sugar which may create intermolecular hydrogen bonds.

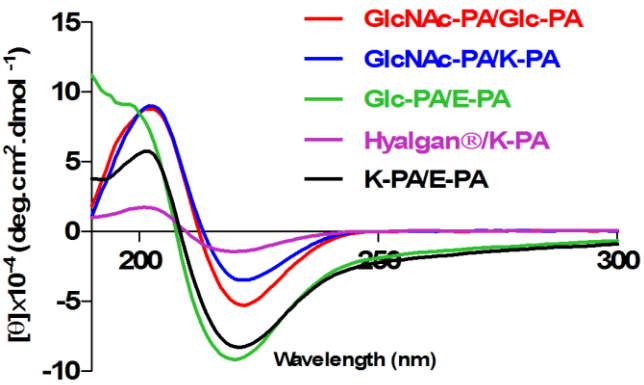

Figure 3.10 CD spectra of peptide amphiphile nanofibers at physiological pH. CD wavelengths revealed that obtained nanofibers have β-sheet secondary structure.

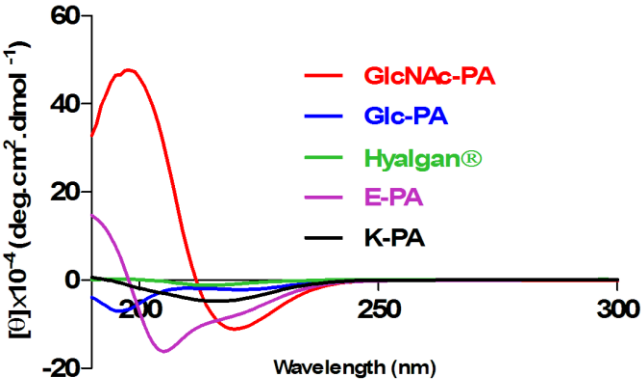

Figure 3.11 CD spectra of single peptide amphiphile solutions at physiological pH. CD wavelengths revealed the secondary structures of PA molecules.

3.2.4.2 Morphological Analyses of PA Nanofibers

The co-assembled PA nanostructures were visualized by SEM, TEM or scanning transmission electron microscopy (STEM). These images revealed the porous and nanoscale structure formed by counter-charged PA molecules that resemble the nanofibrous network of native extracellular matrix. In TEM images, fibers of PA molecules are shown in nanometer scale. Additionally, it is seen that nanofibers came together and seen as larger fibers in some parts of the images. In conclusion, while SEM images showed ECM-like porous network of co-assembled PA systems, TEM and STEM images revealed that porous network was formed by bundles of nanofibers (Figure 3.12 and 3.13).

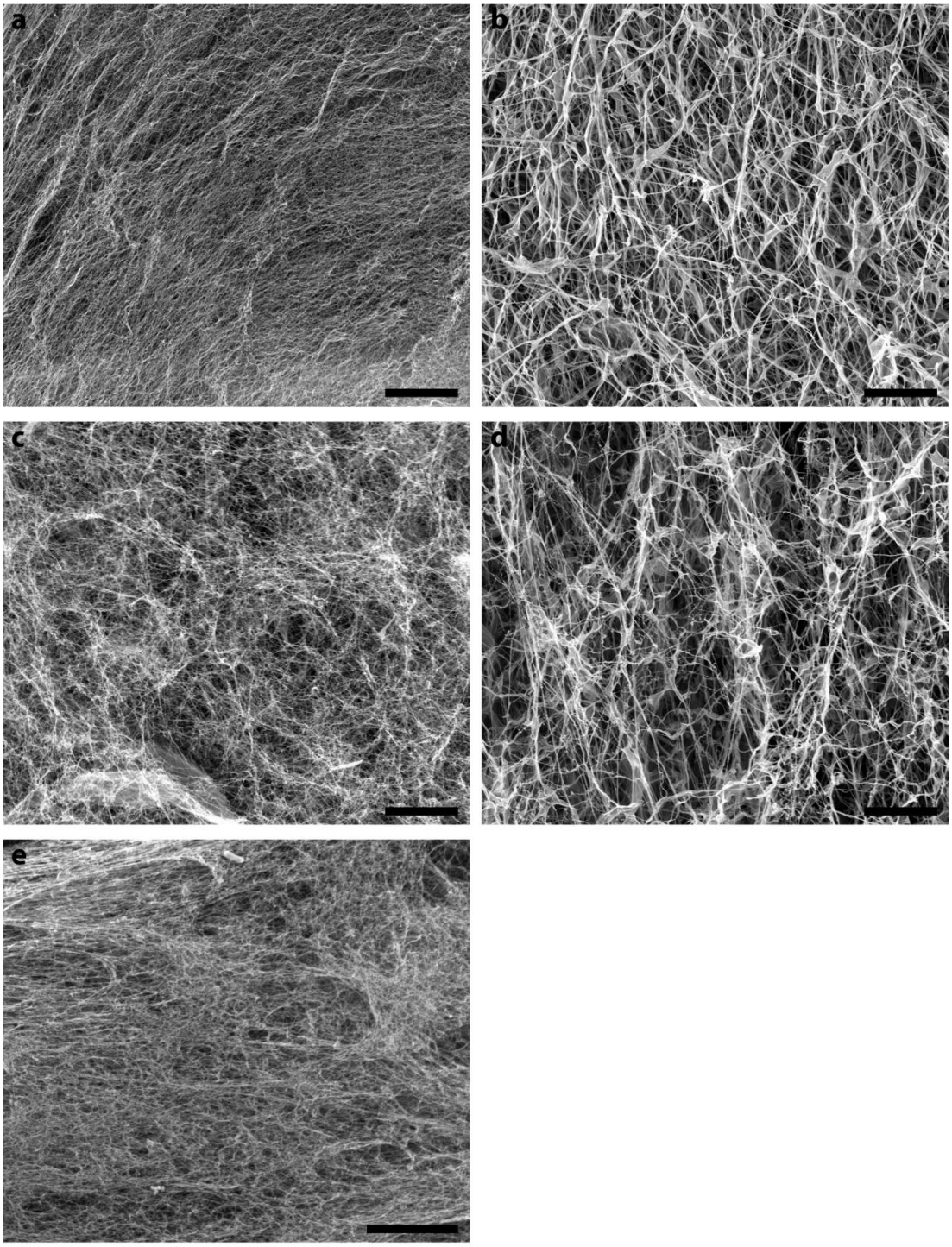

Figure 3.12 SEM micrographs of PA scaffolds. GlcNAc-PA/Glc-PA nanofibers (a), Glc-PA/E-PA (b), GlcNAc-PA/K-PA (c), K-PA/E-PA nanofibers (d), and Hyalgan®/K-PA (e). Scale bars = 10 μm.

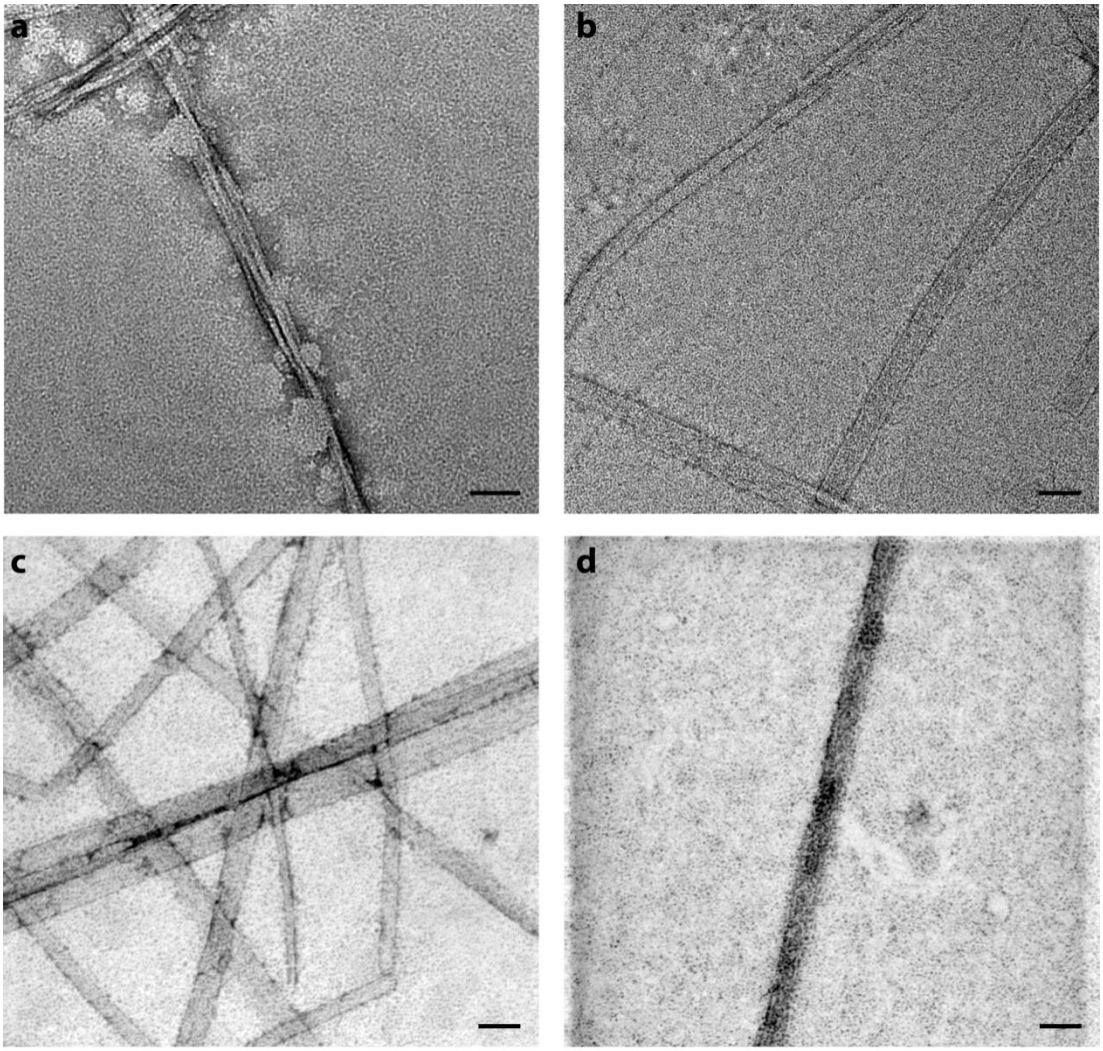

Figure 3.13 TEM (a,b) and STEM (c,d) micrographs of PA nanofibers. GlcNAc-PA/Glc-PA nanofibers (a), GlcNAc-PA/K-PA (b), Glc-PA/E-PA (c), and K-PA/E-PA nanofibers (d). Scale bar = 50 nm.

3.2.5 Biocompatibility of Peptide Amphiphile Nanofiber Networks

Cell viability on peptide amphiphile scaffolds is an important parameter for analyzing biocompatibility of PA nanofiber network with MSCs. Cellular viability was checked by using MTT assay after cells were incubated on the PA nanonetwork for 12 h (Figure 3.14). 12 h was settled as time point to check cell viability because

we want to eliminate interference of proliferation profile on viability results. MTT assay determines viability by measuring mitochondrial activity of viable cells.[100] For this reason, altered cell proliferation might interfere with viability results obtained by MTT assay. As cells might alter their proliferation profile when cultured on PA scaffolds, and interference of proliferation on viability results is not desired, we checked viability at a time point before natural proliferation cycle of MSCs. MTT assay OD values were transformed into relative viability data upon accepting OD values obtained from cells cultured on bare surface as 100% viability. Results indicate that there is a ~10% increase in relative viability in GlcNAc-PA/Glc-PA scaffold and a~14% increase in Glc-PA/E-PA scaffold compared to bare surface. K-PA/E-PA and bare surface were comparable in each other. Additionally, viability on GlcNAc-PA/K-PA and Hyalgan®/K-PA were more than 82% and 84% compared to bare surface, respectively.

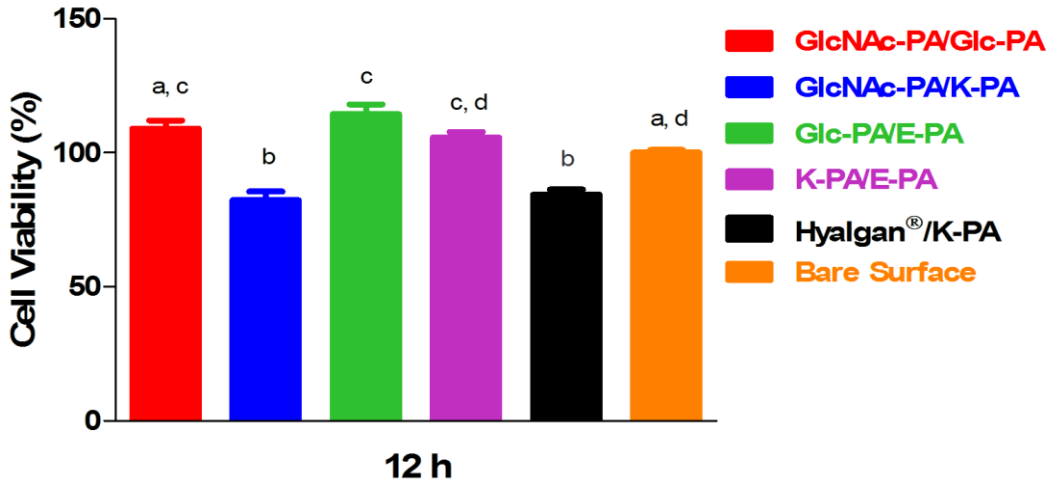

Figure 3.14 Relative cellular viability of rMSCs cultured on PA nanofiber networks and on bare surface after 12 h incubation. Different letters denote significance at $p<0.05$.

3.2.6 Proliferation Analyses of rMSCs on PA Nanofiber Network

MSCs can alter proliferation upon environmental signals.[101] For this reason it is important to investigate the proliferation rate of MSCs cultured on PA scaffold in order to characterize cellular response to our PA scaffold. Proliferation of rMSCs on GlcNAc-PA/Glc-PA was found to decrease by 60% compared to bare surface (Figure 3.15). Proliferation rates of GlcNAc-PA/K-PA, Glc-PA/E-PA and K-PA/E-PA did not give statistically significant difference although Glc-PA/E-PA showed 15% arrest in proliferation compared to bare surface. Cells cultured on Hyalgan®/K-PA decreased proliferation by 25% compared to bare surface but it was not as much drastic as GlcNAc-PA/Glc-PA. As rMSCs are heterogeneous, these results can also be interpreted that 40% and 75% of total cells proliferate after 48 h culture period on GlcNAc-PA/Glc-PA and Hyalgan®/K-PA, respectively.[102]

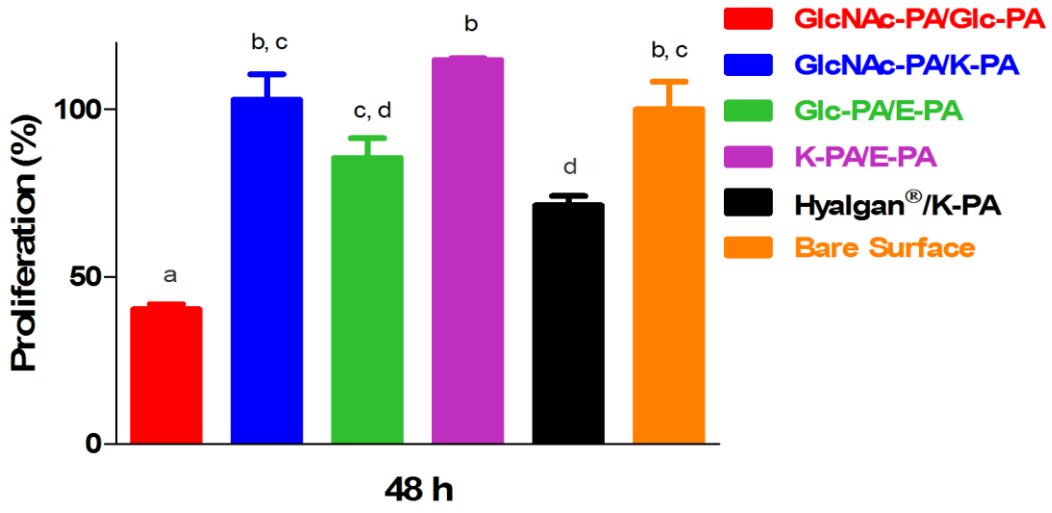

Figure 3.15 Relative proliferation of rMSCs cultured on PA nanofiber networks and on bare surface after 48 h incubation. Different letters denote significance at $p<0.05$.

3.2.7 Adhesion Analyses of rMSCs on PA Nanofiber Network

Adhesion is one of the early events of cellular response that is triggered by a material.[103] Relative adhesion data was obtained by normalization of total number of adhered cells on peptide nanofiber network to total number of cells on bare surface, which is tissue culture plate. Total number of cells on bare surface was accepted as 1 and cell numbers of other groups were normalized to cells on bare surface. Interference of any endogenous proteins to adhesive behavior of cells to PA scaffold was minimized by a protein synthesis inhibitor (cycloheximide, translational elongation inhibitor) treatment.[104] 5 h after cell seeding total number of cells were counted. Results indicate that adhesion of rMSCs on GlcNAc-PA/Glc-PA, Glc-PA/E-PA and Hyalgan®/K-PA were comparable with each other and were increased more than 4 fold compared to bare surface (Figure 3.16). Remaining two PA networks and bare surface groups were comparable in each other. Although statistically significant difference was not observed between GlcNAc-PA/K-PA, K-PA/E-PA and bare surface, GlcNAc-PA/K-PA and K-PA/E-PA showed 0.7 fold (approximately) increase in adhesion compared to bare surface.

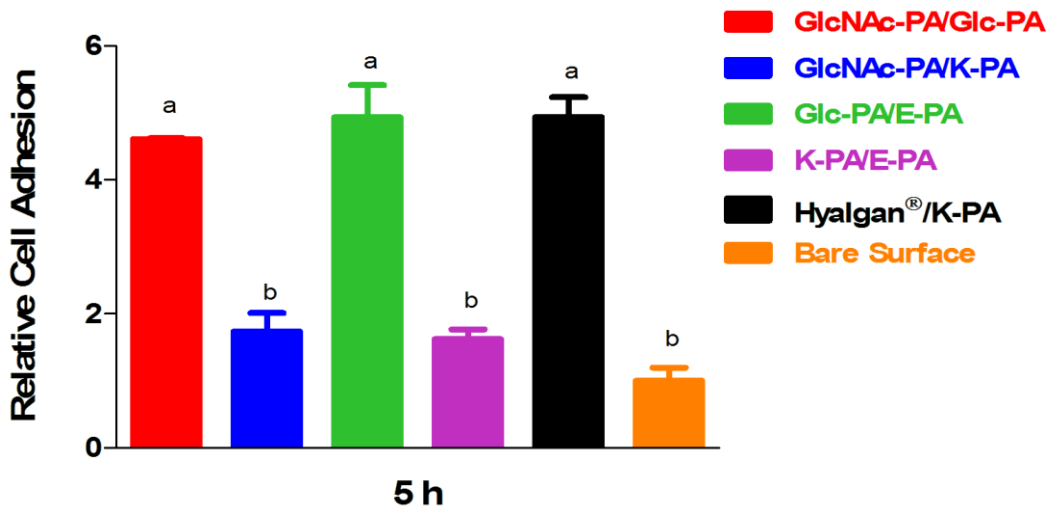

Figure 3.16 Relative adhesion of rMSCs cultured on PA nanofiber networks and on bare surface after 5 h incubation. Different letters denote significance at $P<0.05$.

3.2.8 sGAG Production Analyses

3.2.8.1 Safranin-O staining: Visualization of sGAGs

Chondrogenic differentiation of stem cells can be evidenced by elevated production of GAGs. Natural ECM of cartilage is composed of high amounts of GAGs as indicated in introduction. Stem cells that are induced to differentiate into chondrocytes increase their GAG production. In order to determine chondrogenic differentiation of rMSC cultured on PA networks and on bare surface, cells were stained with Safranin-O. Safranin-O is widely used for chondrogenic phenotype evaluation.[105–108] It is a cationic dye that specifically/stoichiometric binds to sulfated glycosaminoglycans.[95]

Images showed that Safranin-O distinctly stained cell aggregates formed on PA scaffolds with clear boundaries (Figure 3.17). Cells that conserve fibroblastic morphology were stained faintly compared to cell aggregates. Intensity of staining increased gradually with culturing period for all groups (Figure 3.18 and 3.19). However, this elevated staining intensity was more clearly observed in cell aggregates. GlcNAc-PA/Glc-PA combination stands out in terms of aggregate formation. It triggers aggregate formation at a very early culture period. When other groups showed any symptoms that they would form aggregates at day 3, cells had already formed distinct and uniformly distributed aggregates all over GlcNAc-PA/Glc-PA network. At day 7, cell aggregates on GlcNAc-PA/Glc-PA were enlarged and more intensely stained (Figure 3.18). Cells on GlcNAc-PA/K-PA formed reticulated structure with aggregated cells. These aggregates were not independent; rather they were linked to monolayer of cells. This might be a sign of initial aggregate formation. This hypothesis was proved with day 14 Safranin-O stained images (Figure 3.19). Independent cell aggregates having clear boundaries are shown on GlcNAc-PA/K-PA at day 14. Aggregate-like cell accumulations were also shown on Glc-PA/E-PA scaffold. However, although some independent aggregates formed, most of these cell aggregates are linked with monolayer of cells. At day 7, conglomeration of cells were observed in K-PA/E-PA group, but at day 14, cells twisted on top of each other due to confluency. For this reason the nodule-like structures on K-PA/E-PA were not considered as a sign of cartilage cell aggregations. No aggregation was observed on Hyalgan®/K-PA and bare surface.

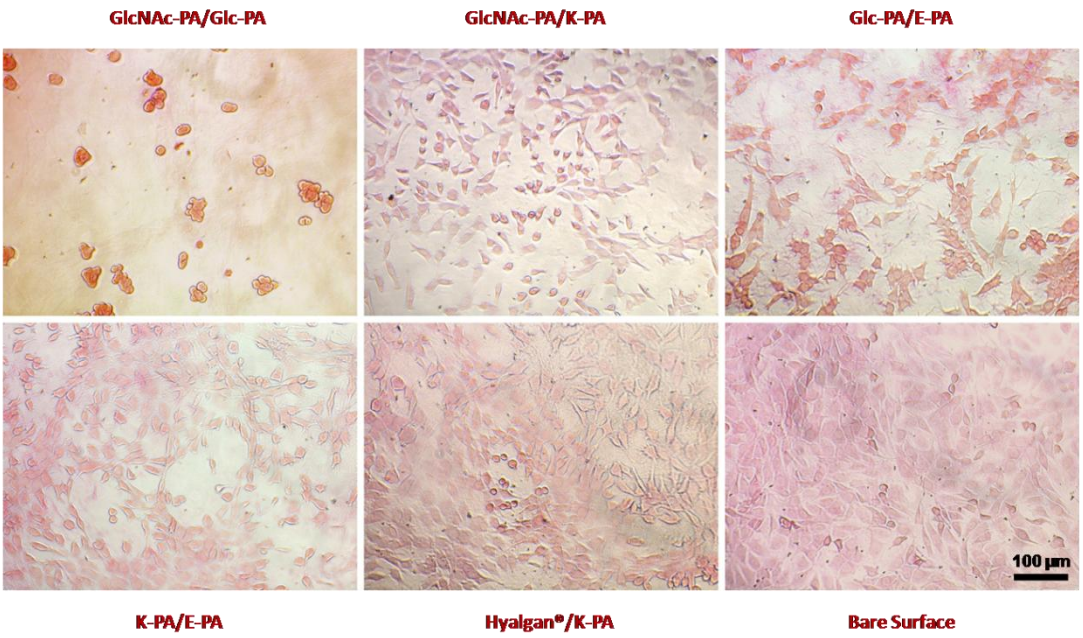

Figure 3.17 Safranin-O staining of rMSCs in growth medium at day 3, showing the extent of sulfated glycosaminoglycan incorporation. Scale bar is 100 µm and equal for all images.

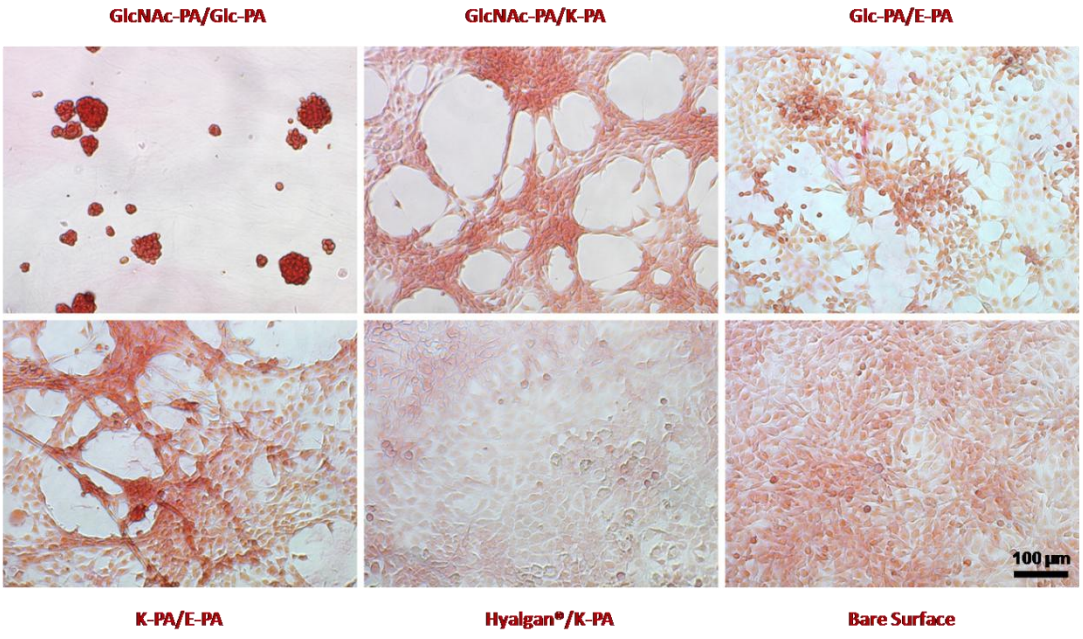

Figure 3.18 Safranin-O staining of rMSCs in growth medium at day 7, showing the extent of sulfated glycosaminoglycan incorporation. Scale bar is 100 µm and equal for all images.

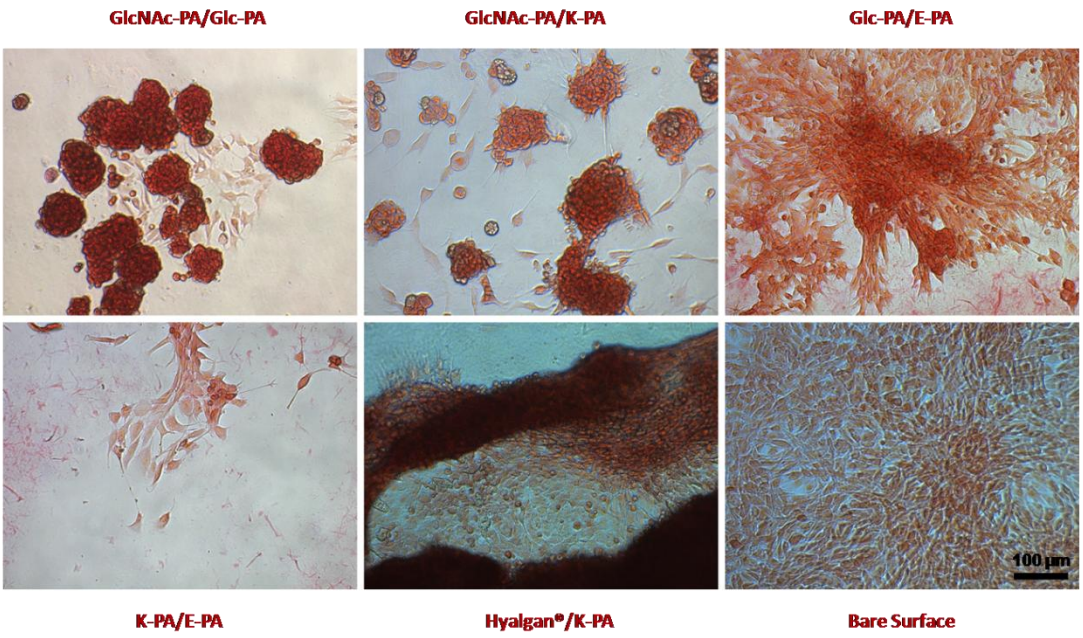

Figure 3.19 Safranin-O staining of rMSCs in growth medium at day 14, showing the extent of sulfated glycosaminoglycan incorporation. Scale bar is 100 µm and equal for all images.

3.2.8.2 DMMB Analysis: Spectroscopic Quantification of sGAGs

Safranin-O staining is a strong indicator of hyaline like cartilage matrix deposition. Visualization of cell aggregates stained with Safranin-O is a strong and undeniable evidence for GAG deposition, but Safranin-O staining is not a quantitative tool. Quantitative analysis of sGAG production of cells which is performed by DMMB assay is not in concert with Safranin-O images. Although discrete, independent and intensely stained cell aggregates are a strong indicator of chondrogenesis for cells of GlcNAc-PA/Glc-PA group, sGAG quantification indicates the highest amount of sGAG deposition at day 3 was formed on Glc-PA/E-PA (Figure 3.20). However,

significant increase in GAG deposition per DNA amount compared to K-PA/E-PA and bare surface was observed on GlcNAc-PA/Glc-PA network. Additionally, day 7 quantifications reflect the ability of GlcNAc-PA/Glc-PA and Glc-PA/E-PA scaffolds to trigger GAG deposition of rMSCs more than the other groups (Figure 3.21). At day 14, GAG deposition on bare surface was significantly decreased compared to PA coated surfaces, which furthermore indicates the positive contribution of PA scaffolds on GAG production for rMSCs (Figure 3.22).

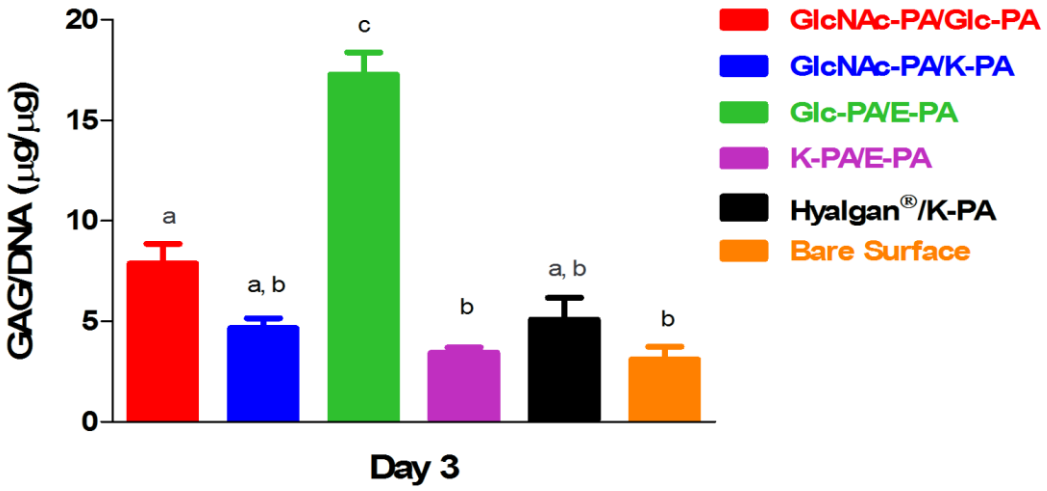

Figure 3.20 sGAG levels of rat mesenchymal stem cells at day 3, analyzed by DMMB assay. DMMB assay showing sGAG content of MSCs normalized to DNA content. Different letters denote significance at $P < 0.05$.

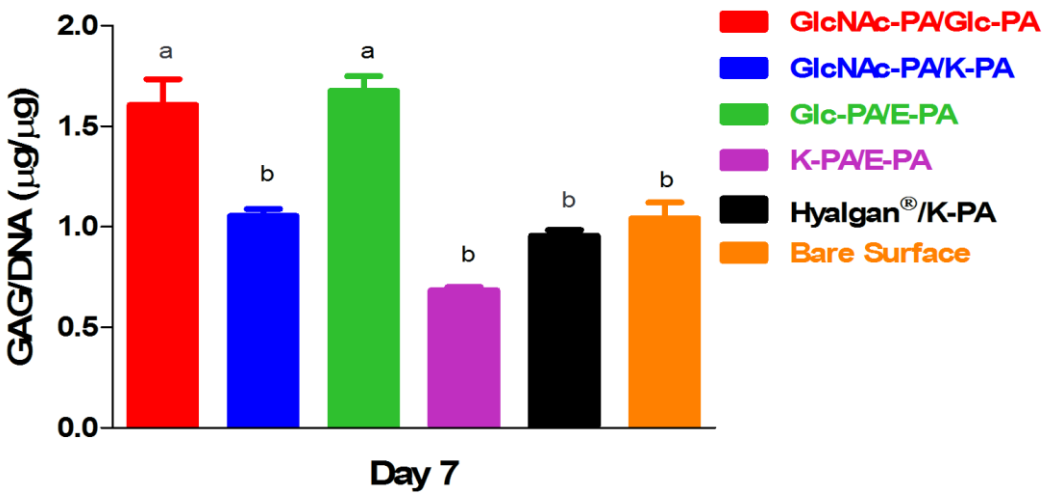

Figure 3.21 sGAG levels of rat mesenchymal stem cells at day 7, analyzed by DMMB assay. DMMB assay showing sGAG content of MSCs normalized to DNA content. Different letters denote significance at $P < 0.05$.

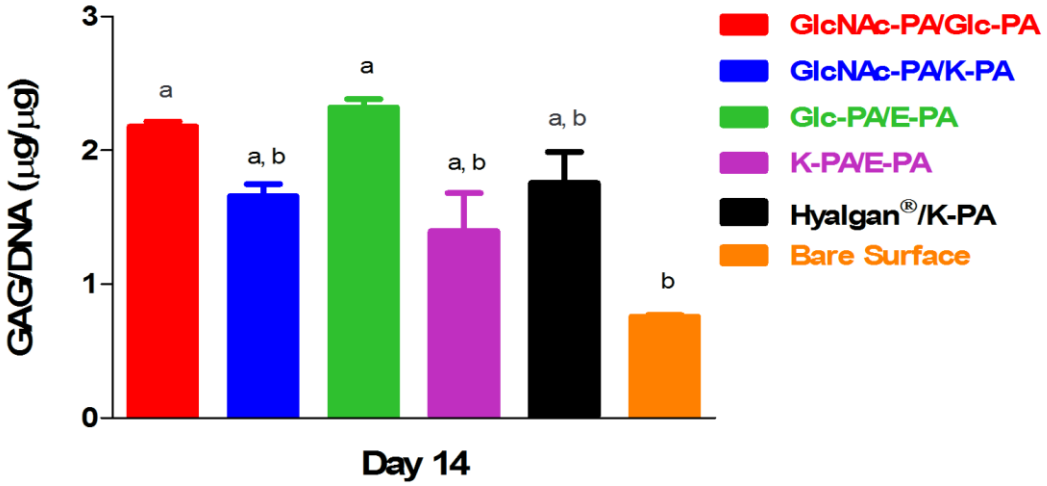

Figure 3.22 sGAG levels of rat mesenchymal stem cells at day 14, analyzed by DMMB assay. DMMB assay showing sGAG content of MSCs normalized to DNA content. Different letters denote significance at $P < 0.05$.

3.2.9 Gene Expression Analyses of Chondrogenic Differentiation Gene Markers

Stem cells alter expression of certain genes as they differentiate.[109] These genes change depending on the lineage that they are committed to differentiate. Since morphological observations indicated that MSCs differentiated through chondrogenesis on HA-mimetic PA systems, gene expression profiles of rMSCs were analyzed in order to investigate how signals supplied by the PA scaffolds alter the expression of certain chondrogenic marker genes. Expression levels of cartilage specific genes Sox9, aggrecan, Collagen II and hyaline cartilage dedifferentiation marker Collagen I were analyzed on day 3, day 7 and day 14.

Raw relative expression values, values that are not compared to any of the groups, were analyzed in order to track expression profiles of the gene of interests between the time points (Figure 3.23-3.24). It is revealed that only cells cultured on GlcNAc-PA/Glc-PA scaffold gradually increased Sox9 expression in concert with the extending culture period. In contrast, there was a gradual decrease in expression of Sox9 for cells cultured on Glc-PA/E-PA, GlcNAc-PA/K-PA, K-PA/E-PA and Hyalgan®/K-PA showed a decrease on day 7 compared to day 3 and increase on day 14 compared to day 7. Expression of Sox9 on bare surface decreased on day 7 and kept this expression value on day 14. Day 1 expression was also analyzed to determine very early differentiation in Sox9 expression. It was observed that expression of Sox9 on Glc-PA/E-PA, GlcNAc-Glc-PA, Hyalgan®/K-PA and bare surface showed similar levels. There was a decrease in K-PA/E-PA and a significant increase at day 1 was observed for GlcNAc-PA/K-PA group.

GlcNAc-PA/Glc-PA group showed the same pattern for aggrecan; its expression gradually increased from day 3 to day 14. In the same manner, pattern for aggrecan expressions were similar with Sox9 expression patterns of GlcNAc-PA/K-PA, K-PA/E-PA and Hyalgan®/K-PA groups. While aggrecan expression of Glc-PA/E-PA remained the same between day 3 and day 7, more than two fold increase was observed on day 14. Cells cultured on bare surface decreased aggrecan expression on day 7 and recovered it on day 14.

Expression levels of Col II, which is a late marker of chondrogenesis, progressively increased on GlcNAc-PA/K-PA and K-PA/E-PA groups.[110] Hyalgan®/K-PA and bare surface trigger higher expression of Col II on day 7 compared to day 3. Although the Col II expression values of day 14 were higher than that of day 3, Col II expression decreased on day 14 compared to day 7. Col II expression remained almost the same for all time points for Glc-PA/E-PA. Although the changes are moderate, there was a decrease on day 7 compared to day 3 and increase on day 14 compared to day 7 for cells on GlcNAc-PA/Glc-PA.

Col II/I ratio which is an important index for hyaline-type chondrogenesis, was found gradually increased on GlcNAc-PA/K-PA and K-PA/E-PA groups, as observed for Col II expressions.[111] However, increase in Col II/I ratio in K-PA/E-PA is less significant compared to GlcNAc-PA/K-PA although higher increases between time points were observed for Col II expression on the same group. With decrease on day 7 and increase on day 14, GlcNAc-PA/Glc-PA and Glc-PA/E-PA groups had similar pattern for Col II/I ratio. Col II/I ratio on day 14 decreased for cells on Hyalgan®/K-PA and bare surface following an increase on day 7.

When we analyzed the Col I gene expression values separately, we observed the arrest effect of PA scaffolds on increase in Col I expression. Its expression gradually increased for Hyalgan®/K-PA and K-PA/E-PA and highest value was found in bare surface cells. On the other hand, GlcNAc-PA/Glc-PA, GlcNAc-PA/K-PA and Glc-PA/E-PA, which are the groups having glycol units, either retained the same level of Col I expression, or increased slightly or even decreased over the culturing time period.

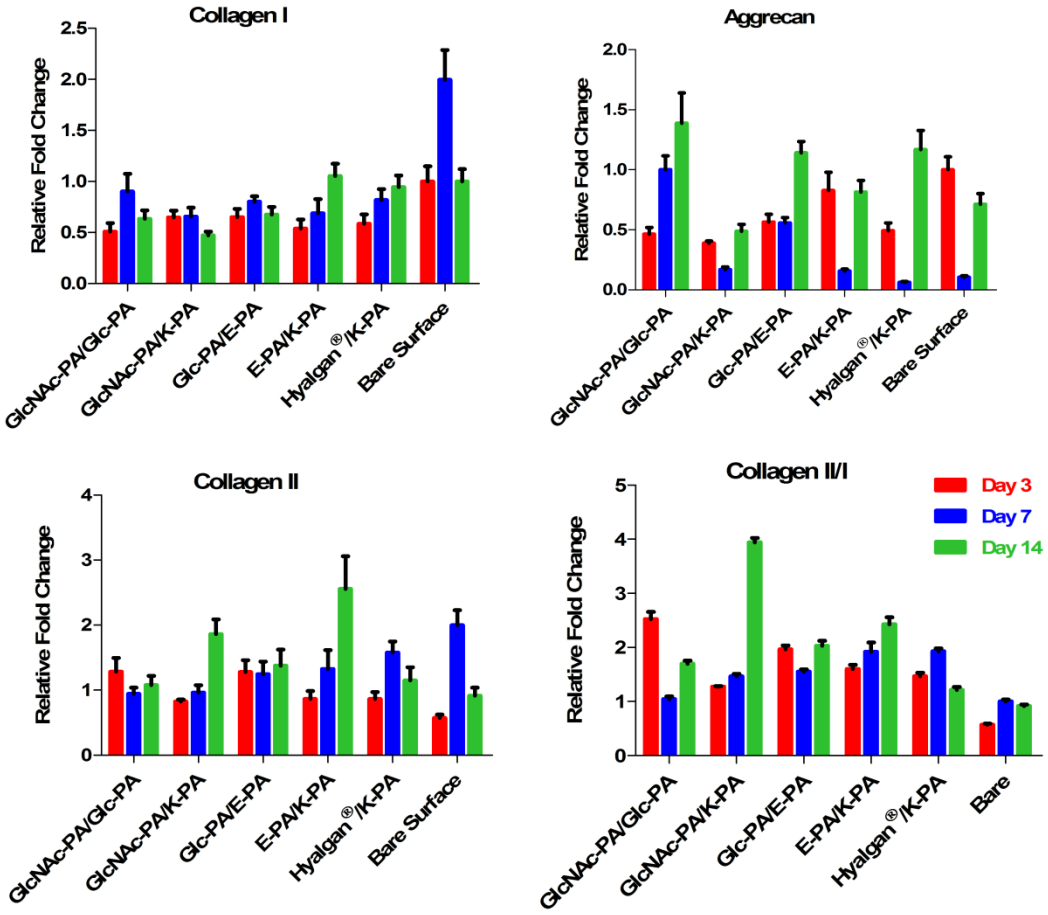

Figure 3.23 Gene expression analyses of rMSCs cultured with growth medium at different time points. The expression level of each gene was normalized against

GAPDH. The results that are normalized against bare surface indicate the changes in expression levels between different time points.

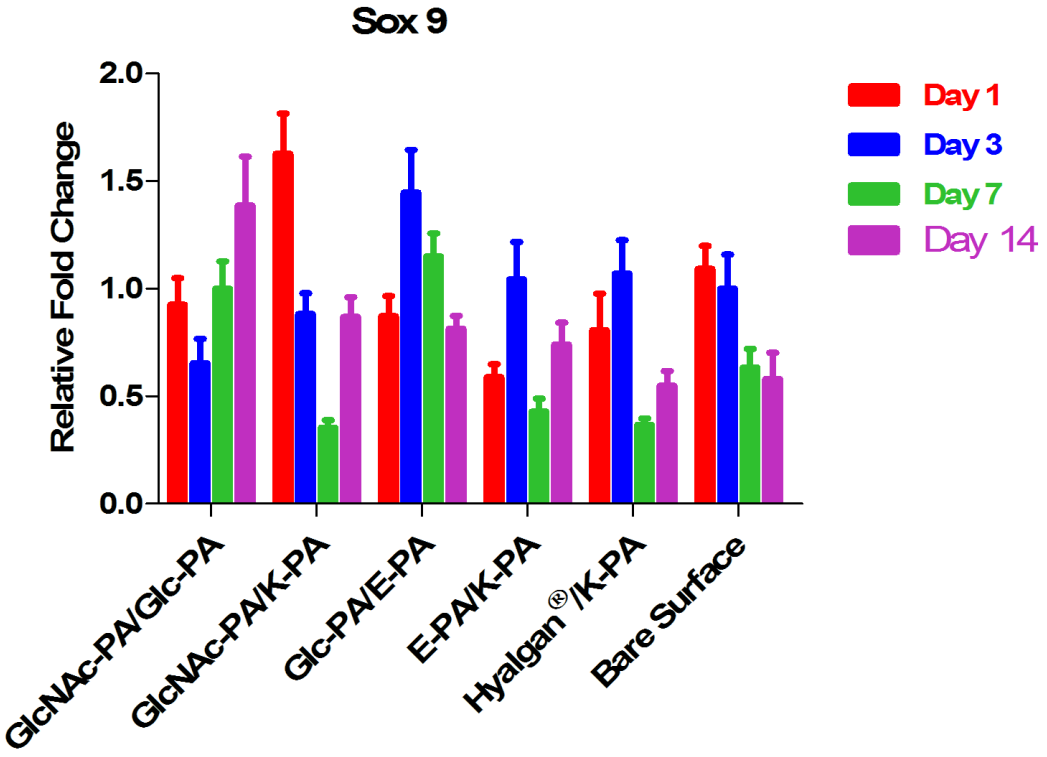

Figure 3.24 Sox9 gene expression analyses of rMSCs cultured with growth medium at different time points. The expression level of each gene was normalized against GAPDH. The results that are normalized against bare surface indicate the changes in expression levels between different time points.

In order to better visualize and analyze the changes between the groups on the same experimental day, bare surface group was chosen as control sample and relative normalized expression values were graphed accordingly (Figure 3.25-3.27). When we checked the fold increase in gene expression values compared to bare surface, it

was observed that while Sox9 expression is highest for Glc-PA/E-PA group on day 3, GlcNAc-PA/Glc-PA comes up to the level of Glc-PA/E-PA on day 7 and get ahead of Glc-PA/E-PA on day 14, so has the highest Sox9 expression value on day 14.

Aggrecan expressions were higher for K-PA/E-PA and bare surface groups compared to others on day 3. On day 7, almost 10 fold and more than 5 fold increase in aggrecan expression was observed for GlcNAc-PA/Glc-PA and Glc-PA/E-PA, respectively. There was a slight increase in expression (~0.5 fold) of Aggrecan for GlcNAc-PA/K-PA and K-PA/E-PA. Expression of Aggrecan for cells cultured on Hyalgan®/K-PA was 0.4 fold less than bare surface. On day 14, all PA coated groups except GlcNAc-PA/K-PA were close to GlcNAc-PA/Glc-PA group in terms of aggrecan expression, except GlcNAc-PA/K-PA group. When we combine raw expression value results with this data, it is seen that although GlcNAc-PA/K-PA significantly increased aggrecan expression on day 14 compared to day 7, GlcNAc-PA/K-PA has the least expression of aggrecan on day 14 since this increase was more significant for other groups.

Collagen II expression on day 3 was more than two fold elevated in GlcNAc-PA/Glc-PA and Glc-PA/E-PA relative to bare surface. GlcNAc-PA/K-PA, K-PA/E-PA and Hyalgan®/K-PA increased Col II expression in a similar manner, slightly but not significantly (~0.5 fold). Pattern observed on day 3 drastically changed on day 7. Bare surface held the highest Col II expression value. This value is two folds of GlcNAc-PA/Glc-PA and GlcNAc-PA/K-PA and this is statistically significant difference. There was no statistically significant difference between any other groups. On day 14, GlcNAc-PA/Glc-PA, Hyalgan®/K-PA and bare surface were

comparable to each other for Col II expression. Col II expression of GlcNAc-PA/K-PA and Glc-PA/E-PA were 1.5 and 2 folds of bare surface's expression. Highest Col II expression value was observed on K-PA/E-PA with 2.7 fold increase on day 14.

Col II/I ratio is an index that can be accepted as hyaline cartilage/fibrocartilage ratio or hyaline cartilage/osteogenesis. Col II/I ratios were significantly increased on all coated surfaces compared to uncoated surface. GlcNAc-PA/Gluco-PA showed the highest expression with 4.42 fold increase. Glc-PA/E-PA, K-PA/E-PA, Hyalgan®/K-PA and GlcNAc-PA/K-PA followed it with decreasing expression values. On day 7, fold increase in Col II/I ratios of K-PA/E-PA and Hyalgan®/K-PA were same with 1.92 folds. Similarly, GlcNAc-PA/Glc-PA did not show any alteration in terms of expression compared to bare surface. GlcNAc-PA/K-PA and Glc-PA/E-PA had the similar values for Col II/I expression on day 7. All PA coated surfaces had higher Col II/I expression ratio on day 14, at least with two-fold increase. Differently, GlcNAc-PA/K-PA had the highest Col II/I ratio (4.315 folds) on day 14 in contrast to day 3.

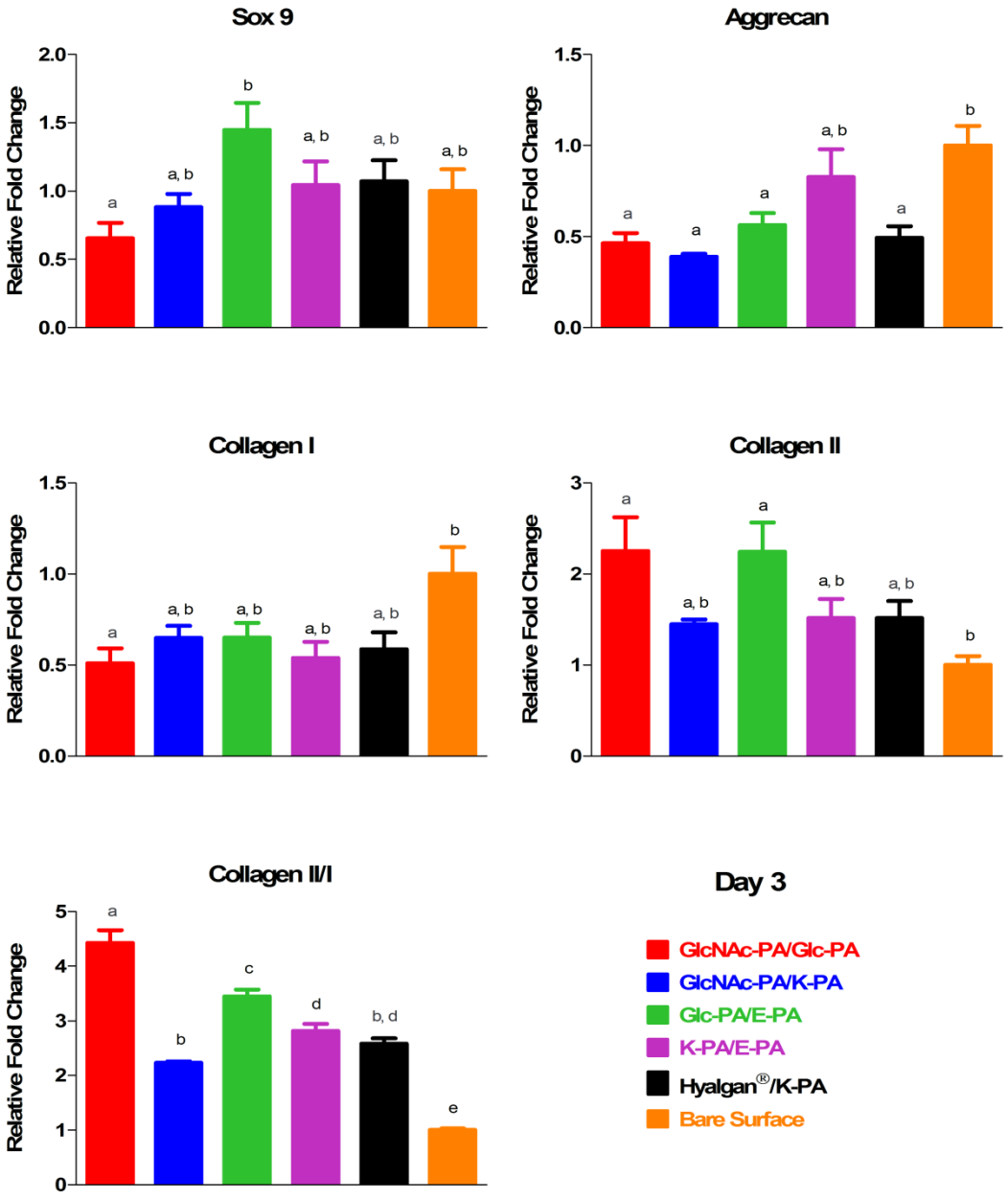

Figure 3.25 Gene expression analyses of rMSCs cultured with growth medium at day 3. The expression level of each gene was normalized against GAPDH and bare surface. Different letters denote significance at $p < 0.05$.

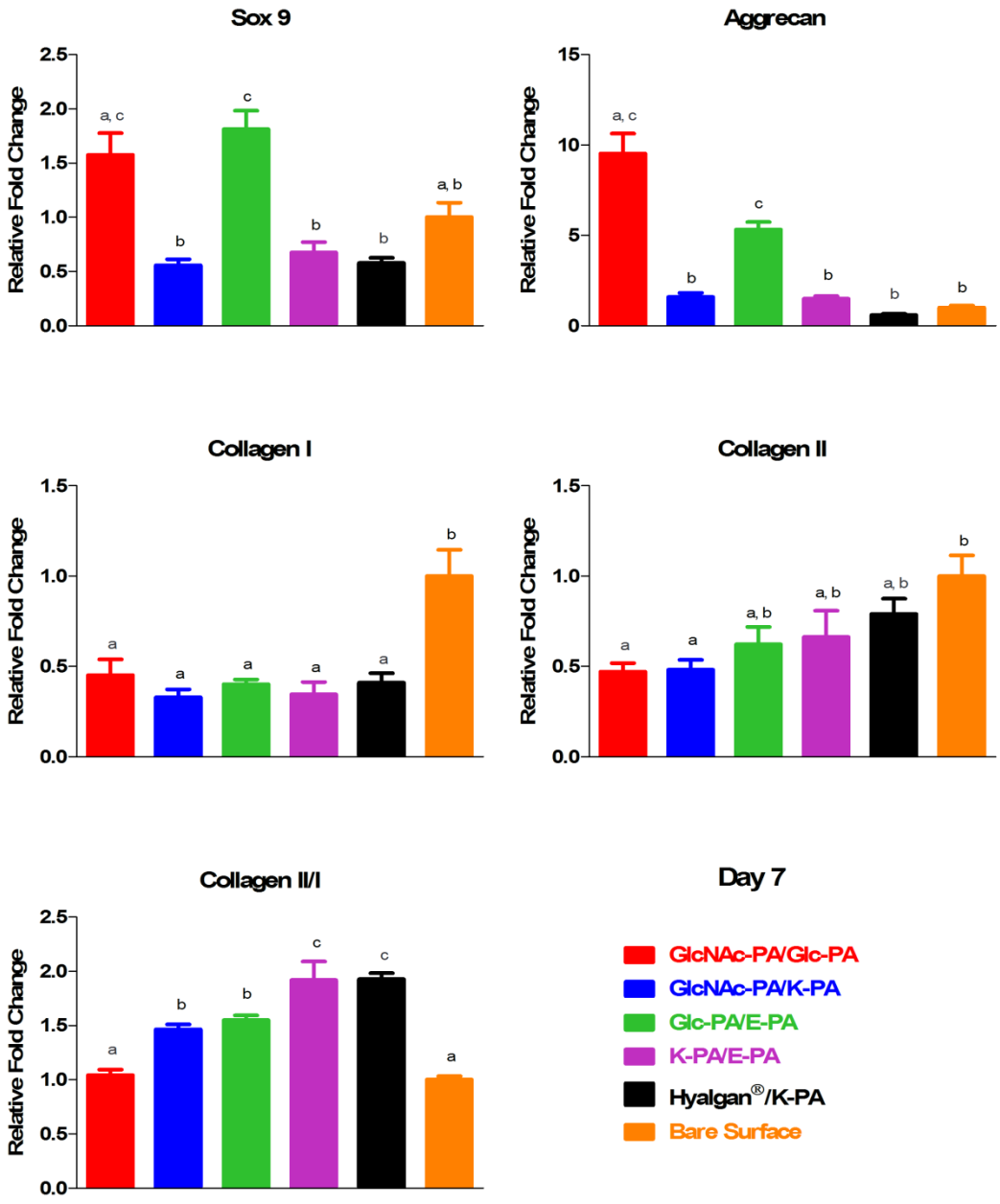

Figure 3.26 Gene expression analyses of rMSCs cultured with growth medium at day 7. The expression level of each gene was normalized against GAPDH and bare surface. Different letters denote significance at $p < 0.05$.

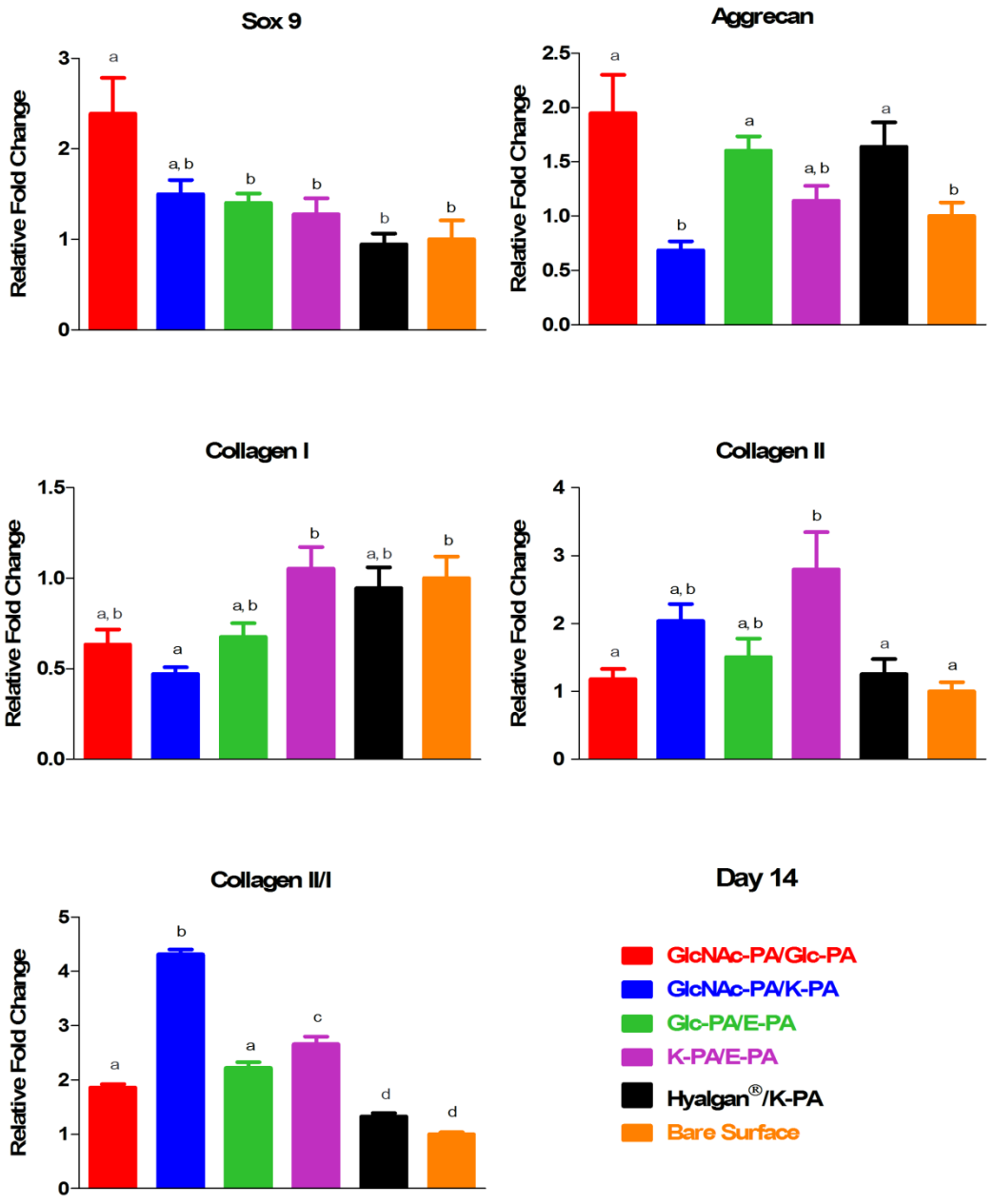

Figure 3.27 Gene expression analyses of rMSCs cultured with growth medium at day 14. The expression level of each gene was normalized against GAPDH and bare surface. Different letters denote significance at $p < 0.05$.

3.3 DISCUSSION

Peptide amphiphiles with opposite charges self-assemble and form nanofiber network when they mixed with each other. Hydrophobic collapse, electrostatic interactions and β-sheet formation drive self-assembly, and van der Waals, hydrophobic forces, and hydrogen bonding stabilize obtained nanofibers.[112] SEM and TEM imaging showed that PA molecules formed highly porous networks that are composed of nanofibers. CD spectroscopy revealed that co-assembled peptide amphiphiles have β-sheet secondary structure. It means that incorporation of β-sheet driving amino acids into the peptide amphiphile backbone forms the desired structure.

It is proven that PA scaffolds do not induce specific toxicity with at most ± 20% deviation of viability relative to bare surface. Increase in viability of cells cultured on GlcNAc-PA/Glc-PA and Glc-PA/E-PA indicates that they create a more suitable environment for rMSCs than bare tissue culture plate surface. Another conclusion that can be obtained by this result is that cells cultured on these networks increase their mitochondrial activity. For GlcNAc-PA/Glc-PA, this increase in mitochondrial activity can be required to perform the initial and drastic morphology changes as observed on Safranin-O staining images.[113] Viability observed on Hyalgan®/K-PA was high enough to conclude that scaffold is compatible with rMSCs. The variation of viability compared to bare surface might stem from adaptation of rMSCs to the environment. Similar to increase on GlcNAc-PA/Glc-PA surface, cells on Hyalgan®/K-PA might have decreased mitochondrial activities due to signals coming from scaffold environment. Another reason of this slight difference might be the

heterogeneity of the MSC population.[114] 20% of total cells may adapt scaffold later than the rest of the cells.

It is obvious that PA niche promotes adhesion of cells more than uncoated surface. On the other hand, there were significant differences between some PA coated surfaces. PA scaffolds that contain bioactive epitopes on positively charged backbone and polymer of Hyalgan® trigger adhesion of two fold higher numbers of cells compared to GlcNAc-PA/K-PA and K-PA/E-PA. Less number of adhered cells on K-PA/E-PA probably results from absence of glyco unit. Glyco-bearing PAs with negatively charged backbone do not trigger adhesion as much as positively charged ones. This fact is further supported by data obtained for adipogenesis study of rMSCs. E-Glc-PA which is a negatively charged PA that contains glucose had the similar adhesion value for rMSCs.

Although PA molecules were mixed with counter charged ones, and overall charge set to zero theoretically, it might not be the case. Glyco-PAs with negative backbone (GlcNAc-PA and E-Glc-PA) might introduce more negative charge even after mixing with K-PA, which is positively charged. Cells having negatively charged membrane probably did not adapt on this overall negativity.[115] Similarly, scaffolds with positively charged glyco-PAs hold more cells due to charge interaction. Another reason might stem from lysine effect. Poly-lysine coatings are extensively used for cells that are not able to adhere to bare tissue culture plate surfaces to facilitate attachment.[116] Mechanism of action of lysine coatings are again based on electrostatic interactions. For K-PA/E-PA group, on the other hand, that cannot be observed as much as glyco-bearing groups.

Cell proliferation was arrested more in scaffolds where cell adhesion was higher. Stem cells lose their proliferative potential during the terminal differentiation.[117,118] It can be concluded that cells receive more differentiation signals when there are higher number of epitopes that cells adhere on. In accordance with epitope density hypothesis, most drastic alteration in proliferation was observed on GlcNAc-PA/Glc-PA. This result is in accordance with the drastic morphology change of rMSCs on the same scaffold. Morphology change of cells on GlcNAc-PA/Glc-PA group is not only formation of nodule-like cell clusters; but single cells on this scaffold also lost their fibroblastic morphology and became rounded even as early as 12 h (observed during the viability test). Fibroblastic shape is the basal morphology of undifferentiated MSCs.[119] They change fibroblastic morphology as they differentiate. So, probably, the drastic increase in cell proliferation is linked to early terminal differentiation of MSCs on GlcNAc-PA/Glc-PA scaffold.

Safranin-O staining of cells does not only show the sulfated GAGs, but also clearly indicates the morphology changes of cells. GAG deposition and morphology change, which is similar to aggregate formation, are considered to be evidence of chondrogenic differentiation. When these properties and healthy culturing period are considered, glyco-bearing PA scaffolds emerges as appropriate scaffolds to induce MSC differentiation into chondrogenesis. When loss of fibroblastic morphology at single cell level, high number of independent cell aggregates and early occurrence of these alterations are taken into consideration, GlcNAc-PA/Glc-PA is the most prominent combination for differentiation of rMSCs into chondrocytes. On the other hand, quantification of sulfated GAGs (DMMB assay) did not exclusively indicate GlcNAc-PA/Glc-PA as the most prominent scaffold for rMSC culturing to induce

chondrogenic differentiation in terms of quantified sulfated GAGs. DMMB assay do not quantify hyaluronic acid as it is not sulfated. Therefore, it is not sensitive to GAG composition of hyaline-cartilage which is the cartilage type that we differentiate rMSCs into. For this reason, morphological observations seem more reliable to assess cellular behavior and differentiation of rMSCs into chondrocytes, especially into hyaline type ones. A persisting trend for expressions patterns of all gene markers was not obtained. On the other hand, day 3 expression levels of Col II, Col I and Col II/I ratio reveal the contributions of glyco PA network on chondrogenesis. Highest elevation in fold change of Col II in GlcNAc-PA/Glc-PA and Glc-PA/E-PA groups indicate that they are optimal surfaces for hyaline like chondrogenesis. Col I expression levels showed that networks, especially GlcNAc-PA/Glc-PA group suppress bone like or fibrocartilage like differentiation of rMSCs compared to bare surface with statistical significance. Additionally, highest fold change in Col II/I ratio on GlcNAc-PA/Glc-PA, which is the hyaluronic acid mimetic group, indicates its eligibility as an early inducer of hyaline chondrogenesis for MSCs. Prominent role of hyaluronic acid mimetic PA group in early chondrogenesis is underlined by the 10 fold increase in aggrecan expression at day 7.

3.4 CONCLUSION

Articular hyaline cartilage regeneration has an exclusive importance as it is a tissue which lacks regeneration capacity, and degeneration of articular cartilage impairs the daily life of many humans. Mesenchymal stem cell therapy is a promising option and controlling their differentiation is crucial for regeneration purposes. Herein, we presented a bioactive peptide amphiphile nanofiber scaffold system for early induction of mesenchymal stem cell differentiation into hyaline cartilage chondrocyte phenotypes. Chemical, spectroscopic, and physical characterization of PA nanofiber scaffolds proved that they are eligible as ECM mimicking environment. Studies that were performed with rMSCs demonstrated that PA scaffolds create a friendly environment for cells to live and adhere, and to proliferate. Although there are some contradictions between different differentiation experiments, our hyaluronic acid mimicking PA system, which is GlcNAc-PA/Glc-PA combination, emerges as a very successful scaffold to induce early differentiation of chondrogenesis into hyaline type. It is also demonstrated that HA mimicking scaffold is more prominent than our positive control system Hyalgan®/K-PA group. Hyaluronic acid mimicking PA system creates an environment for rMSCs to adhere more, provides signals to induce early and drastic chondrocyte-like morphology change and increases expression of late gene markers of chondrogenesis (aggrecan and Col II) at early time points (day 3 and day 7). Overall, *in vitro* studies showed that hyaluronic acid mimicking environment is a promising biomaterial for *in vivo* regeneration studies.

CHAPTER 4

MONITORING EFFECTS OF SINGLE AMINO ACID CHANGE ON DIFFERENTIATION FATE OF rMSCs

4.1 INTRODUCTION

Self-assembled peptide amphiphile (PA) nanofibers are powerful and exclusive tools for fabrication of nanometers and micrometers scale materials.[120] PAs can be designed for different tasks, as they can show bioactivity depending on the purpose. Understanding the factors affecting bioactivity and self-assembly mechanism of PAs has a lot of importance for the successful engineering of supramolecular architectures with predictable properties, functions, and for better understanding the biological processes. One of the features that affects bioactivity, and self-assembly, is amino acids that are flanking the bioactive sequences.[121–123] In the literature, there are various examples indicating the importance of flanking amino acid sequences. They can be determinative for activity and specificity of the bioactive amino acid sequences. Makagiansar *et al.* showed that residues flanking the HAV sequence are important in the binding selectivity of HAV peptides to E-cadherin. A study by Bertram *et al.* indicates that adding flanking amino acids to the RGD motif, found within many adhesion proteins,[124] produces a more active binding conformation.[123] Naturally occurring flanking amino acids also alter the activity of the bioactive amino acid sequence, and not only the type but also the number of flanking amino acids affects the process. It is reported that number of amino acids flanking the RGD sequence varies in different types of adenoviruses and their affinity to binding with integrins differ from each other.[122] With the light of these studies, in order to understand the effect of flanking amino acids in our PA systems, we designed two different gluco-bearing PAs with a single amino acid change in the location flanking the gluco-conjugated amino acid. K-Glc-PA was previously reported as a chondrogenesis inducer and an effective material for cartilage regeneration in our

group.[10] For this study, we replaced the lysine amino acid in the K-Glc-PA with glutamic acid and designed E-Glc-PA. We tested the effects of the amino acid change of gluco-bearing PAs on cellular response of rat mesenchymal stem cells by creating peptide amphiphile scaffolds. We observed a striking difference between the cell behaviors on E-Glc-PA/K-PA and K-Glc-PA/E-PA scaffolds. Our results demonstrate that E-Glc-PA/K-PA scaffold induced adipogenesis, specifically the brown fat differentiation of MSCs significantly higher than the K-Glc-PA/E-PA and other surfaces. This result reports that single amino acid change in our self-assembled system results in a significant difference on cell behavior of mesenchymal stem cells.

4.2 RESULTS

4.2.1 Synthesis and Characterization of Peptide Amphiphile Molecules

K-Glc-PA and E-Glc-PA molecules were designed for studying the effect of single amino acid change on the PA backbone of a sugar bearing PA molecule on MSC differentiation (Figure 3.1 i and ii). K-Glc-PA (Lauryl-VVAGKS(β-*D*-Glc)-Am) was previously designed and synthesized by our group. It was demonstrated that nanofibers formed with K-Glc-PA induce early commitment of rMSCs to the chondrogenic lineage and their capacity on *in vivo* cartilage regeneration was demonstrated in microfracture treated osteochondral defect healing.[10] E-Glc-PA (Lauryl-VVAGES(β-*D*-Glc)-Am) was designed to study the effects of backbone amino acids on bioactivity of the PA molecules. E-PA (Lauryl-VVAGE) and K-PA (Lauryl-VVAGK-Am) were designed as control PAs, to study the amino acid changes in the non-sugar bearing PA backbone (Figure 3.1 iii and iv).

PA molecules are composed of hydrophobic alkyl tail (lauryl moiety), β-sheet forming amino acid sequence (-VVAG-) and charged amino acid for solubility and charge control.[125] Glucose bearing PA molecules (K-Glc-PA and E-Glc-PA) have additional Ser-linked acetyl-protected β-D-glucose glyco-amino acid as bioactive unit (Figure 4.1). Nanofiber scaffolds were generated through self-assembly that is triggered by mixing counter-charged PA molecules.

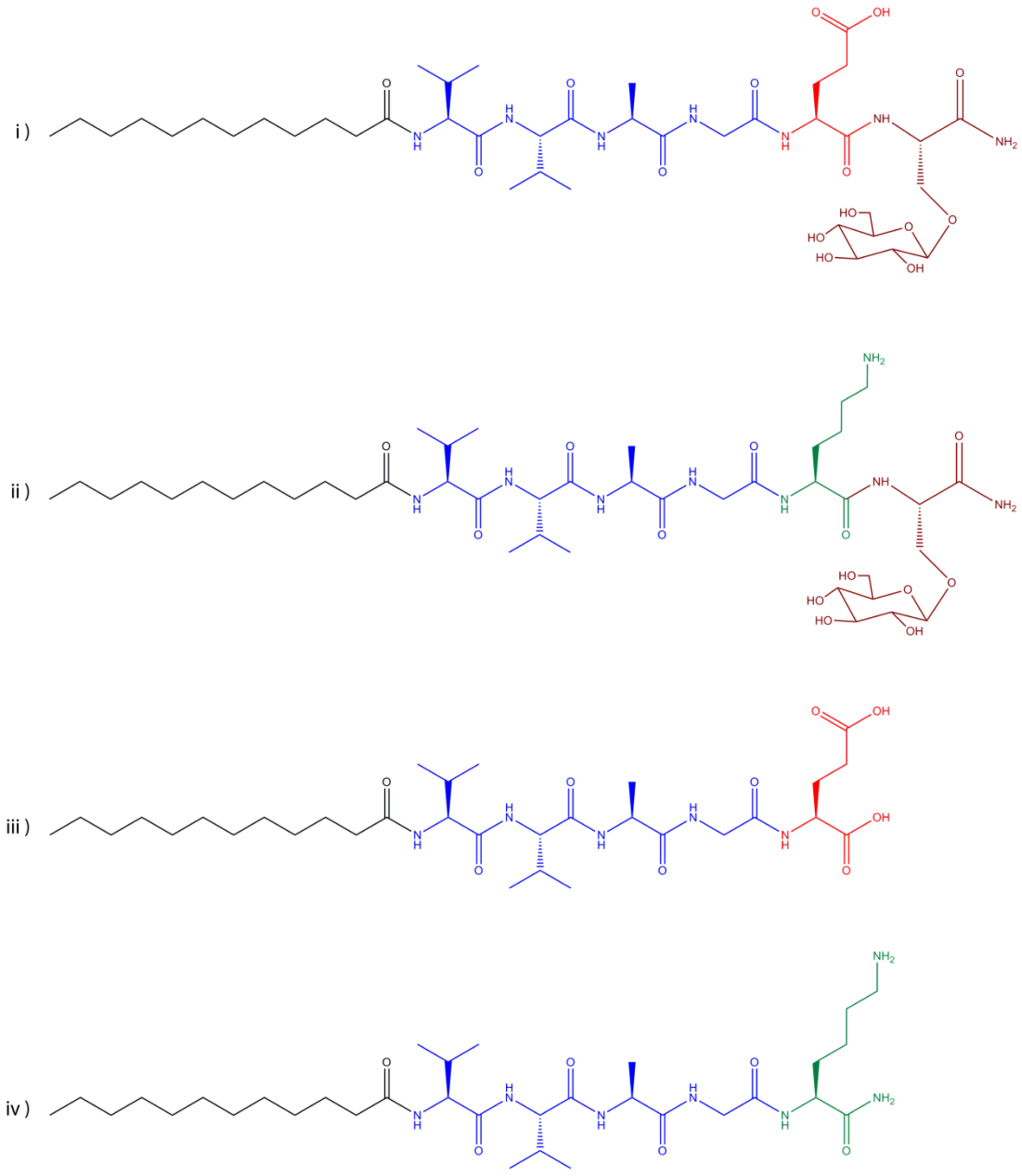

Figure 4.1 Chemical structures of the peptide amphiphiles. E-Glc-PA (i), K-Glc-PA (ii), E-PA (iii), and K-PA (iv). Color codes of the structures indicate alkyl tail (black), beta sheet forming units (blue), positively charged amino acids (green), and negatively charged amino acids (red).

All PA molecules were synthesized by solid phase peptide synthesis method, characterized by LC-MS and purified by preparative HPLC. LC-MS spectroscopy showed the purity of the PA molecules. Experimental molecular masses of the PA molecules were shown as 654.4975 for K-PA ($[M+H]^+$), 903.5758 for K-Glc-PA ($[M+H]^+$), 902.4545 for E-Glc-PA ($[M-H]^-$), and 654.2844 for E-PA ($[M-H]^-$). These results matched with the theoretical masses of the designed PA molecules (Table 4.1), and this proved the success of the synthesis. Regardless of the purity of PA molecules, prep-HPLC purification was performed for all PA molecules before they are used in cell culture studies. A second round of LC-MS was performed after prep-HPLC purification of the PAs to check the final purity of PA molecules (Figure 4.2-4.5).

Table 4.1 Sequences, molecular weights and theoretical overall charges of the peptide amphiphiles at neutral pH.

Peptide Amphiphile	Sequence	Molecular Weight	Net Charge
E-Glc-PA	Lauryl-VVAG**E**S(β-*D*-Glc)-Am	903.52	-1
K-Glc-PA	Lauryl-VVAG**K**S(β-*D*-Glc)-Am	902.57	+1
E-PA	Lauryl-VVAG**E**	655.42	-2
K-PA	Lauryl-VVAG**K**-Am	653.48	+1

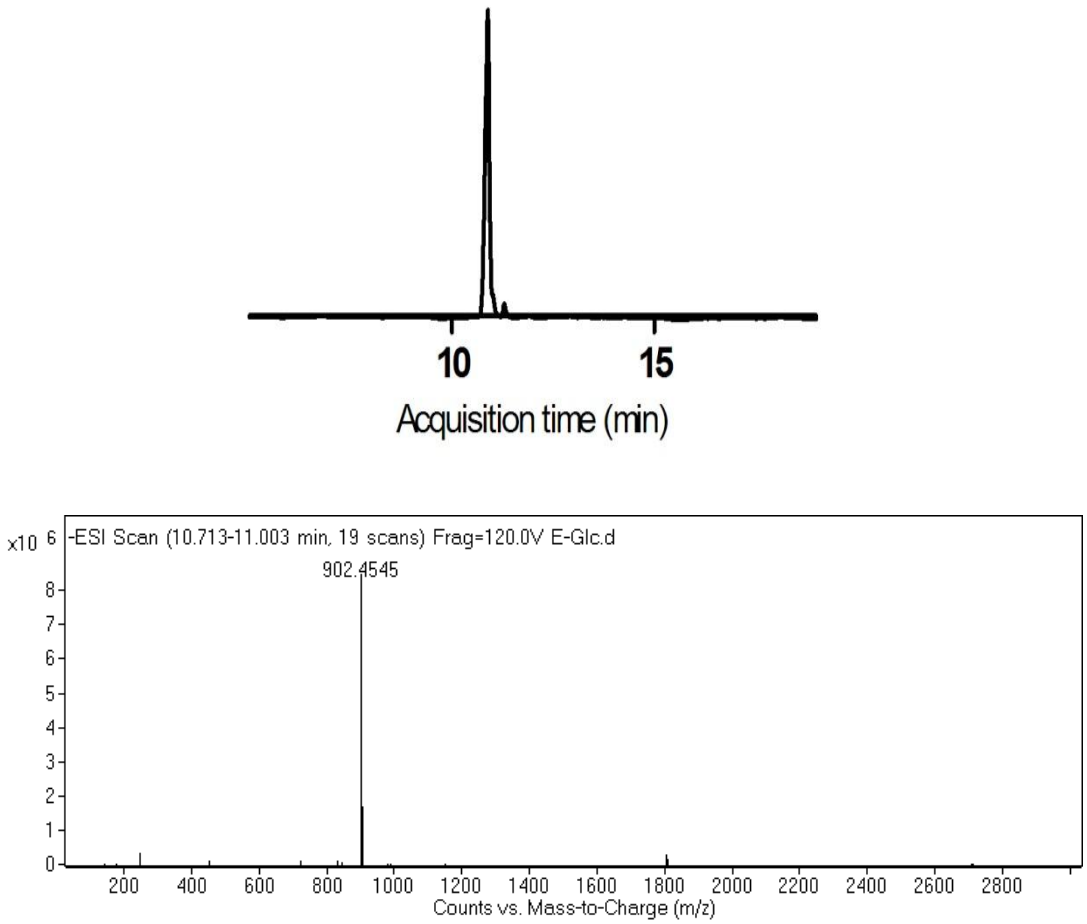

Figure 4.2 Liquid chromatography-mass spectrometry (LC-MS) analysis of E-Glc-PA. The purity of the crude product was analyzed according to the optical density at 220 nm. Experimental m/z $[M-H]^-$ = 902.4545, calculated m/z $[M-H]^-$ = 902.52.

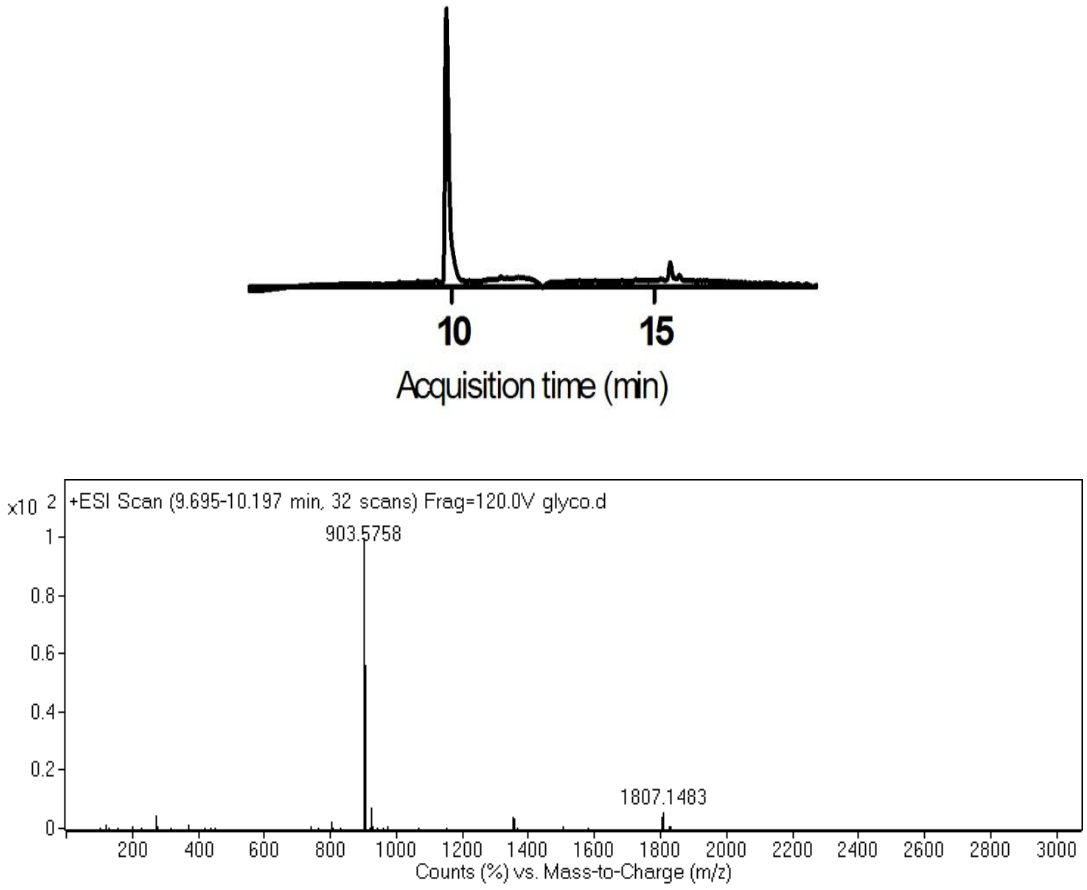

Figure 4.3 Liquid chromatography-mass spectrometry (LC-MS) analysis of K-Glc-PA. The purity of the crude product was analyzed according to the optical density at 220 nm. Experimental m/z $[M+H]^+$ = 903.5758, $[(M+H)*2]^+$ = 1807.1483, calculated m/z $[M+H]^+$ = 903.57.

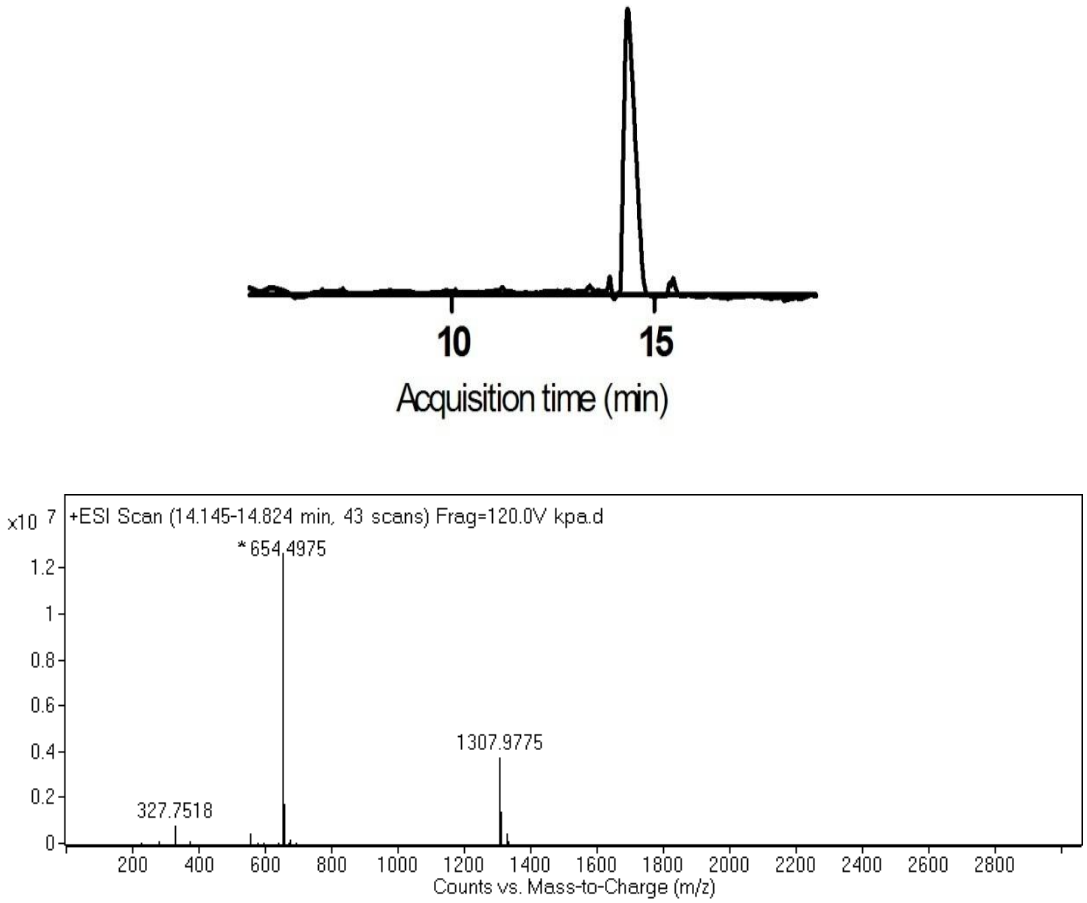

Figure 4.4 Liquid chromatography-mass spectrometry (LC-MS) analysis of K-PA. The purity of the crude product was analyzed according to the optical density at 220 nm. Experimental m/z $[M+H]^+$ = 654.4975, $[(M+H)*2]^+$ = 1307.9775, $[(M+H)/2]2^+$ = 327.7518, calculated m/z $[M+H]^+$ =654.48.

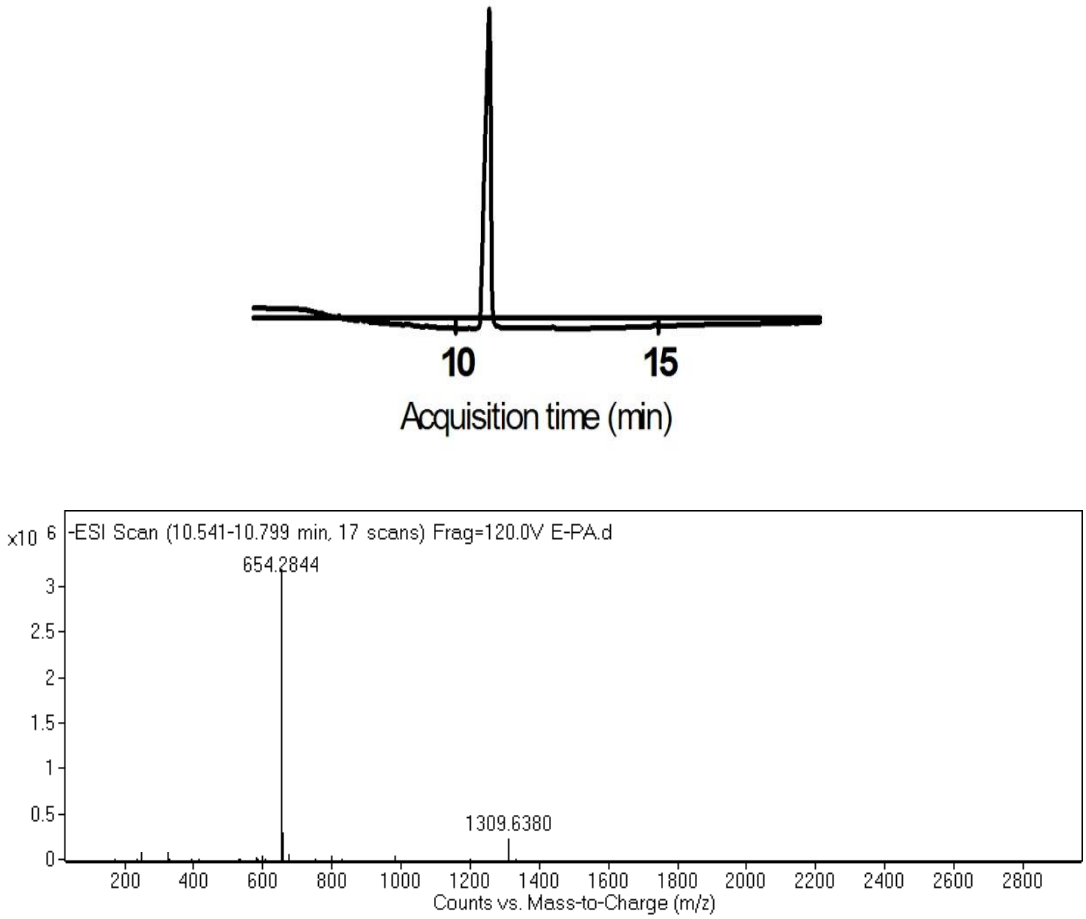

Figure 4.5 Liquid chromatography-mass spectrometry (LC-MS) analysis of E-PA. The purity of the crude product was analyzed according to the optical density at 220 nm. Experimental m/z $[M-H]^-$ = 654.2844, $[(M-H)*2]^-$ = 1309.6380, calculated m/z $[M-H]^-$ = 654.42.

4.2.2 PA Nanofiber Formation

In this study, four different combinations of peptide amphiphile nanofiber scaffolds which are E-Glc-PA/K-Glc-PA, E-Glc-PA/K-PA, K-Glc-PA/E-PA and K-PA/E-PA scaffolds were prepared. E-Glc-PA/K-PA and K-Glc-PA/E-PA nanofiber networks were constructed to study the effects of flanking amino acid differences around

glyco-conjugated amino acid in a counter-charged PA mixed system on cellular behavior. E-Glc-PA/K-Glc-PA was added to observe the combinatorial effects of two glucose units. As a negative PA scaffold control, K-PA/E-PA combination was used. This scaffold does not bear glyco group but has the remaining PA backbone with the same amino acid sequences of glyco-bearing PAs. Bare tissue culture plate surface is an essential negative control for our cell culture systems and was used to compare effects of PA scaffolds on cellular behavior.

4.2.3 PA Nanofiber Characterizations

Biophysical and morphological characterizations of single PA molecules and PAs mixtures were performed with circular dichroism (CD), scanning electron microscopy (SEM) and transmission electron microscopy (TEM).

4.2.3.1 Secondary structure analysis

CD analyses were performed to understand the secondary structure of pure PA molecules and mixed PA molecule systems. CD determines the unequal absorbance of left-handed and right-handed circularly polarized light which is exhibited by optically active chiral molecules and this value is used to evaluate the secondary structures of proteins and peptides.[99] As different molecular secondary structures result in different polarization, CD spectrometry is widely used to determine the secondary structure.[126] The CD spectra results revealed that mixed PA molecule systems show β-sheet structure, displaying a minimum around 220 nm and a maximum around 204 nm (Figure 4.6). Single PA molecules at neutral pH showed disordered conformation (Figure 4.7). E-Glc-PA molecule was the exception with its

β-sheet indicating CD peaks. This result indicates that how single amino acid change might change the structural shape.

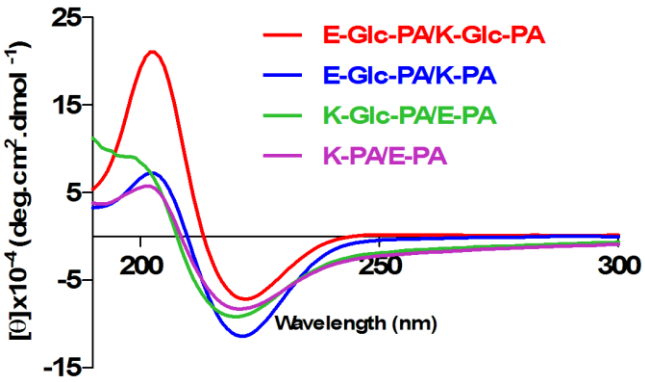

Figure 4.6 CD spectra of peptide amphiphile nanofibers at physiological pH. CD wavelengths revealed that obtained nanofibers have β-sheet secondary structure.

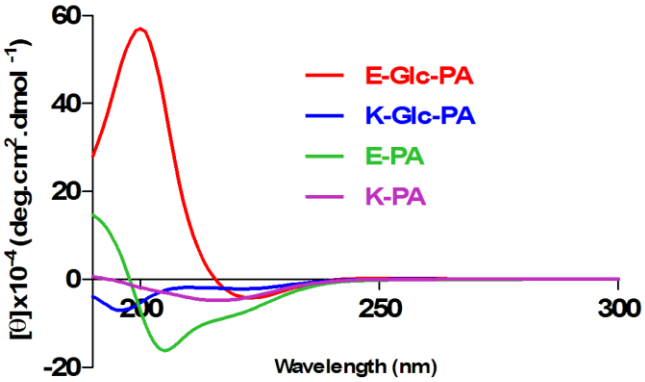

Figure 4.7 CD spectra of single peptide amphiphile solutions at physiological pH. CD wavelengths revealed the secondary structures of PA molecules.

4.2.3.2 Morphological Analyses of PA Nanofibers

The co-assembled PA nanostructures were visualized by SEM. Results showed that oppositely charged PA molecules formed nanofiber network upon mixing. These networks are porous and composed of nanofibers. In that sense, obtained PA

networks highly resemble the native extracellular matrix found around the cells. This resemblance makes PA nanofibers a suitable microenvironment for the cells to attach, live and proliferate. The closer visualization of PA nanofibers was performed by TEM or STEM. TEM and STEM images revealed that ECM-like structure was formed by high-aspect-ratio nanofibers with diameters in the order of 8-10 nm and lengths reaching several micrometers.

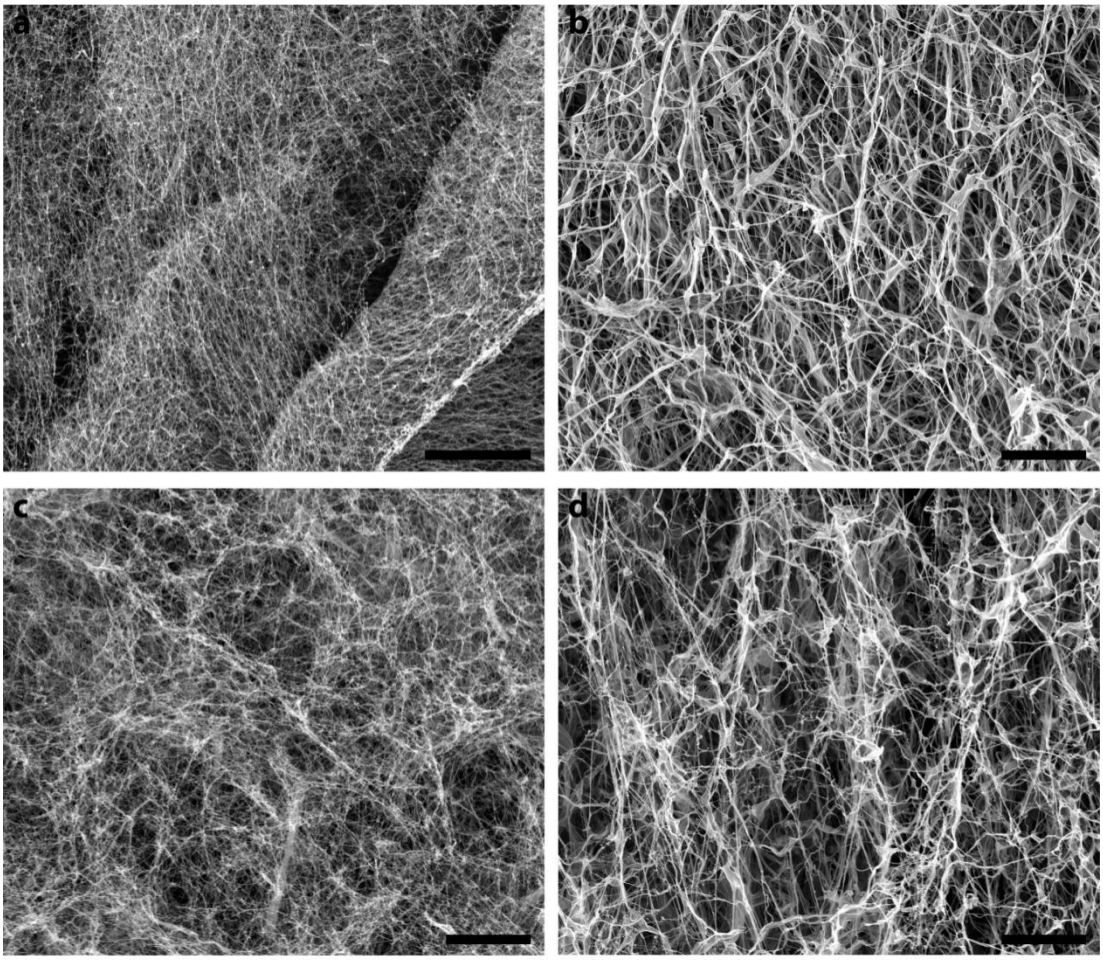

Figure 4.8 SEM micrographs of PA scaffolds. E-Glc-PA/K-PA nanofibers (a), K-Glc-PA/E-PA (b), E-Glc-PA/K-Glc-PA (c), and K-PA/E-PA nanofibers (d). Scale bars = 10 μm.

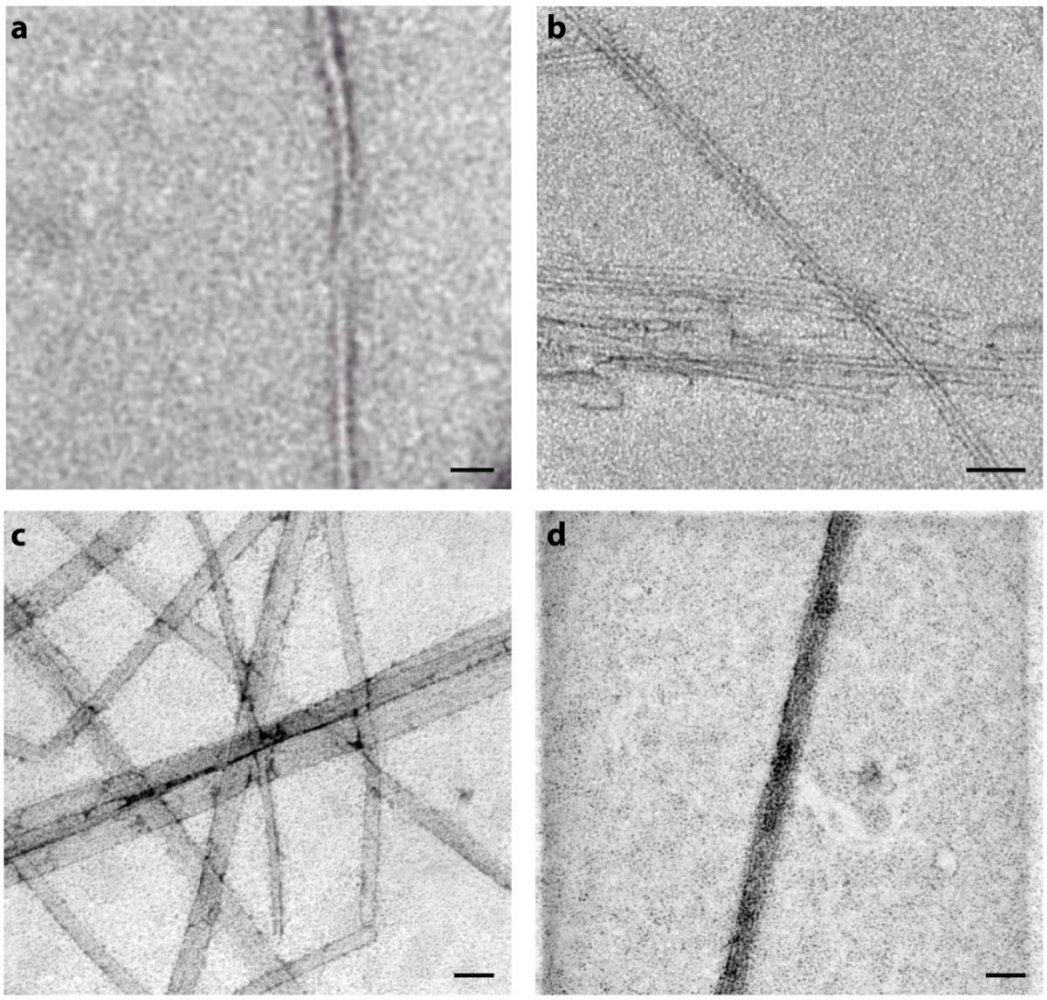

Figure 4.9 TEM (a,b) and STEM (c,d) micrographs of PA nanofibers. E-Glc-PA/K-PA (a), E-Glc-PA/K-Glc-PA (b), K-Glc-PA/E-PA (c), and K-PA/E-PA nanofibers (d). Scale bars = 50 nm.

4.2.4 Cell Viability on Peptide Amphiphile Nanofiber Networks

Biocompatibility of peptide amphiphile nanofibers was assessed by monitoring viability of cells that are cultured on PA nanofiber network. Cellular viability was checked after 12 h incubation on the PA nanonetwork, in order to discriminate interference of proliferation that can be altered by PA nanofibers, on viability results.

The cellular viability of the cells cultured on PA nanonetwork and on tissue culture plate was at comparable levels. 12 h viability results showed that PA nanofibers did not have intrinsic toxicity to rMSCs (Figure 4.10). This result also means that flanking amino acid change in a self-assembled system did not interfere with the cellular viability for rMSCs.

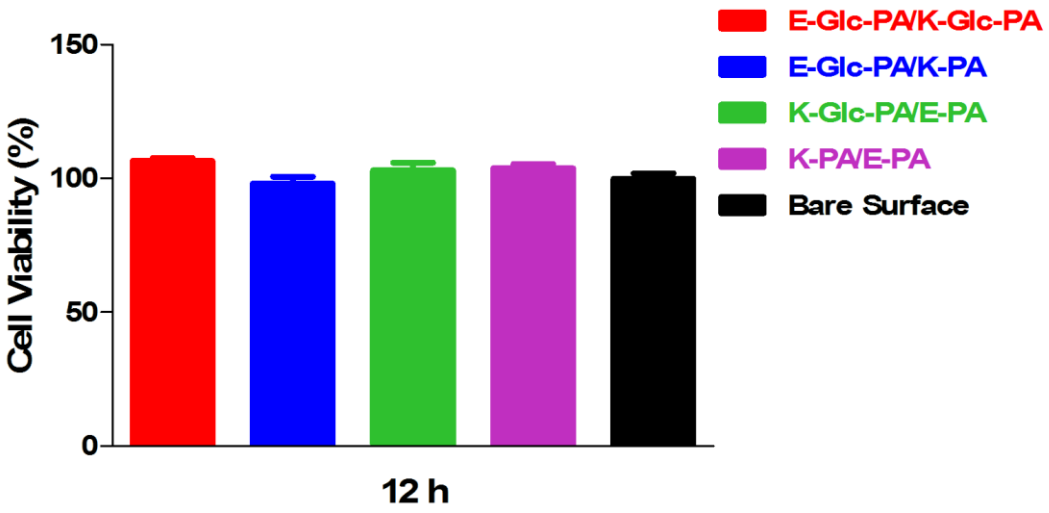

Figure 4.10 Relative cellular viability of rMSCs cultured on PA nanofiber networks and on bare surface after 12 h incubation. No significant difference (One-way ANOVA, Bonferroni post test) was found between the groups.

4.2.5 Adhesion Profile of rMSCs on PA Nanofibers

Adhesion of cells on peptide nanofiber network system is another sign to check the compatibility of our system for rMSC culturing. For this reason, adhesion of cells on peptide nanofiber network was studied. Relative adhesion data was obtained by normalization of total number of adhered cells on peptide nanofiber network to total number of cells on bare surface which is tissue culture plate. Total number of cells on bare surface was accepted as 1 and cell numbers of other groups were normalized

to cells on bare surface. Results showed that 5 h after cell seeding cells adhered more on peptide nanofiber networks compared to bare surface. It indicates that PA nanofiber network present epitopes for cells to adhere. Another result obtained from this data is the difference between adhesive properties of glucose-bearing PA scaffolds. In terms of adhesion, there is significant difference between K-Glc-PA/E-PA and E-Glc-PA/K-PA groups. This result underlines the difference of our system based on cellular behavior. Actually, the number of adhered cells on K-Glc-PA/E-PA group is significantly higher than all other groups, including E-Glc-PA/K-Glc-PA. This demonstrates that E-Glc-PA has a suppressive effect on adhesion in two-sugar bearing scaffold system.

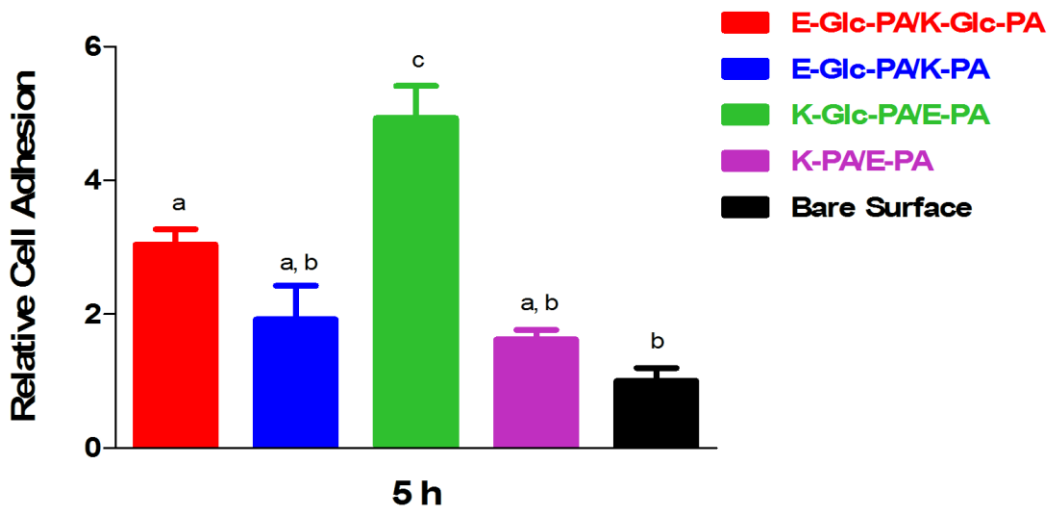

Figure 4.11 Relative adhesion of rMSCs cultured on PA nanofiber networks and on bare surface after 5 h incubation. Different letters denote significance at $p<0.05$.

4.2.6 Effects of PA Nanofiber Network on Cell Proliferation

Effect of culturing rMSCs on PA nanofibers on proliferation profile was studied by BrdU incorporation assay. Proliferation rates of cells cultured on PA nanofibers were compared to that of cells cultured on tissue culture plate. After 48 h of incubation, results indicated that 25% of total cell population, compared to cells cultured on tissue culture plate, completed proliferation when cultured on E-Glc-PA/K-Glc-PA. Proliferation percentages of rMSCs were found to be 62% for E-Glc-PA/K-PA, 85.54% for K-Glc-PA/E-PA, and 114.8% for K-PA/E-PA group. Obtained data showed that two glyco groups had a combinatorial effect on proliferation. Proliferation on E-Glc-PA/K-Glc-PA was significantly less than either E-Glc-PA/K-PA or K-Glc-PA/E-PA groups. When the data was compared with bare surface, we saw that K-Glc-PA/E-PA and K-PA/E-PA groups did not significantly alter the proliferation compared to bare surface. It was also observed that E-Glc-PA/K-PA and K-Glc-PA/E-PA scaffolds affect the proliferation at different levels. Although not statistically significant, there was 23% difference between the groups in terms of proliferation.

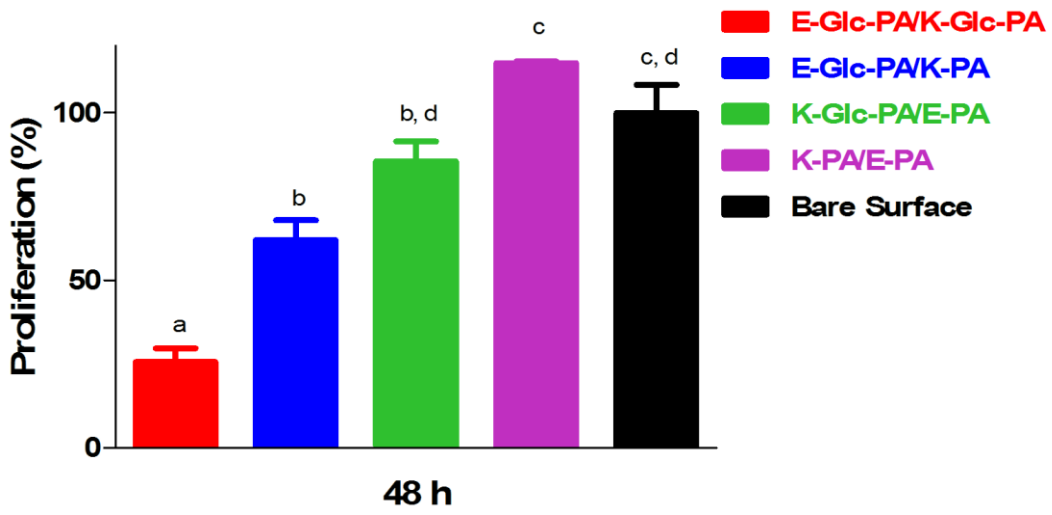

Figure 4.12 Relative proliferation of rMSCs cultured on PA nanofiber networks and on bare surface after 48 h incubation. Different letters denote significance at $p<0.05$.

4.2.7 Investigation the Differentiation Response of rMSCs to Different Glucose Bearing Nanofiber Scaffolds

Cells were seeded on PA nanofiber network groups and morphological changes were tracked, in order to observe any changes triggered by different PA networks. During initial observations, lipid-droplet-like accumulations were repeatedly observed in E-Glc-PA/K-PA group (Figure 4.13) whereas they were barely observed in other groups. For this reason, investigation on the effect of single amino acid change in PA molecules on rMSC differentiation fate was specifically focused on the adiopogenesis profile. Investigation of rMSC differentiation into adipogenic lineage was analyzed by Oil Red-O for investigating deposition of lipid droplets and by mRNA expression analyses of adipogenic marker genes adiponectin, FABP4 and UCP1.

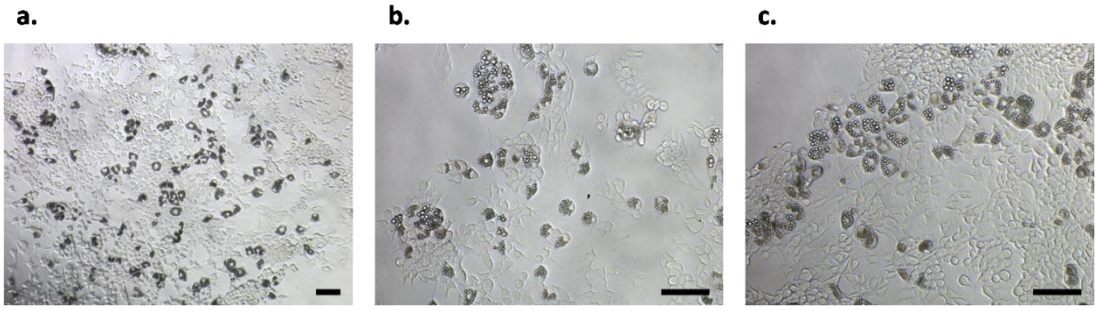

Figure 4.13 Optical microscope images of rat mesenchymal stem cells cultured on E-Glc-PA/K-PA nanonetwork after 7 days of incubation. Darker areas are lipid droplets. a., b., c., all belong to the same group. Scale bars = 100 μm.

4.2.7.1 Lipid Droplet Accumulation by Oil Red-O Staining

As noted above, rMSCs cultured on E-Glc-PA/K-PA nanofiber network showed drastic morphological difference compared to other groups. Adipogenic differentiation of MSCs can be evidenced by fat globules also called as lipid droplets.[119] To determine whether the above mentioned morphological changes are indicators of adipogenesis, Oil Red-O staining was performed. Oil Red-O is a fat-soluble diazol dye and stains neutral lipids such as triglycerides, diacylglycerols and cholesteryl esters but not polar lipids (i.e., phospholipids, sphingolipids and ceramides).[127,128] Oil Red-O is minimally soluble in the solvent, and the solubility is further decreased by diluting stock solution of Oil Red-O in water before use. When there are lipids and cholesteryl esters found in the area, Oil Red-O passes from the solution to the lipid as there is better solubility for them.[127] After 7 days culturing rMSCs on peptide nanofiber network, Oil Red-O staining demonstrated that rMSCs accumulate lipid droplets in significantly high numbers when peptide nanofiber network includes E-Glc-PA (Figure 4.14). It was also observed that there are

differences between E-Glc-PA containing scaffolds. On E-Glc-PA/K-PA scaffold lipid droplets were homogeneously distributed and cells were in fibroblast like morphology. On the other hand, on E-Glc-PA/K-Glc-PA group, cell aggregation was observed which is generally accepted as a sign of chondrogenic differentiation and so lipid droplets were shown in these aggregates. Lipid accumulating cells on bare surface was in negligible amount in terms of number. Some populations of rMSCs on K-Glc-PA/E-PA and E-PA/K-PA combinations accumulated lipids, but their number and amount of total lipid droplets stained by Oil Red-O was very few compared to E-Glc-PA containing groups. Day 7 trend was observed on day 11 Oil Red-O staining with the increase in formation of lipid droplets in all experimental groups. Elevated number of lipid droplets underlines the significant effect of E-Glc-PA containing networks on lipid droplet formation of rMSCs. On the other, specifically E-Glc-PA/K-PA combination stands out in terms of lipid formation on day 11 (Figure 4.15). The highest number and widest distribution of multilocular lipid droplets were observed on E-Glc-PA/K-PA nanofiber network. In this sense, E-Glc-PA/K-PA distinguished itself from E-Glc-PA/K-Gluco-PA combination. Additionally, day 11 Oil Red-O staining underlines the significantly different effects of E-Glc-PA/K-PA and K-Glc-PA/E-PA on rMSCs adipogenesis. There were a few numbers of lipid droplets on K-Glc-PA/E-PA at day 11. On K-PA/E-PA, cells rolled upon themselves due to increased confluency at day 11.

Morphology of lipid droplets differs between white and brown adipocytes. White adipocytes contain single or a few large lipid droplets that appear to comprise the majority of cell volume. The cytoplasm and nucleus of white adipocytes are found at the cell periphery.[34,129] Brown adipocytes, on the other hand, are characterized by

small and multilocular lipid droplets.[34,129] Lipid droplet morphologies of rMSCs cultured on our PA nanofiber systems were typical of brown-like adipocytes. There was a nuance on E-Glc-PA/K-Glc-PA in terms of lipid droplet morphology. Some of the lipid droplets E-Glc-PA/K-Glc-PA had larger volumes, however, they were not unilocular, so they were not white-adipocyte indicators. The numbers of lipid droplets were increased but their brown-like morphology did not alter during 11 days of culturing.

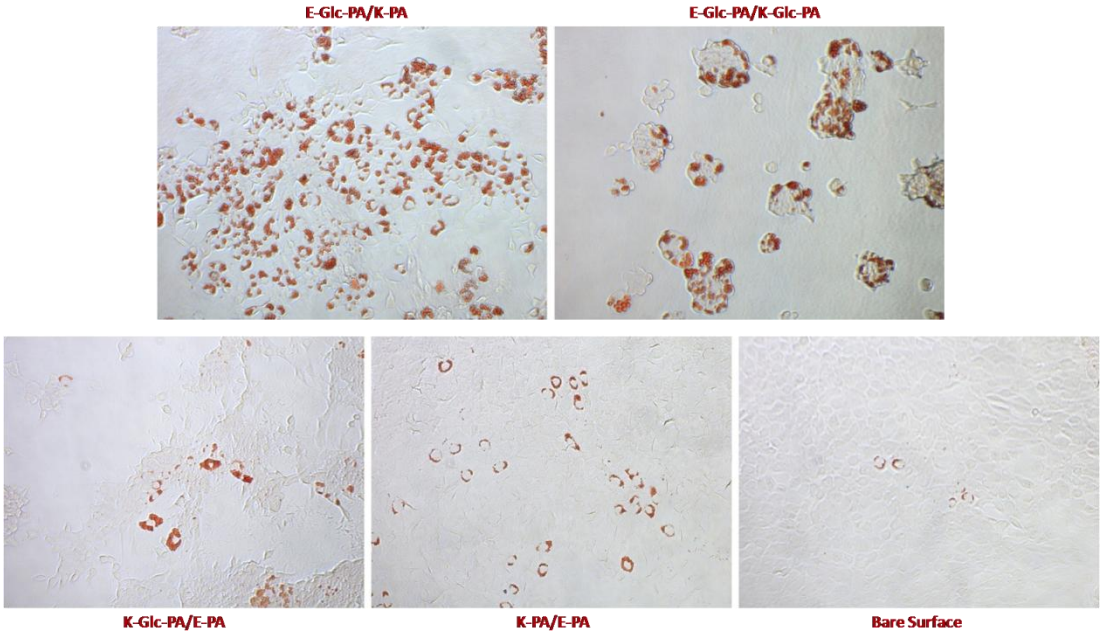

Figure 4.14 Oil Red-O staining of cells in growth medium at day 7, showing the lipid droplet accumulation. Red colors indicate lipid droplets inside cells. Scale bars = 100 μm.

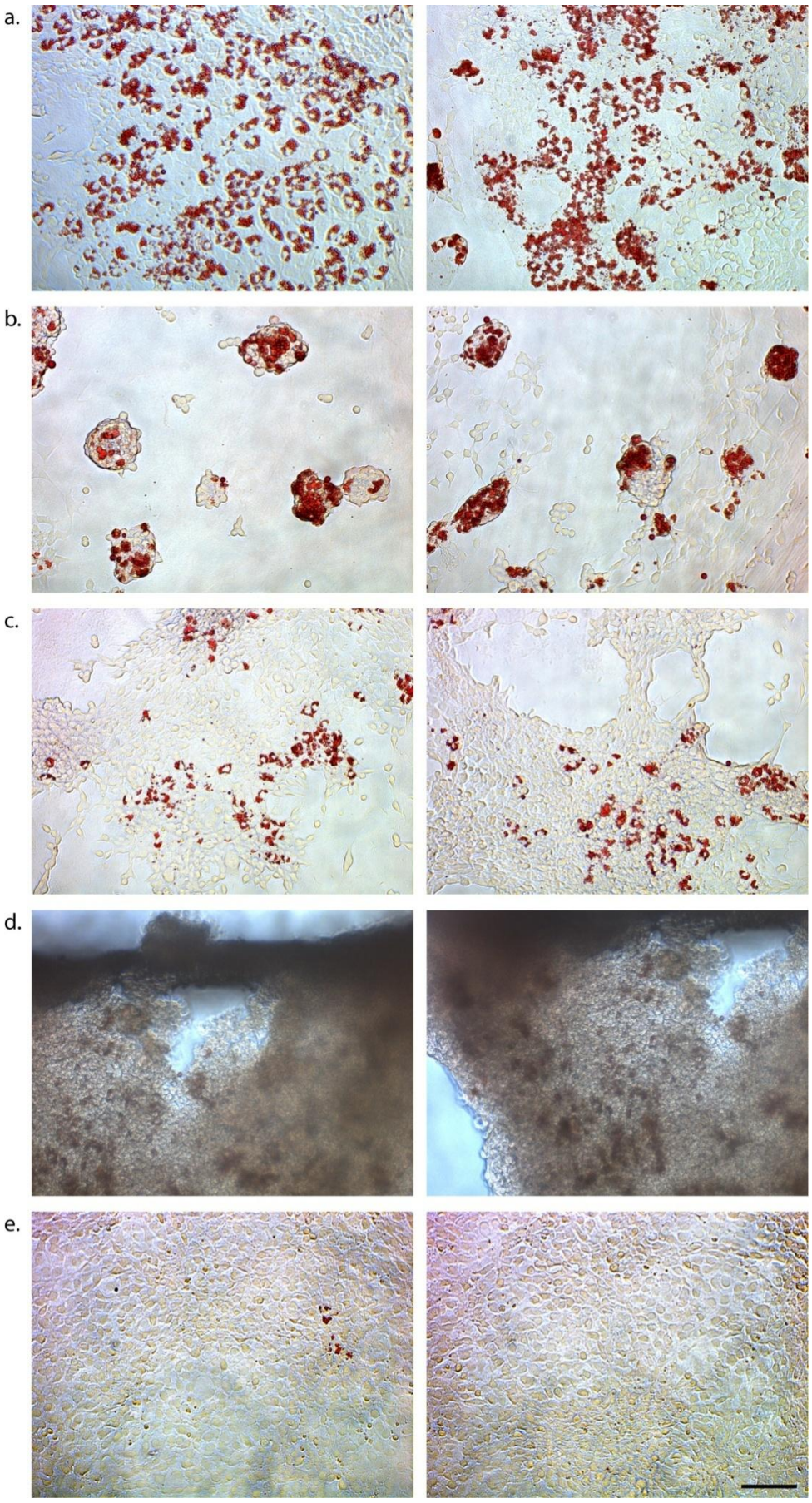
a.
b.
c.
d.
e.

Figure 4.15 Oil Red-O staining of cells in growth medium at day 11, showing the lipid droplet accumulation. Red colors indicate lipid droplets inside cells. E-Glc-PA/K-PA (a), E-Glc-PA/K-Glc-PA (b), K-Glc-PA/E-PA (c), K-PA/E-PA (d), and bare surface (e). Scale bar is 100 μm and equal for all images.

4.2.7.2 Expression Analyses of Adipocyte Gene Markers

To better understand whether the elevated lipid accumulation of rMSCs is a result of adipogenic differentiation, gene expression profiles of rMSCs cultured on peptide nanofiber network and on bare surfaces were analyzed. Expression levels of two widely used adipogenesis markers adiponectin (ADIPOQ) [34,130–133] and fatty acid binding protein 4 (FABP4) [134–137], and brown fat specific gene marker uncoupled protein 1 (UCP1)[41,138–141] were examined on day 7 and day 11.

Relative expression values were transformed to fold change in expression according to control group, which is bare surface, in order to better analyze the changes between the groups on the same experimental day. The trend in relative fold changes of adiponectin and FABP4 gene expressions on both experimental days were similar. The remarkable increase in expression of these adipogenesis gene markers for E-Glc-PA/K-PA and E-Glc-PA/K-Glc-PA compared to three other groups were observed on both day 7 and day 11 analyses. While E-Glc-PA/K-Glc-PA group showed highest elevation of expression on day 7, E-Glc-PA/K-PA held this appellation on day 11. Slight increase in expressions of both genes were observed for K-Glc-PA/E-PA, when compared with K-PA/E-PA and bare surface groups. These fold increases decreased at day 11 compared to day 7 results. In terms of gene expressions, K-PA/E-PA and bare surface groups were comparable for both genes on both days.

As there were drastic increases in expression of adiponectin and FABP4 of rMSCs on E-Glc-PA containing scaffolds, we moved on to analysis of a more determinant gene marker for brown fat cells. To check whether the elevated expression of common adipogenic markers is a cue for brown fat cell formation, UCP1 (uncoupled protein 1) gene was chosen as marker. UCP1 is a mitochondrial protein which is uniquely expressed by the mitochondrion-rich brown adipocytes and its function is to uncouple respiration from ATP synthesis.[142,143] UCP1 uncouples respiration by creating a proton leak across the inner mitochondrial membrane, so it interferes with the proton gradient and dissipates the chemical energy as heat.[143,144] This process is known as adaptive, facultative or non-shivering thermogenesis.[142,143] In terms of body temperature regulation, this process is vital. It was observed that expression levels of E-Glc-PA bearing scaffolds were remarkably high compared to remaining three groups on day 7. Expression levels of cells on K-Glc-PA/E-PA, K-PA/E-PA and bare surface were comparatively in the same range. On day 11, while K-PA/E-PA and bare surface group kept day 7 trend, slight up-regulation of expression on K-Glc-PA/E-PA group (3.3 fold) was observed. E-Glc-PA/K-Gluco-PA group also enhanced UCP1 expression 40 fold compared to bare surface. Although 40 fold increase in gene expression can be accepted as striking, this level is statistically less significant than the E-Glc-PA/K-PA group. Fold increase in UCP1 expression of E-Glc-PA/K-PA at day 11 was outstanding. UCP1 expressed by cells on E-Glc-PA/K-PA was 100 times higher than the bare surface.

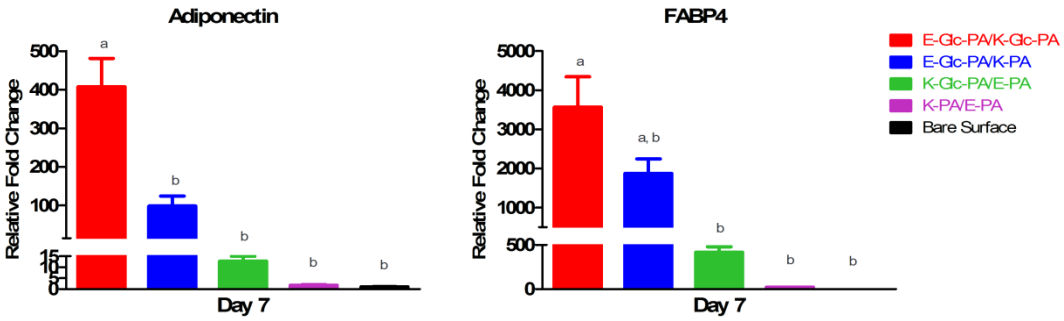

Figure 4.16 Adiponectin and FABP4 gene expression analyses of rat mesenchymal stem cells cultured with growth medium at day 7. The expression level of each gene was normalized against GAPDH and bare surface. Different letters denote significance at $p < 0.05$.

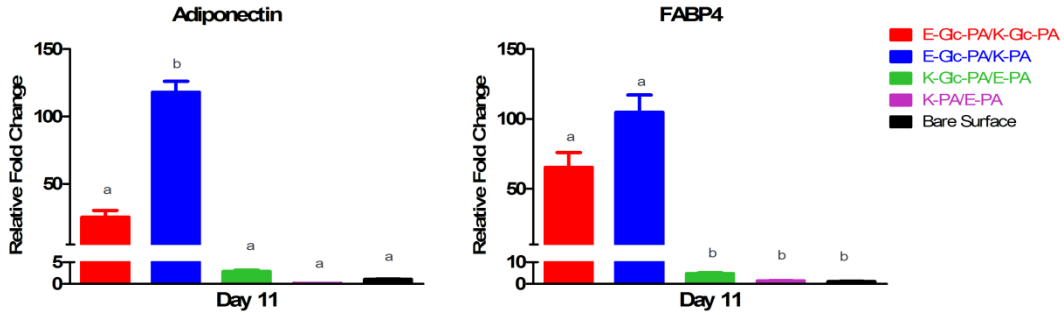

Figure 4.17 Adiponectin and FABP4 gene expression analyses of rat mesenchymal stem cells cultured with growth medium at day 11. The expression level of each gene was normalized against GAPDH and bare surface. Different letters denote significance at $p < 0.05$.

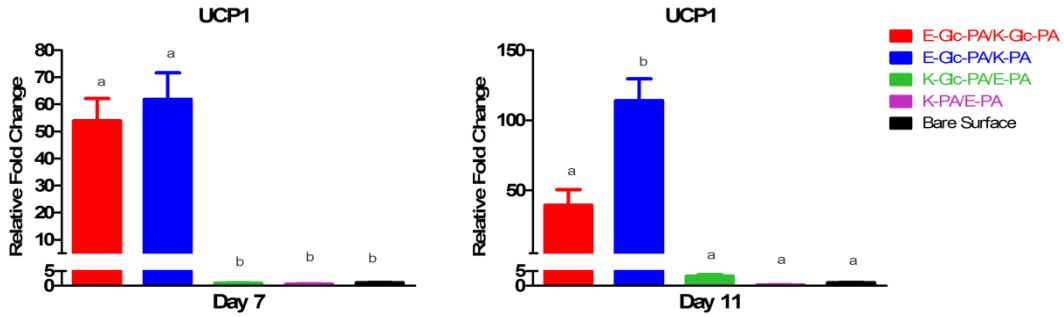

Figure 4.18 UCP1 gene expression analyses of rat mesenchymal stem cells cultured with growth medium at day 7 and day 11. The expression level of each gene was normalized against GAPDH and bare surface. Different letters denote significance at $p < 0.05$.

Day 7 and day 11 relative expression data of adipogenesis gene markers normalized against housekeeping gene GAPDH, but not normalized against bare surface, were analyzed in order to track expression profiles of the gene of interests between two different time points. To obtain this data, results were not normalized against bare surface. This tracking revealed that overall trend for adiponectin and FABP4 is to increase in expression on day 11 compared to day 7. Additionally, K-PA/E-PA and K-Glc-PA/E-PA combinations showed expression decrease for adiponectin and FABP4 genes, respectively. UCP1 expression of cells cultured on bare surface remained constant between day 7 and day 11 and this result indicates the stable expression of UCP1 gene at normal, un-induced basal conditions. On the other hand, for E-Glc-PA/K-Glc-PA and K-PA/E-PA groups there is a decrease in expression at day 11 compared to day 7 results. As in the overall trend of adiponectin and FABP4 expressions, UCP1 expression was elevated in K-Glc-PA/E-PA and E-Glc-PA/K-PA groups with increased culturing period.

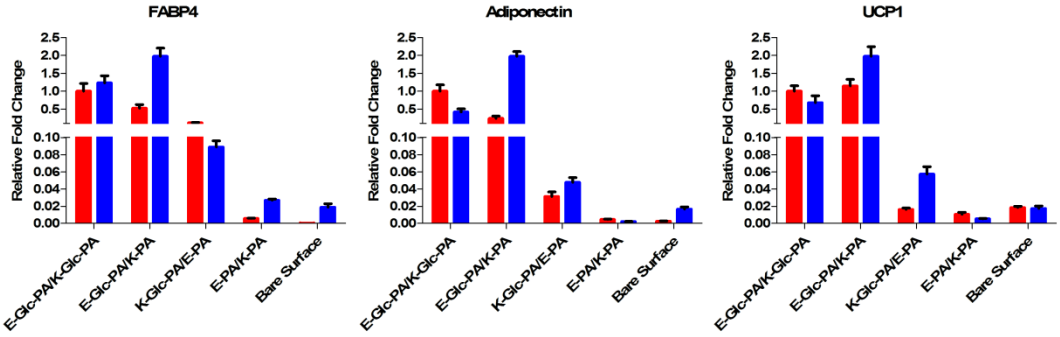

Figure 4.19 Gene expression analyses of rat mesenchymal stem cells cultured with growth medium at different time points. The expression level of each gene was normalized against GAPDH. The results that are normalized against bare surface indicate the changes in expression levels between different time points.

4.3 DISCUSSION

Peptide amphiphiles with counter-charges self-assemble and form nanofiber network when they are mixed. This self-assembly is driven by hydrophobic collapse, electrostatic interactions and β-sheet formation and obtained nanofibers are stabilized by van der Waals, hydrophobic forces, hydrogen bonding.[112] SEM and TEM imaging showed that PA molecules that were designed for this study create an ECM-like highly porous environments formed by nanofibers**.** Circular dichroism spectroscopy revealed co-assembly of peptide amphiphiles have β-sheet secondary structure as expected due to the incorporation of β-sheet driving amino acids into the peptide backbone.

Biocompatible PA scaffolds had different capacity to alter cell adhesion and proliferation among different PA co-assembly combinations. Higher number of cells adhered on nanofiber scaffolds compared to bare surface indicates that peptide amphiphile niche provides more adhesion epitopes than that of tissue culture plate. Additionally, the number of cells adhered on K-Glc-PA containing scaffolds were significantly higher than remaining groups. This might be the effect of lysine in the peptide backbone. Polycationic polylysine is widely used to modify glass or plastic surfaces to culture specific cell types.[116,145] Upon adsorption to culture surface, polylysine increases cationic sites on culture surface which combine with anionic sites of cell surfaces.[146] Lysine residues as cationic amino acids are also rich in cell penetrating peptides.[147,148] Increased cell adhesion on K-Glc-PA including scaffolds might stem from the similar effect of lysine on the backbone chain. On the other hand, we did not observe the same significant increase in adhesion on K-PA/E-PA group. This is probably due to absence of glyco-groups. However, adhesion on E-

Glc-PA/K-PA was significantly less than K-Glc-PA/E-PA group although they have the same amount of lysine and glucose. This difference underlines the effects of flanking amino acid differences in a mixed system on cellular responses. Additionally, this difference can also be examined in terms of self-assembly. Total peptide amounts for K-Glc-PA/E-PA and E-Glc-PA/K-PA are 3X and 4X, respectively. At K-Glc-PA/E-PA, 1X amount E-PA was used in order to achieve charge neutralization. In the self-assembled system, this less amount of E-PA might leave gaps on K-Glc-PA and result in exposure of more amounts of lysines to the surface. Last but not least, the resin type that PA was constructed on might be an issue. E-PA was constructed on Wang resin and so it has additional free carboxyl acid. Carboxylate is an active group, so it might interfere with cellular response. However, we had K-PA/E-PA control group and we did not observe the similar effects on this group. In a similar manner, the decrease in relative adhesion of cells on E-Glc-PA/K-Glc-PA compared to K-Glc-PA/E-PA group might also be attributed as suppressive effect of E-Glc-PA group on adhesion, it might also stem from the absence of sufficient amounts of counter-charged PA group (E-PA) in the system (K-Glc-PA/E-PA). Another conclusion that can be obtained from the adhesion data is the positive effect of glyco-group on adhesion. There are same amount of amino acids, all peptides are constructed on same resin type but there is a difference between E-Glc-PA/K-Glc-PA and E-Glc-PA/K-PA groups. This result obviously indicates that this difference stems from the additional gluco-group, and shows the positive effect of glucose on adhesion.

While other groups were comparable with bare surface, proliferation of E-Glc-PA/K-PA group was 62%, compared to control group, which is tissue culture plate group.

This arrest in cell proliferation may be an indicator of cellular differentiation, as indicated in literature.[117,118] It has been reported that differentiating stem cells are less likely to proliferate.[149] Another reference indicates that mesenchymal stem cells must arrest their growth at a distinct state called predifferentiation state prior to differentiation into adipocytes.[150] Upon combining lipid droplet formation and adipogenic gene marker expression analyses with proliferation data, it is likely that significant arrest of cell division of E-Glc-PA containing scaffolds is due to induced adipogenic differentiation of MSCs. On the other hand, decrease in cell proliferation was much more drastic in K-Glc-PA/E-Glc-PA group when compared to E-Glc-PA/K-PA. The morphology change of cells on K-Glc-PA/E-Glc-PA was significantly more compared to all groups, which will be discussed in lipid droplet staining discussion. Thus, cell proliferation may be arrested more as the cells on E-Glc-PA/K-Glc-PA group spend their energies more for morphology change. We did not claim that these cells did not differentiate. They also up-regulate expression of adipogenic gene markers, in addition to forming aggregates that are commonly formed by chondrocytes. So, cells on two-gluco containing group might decrease proliferation because of induced differentiation, but not specifically for adipogenesis, maybe also for chondrogenesis. Cell proliferation was arrested in glucose bearing peptide scaffolds compared to that of control groups, which are K-PA/E-PA and bare surface. The decrease in proliferation was significant on E-Glc-PA containing groups compared to remaining three groups. In that sense, proliferation results also demonstrate that differences of single amino acid change on PA backbone in our self-assembled systems triggers different responses.

Lipid droplet formation results indicated that E-Glc-PA induces adipogenic differentiation of MSCs. The less number of lipid droplets formed in cells on K-Glc-PA/E-PA, E-PA/K-PA and bare surface (so, not induced by E-Glc-PA group) can be explained by heterogeneity of MSCs. MSC populations are highly heterogeneous in their proliferative and differentiation potentials even though they are single-cell-derived clones.[151] Representative Oil Red-O stained images showed that negligible number of cells formed lipid droplets on bare surfaces due to intrinsic differentiation potential of MSCs. K-Glc-PA/E-PA and E-PA/K-PA scaffolds enhance adipogenic differentiation of fewer numbers of cells compared to bare surface. Apart from the number of cells that formed lipid droplets, high quantity of multilocular lipid droplets in a single cell is important indicator of adipogenesis, especially of brown adipogenesis.[139] In that respect, E-Glc-PA triggers highest quantity of lipid droplets formation and drives great majority of MSCs to adipogenesis. All in all, minor design differences in our PA systems resulted in different levels of lipid droplet formation. Lipid droplet staining not only demonstrated the differential effects of PA scaffolds but also indicated that the adipogenesis of rMSCs goes towards brown fat adipocytes, not the white ones. This conclusion was further be confirmed by brown fat specific gene expression analyses.

Adiponectin is a member of adipocytokines[152], bioactive circularity proteins that are secreted into bloodstream exclusively by adipocytes and acts as a regulator of energy homeostasis.[130] Adiponectin (also known as adipocyte complement-related protein of 30 kDa (Acrp30)[153], AdipoQ[154], and gelatin binding protein of 28 kDa (GBP28)[155] as it is named by different investigators) is involved in food intake, carbohydrate and lipid catabolism.[152] Adiponectin is widely used as a marker of adipogenic

differentiation,[156,133,157,158] as it is highly expressed in differentiated adipocytes.[33] Fatty-acid-binding protein (FABP4, also known as adipocyte protein 2, aP2) is another common gene whose expression is significantly upregulated during differentiation of preadipocytes into adipocytes.[135] FABP4 is the most abundant protein among the proteins ever found in mature adipocytes and adipose tissue.[159] FABP4 regulates lipid metabolism and inflammation, impair insulin action, promotes glucose production, and as lipids have a central role in immune cell signaling FABP4 also has been implicated in immune cell biology by contributing to the pathogenesis of immunometabolic diseases such as diabetes mellitus and atherosclerosis.[134] It is a common gene for white and brown adipocytes.[137] FABP4 and adiponectin are late markers of adipogenesis. They are highly expressed in adipocytes rather than pre-adipocytes.[136] Highly elevated fold changes of two late adipogenic gene markers in our systems indicated that MSCs differentiate into mature adipocytes in the presence of E-Glc-PA.

UCP1 is a mitochondrial protein that dissociates oxidative phosphorylation from energy production, leading to increased thermogenesis.[137] It acts as a long-chain fatty acid (LCFA) anion/H^+ symporter and its activation is done by LCFAs that are released from BAT upon lipolysis of triacylglycerol from lipid droplets by adrenergic stimulation.[143] Brown adipose tissue (BAT) is specialized for thermogenic energy expenditure and it maintains animal body temperature with unique expression of UCP1.[141,143] Significant enhancement of UCP1 expression of cells cultured on peptide scaffolds containing E-Glc-PA shows that these cells differentiate into brown adipocytes. E-Glc-PA/K-PA group expressed all adipogenic gene markers even more than E-Glc-PA/K-Glc-PA group on day 11. Besides, there is a decrease in

expressions of adipogenic genes on E-Glc-PA/K-Glc-PA group significantly at day 11 compared to day 7. These results together indicate that MSCs cultured on E-Glc-PA/K-Glc-PA scaffolds go on another differentiation pathway, as discussed in lipid droplet staining discussion part. Therefore, E-Glc-PA/K-PA group stands out as a brown fat adipogenesis triggering scaffold for MSCs.

Overall, expression levels of adipogenesis marker genes demonstrated that single amino acid change flanking the gluco-conjugated amino acid and presence or absence of gluco-conjugated amino acids result in drastic differences in cellular differentiation of rMSCs. Gene expression analyses also revealed that E-Glc-PA/K-PA combination specifically induces brown fat differentiation, which might have striking importance in terms of obesity fighting treatments.

4.4 CONCLUSION

Our results indicate that minor changes in scaffold design can drastically affect the fate of MSCs. As our design contains counter-charged assembly step, further studies like repeating experiments with soluble treatment of single PA molecules are required in order to better test the effects of single amino acid change of PA backbone on MSCs differentiation. Besides, this study might also reveal the effects of assembly kinetics on cell behavior. Future studies can also reveal the molecular pathways underlying the observed affects. Additionally, induced brown fat cell formation from white fat cells via E-Glc-PA might provide an obesity treatment candidate. Apart from that, we established a simple, easy-to-apply scaffold to differentiate MSCs to mature adipocytes with brown adipocyte characteristics.

CHAPTER 5

CONCLUSIONS AND FUTURE PERSPECTIVES

Tissue regeneration studies are primarily based on material science and comprehensive knowledge on molecular biology. A better understanding of the regeneration at molecular level and development of new materials are essential to improve prospects of tissue regeneration. Peptide amphiphiles arise as versatile tools at this stage. Their design requires in-depth understanding of molecular biology, but can be easily modulated and synthesized, and they can take the form of various types of materials in terms of mechanical, chemical and physical properties. In this thesis, novel glycopeptide nanofibers were formed by supramolecular interactions and used as GAG-mimetic scaffolds to control MSC differentiation.

In the first study, we developed a bioactive peptide amphiphile nanofiber scaffold system for early induction of MSC differentiation into hyaline cartilage chondrocyte phenotypes. Although an apparent trend was not obtained among different type of experiments and between different experimental time points, the hyaluronic acid mimicking PA system (GlcNAc-PA/Glc-PA combination) created an environment for rMSCs to adhere more, provided signals to induce early and drastic chondrocyte-like morphology change and increased expression of late gene markers of chondrogenesis (aggrecan and Col II) at early time points (day 3 and day 7). These *in vitro* studies showed that hyaluronic acid mimicking environment is a promising biomaterial for *in vivo* regeneration studies. For further development of this study, expression of selected chondrogenic gene markers can be analyzed at protein level by western blot analyses. Additionally, new gene markers specific for chondroblasts can be analyzed for investigation of chondroblastic features of the rMSCs cultured on hyaluronic acid mimicking scaffold. In order to demonstrate that hyaluronic acid mimicking glycopeptide system functions in the same biological pathways with

natural hyaluronic acid, the differentiation experiments can be repeated in the presence of CD44 and CD168 antibodies. These antibodies would bind to CD44 and CD168 cell surface receptors, which are HA receptors, and would perform as inhibitors for epitopes of our HA mimicking scaffold. An abolishment of the observed effects of HA mimicking scaffold on cell differentiation proves that our design can target native HA receptors. Besides, HA amount produced by cells cannot be detected by our current analysis method as HA is the only GAG that is not sulfated. An HA detection method can be applied to develop this study.

In the second study, behaviors of rMSCs in terms of adhesion, proliferation and differentiation with respect to the change in single flanking amino acid of gluco-bearing amino acid were monitored. The importance of flanking amino acids on bioactive sequence functions is known. Besides, each amino acid has characteristic chemical structure and so amino acid type that is integrated into the PA backbone can alter the self assembly properties. In order to study these effects in our systems, K-Glc-PA which is also used in the first study was chosen and a new glycopeptide was developed by changing the lysine residue with glutamic acid. It was demonstrated this minor change drastically affects PA molar ratios in our counter charged mixing systems and results in different adhesion, proliferation and differentiation responses. Monitoring cell behaviors revealed the newly designed glycopeptide, E-Glc-PA, as a potential obesity treatment. It was observed that E-Glc-PA induces differentiation of MSCs specifically into brown fat adipocytes. Unlike white fat adipocytes, brown fat adipocytes do not store chemical energy as fat but dissipates it as heat. White-to-brown conversion of adipocytes is in the spotlight

of obesity treatment studies. Our new glycopeptide can be used in brown adipose tissue regeneration and can be used as a scaffold to study brown adipocyte differentiation pathways of MSCs. For further investigations, flow cytometry analyses can be performed in order to determine percentage of the MSCs that differentiate into brown fat adipocytes. Besides, these systems can be tested with white fat cells *in vitro*. This study would demonstrate the potential of this system as an obesity fighting agent. *In vivo* studies would be a better way for understanding the efficacy of this system on obesity.

REFERENCES

1. Principles of Tissue Engineering, 3rd Edition | Robert Lanza, Robert Langer, Joseph Vacanti | ISBN 9780080548845.

2. Devices, P. S. Tissue engineering. Nat. Biotechnol.**18,** 18–20 (2000).

3. Chen, Q. & Thouas, G. Biomaterials: A Basic Introduction. 736 (CRC Press, 2014).

4. Organ Nakli. at <https://organ.saglik.gov.tr/web/#>

5. Cooper, D. K. C. A brief history of cross-species organ transplantation. Proc. (Bayl. Univ. Med. Cent).**25,** 49–57 (2012).

6. Ikada, Y. Challenges in tissue engineering. J. R. Soc. Interface**3,** 589–601 (2006).

7. Chan, B. P. & Leong, K. W. Scaffolding in tissue engineering: General approaches and tissue-specific considerations. Eur. Spine J.**17,** (2008).

8. Biedermann, T. Human eccrine sweat gland cells can reconstitute a stratified epidermis Human Eccrine Sweat Gland Cells Can Reconstitute a Stratified Epidermis. (2011).

9. Atala, A., Bauer, S. B., Soker, S., Yoo, J. J. & Retik, A. B. Tissue-engineered autologous bladders for patients needing cystoplasty. Lancet**367,** 1241–1246 (2006).

10. Yaylaci, S. U. et al. Supramolecular GAG-like Self-Assembled Glycopeptide Nano fi bers Induce Chondrogenesis and Cartilage Regeneration. (2015). doi:10.1021/acs.biomac.5b01669

11. Mammadov, R. et al. Heparin mimetic peptide nanofibers promote angiogenesis. Biomacromolecules**12,** 3508–19 (2011).

12. Sever, M., Mammadov, B., Guler, M. O. & Tekinay, A. B. Tenascin - C Mimetic Peptide Nano fi bers Direct Stem Cell Di ff erentiation to Osteogenic Lineage. (2014).

13. Nguyen, L. H., Kudva, A. K., Guckert, N. L., Linse, K. D. & Roy, K. Unique biomaterial compositions direct bone marrow stem cells into specific chondrocytic phenotypes corresponding to the various zones of articular cartilage. Biomaterials**32,** 1327–1338 (2011).

14. Yuan, T. et al. Collagen hydrogel as an immunomodulatory scaffold in cartilage tissue engineering. J. Biomed. Mater. Res. - Part B Appl. Biomater.**102,** 337–344 (2014).

15. Zhang, J. et al. The influence of scaffold microstructure on chondrogenic differentiation of mesenchymal stem cells. Biomed. Mater.**9,** 035011 (2014).

16. Oberpenning, F., Meng, J., Yoo, J. J. & Atala, a. De novo reconstitution of a functional mammalian urinary bladder by tissue engineering. Nat. Biotechnol.**17,** 149–155 (1999).

17. Stem Cell and Gene-Based Therapy: Frontiers in Regenerative Medicine. 422 (Springer Science & Business Media, 2007).

18. Groeber, F., Holeiter, M., Hampel, M., Hinderer, S. & Schenke-Layland, K. Skin tissue engineering--in vivo and in vitro applications. Adv. Drug Deliv. Rev.**63,** 352–66 (2011).

19. Pearle, A. D., Warren, R. F. & Rodeo, S. A. Basic science of articular cartilage and osteoarthritis. Clin. Sports Med.**24,** 1–12 (2005).

20. Ateshian, G. a. Artificial cartilage: weaving in three dimensions. Nat. Mater.**6,** 89–90 (2007).

21. Zhang, G. & Fenderson, B. A. Lippincott's Illustrated Q&A Review of Histology. 360 (Lippincott Williams & Wilkins, 2014).

22. Stockwell, R. A. Biology of Cartilage Cells. 329 (CUP Archive, 1979).

23. Omelyanenko, N. P., Slutsky, L. I. & Mironov, S. P. Connective Tissue: Histophysiology, Biochemistry, Molecular Biology. 638 (CRC Press, 2013).

24. Hoffman, L. M., Weston, A. D. & Underhill, T. M. Molecular mechanisms regulating chondroblast differentiation. J. Bone Joint Surg. Am.**85-A Suppl,** 124–32 (2003).

25. Cremer, M. a, Rosloniec, E. F. & Kang, a H. The cartilage collagens: a review of their structure, organization, and role in the pathogenesis of experimental arthritis in animals and in human rheumatic disease. J. Mol. Med. (Berl).**76,** 275–88 (1998).

26. Mauck, R. L. & Burdick, J. a. Engineering cartilage tissue. Tissue Eng. From Lab to Clin.**60,** 493–520 (2011).

27. Gartner, L. P. Textbook of Histology. **20,** 672 (Elsevier Health Sciences, 2015).

28. Khoshgoftar, M., Wilson, W., Ito, K. & van Donkelaar, C. C. The effects of matrix inhomogeneities on the cellular mechanical environment in tissue-engineered cartilage: an in silico investigation. Tissue Eng. Part C. Methods**20,** 104–15 (2014).

29. Temenoff, J. S. & Mikos, A. G. Review: Tissue engineering for regeneration of articular cartilage. Biomaterials**21,** 431–440 (2000).

30. Howell, D. S. Biology of Cartilage Cells. R. A. Stockwell. Cambridge, Cambridge University Press, 1979. 329 pages; illustrated. Arthritis Rheum.**23,** 964–965 (1980).

31. Bhosale, A. M. & Richardson, J. B. Articular cartilage: Structure, injuries and review of management. Br. Med. Bull.**87,** 77–95 (2008).

32. Pacifici, M. Introduction to the mini-review series "Articular cartilage: Biology, pathology and repair." Matrix Biol.**39,** 1 (2014).

33. Musi, N. & Guardado-Mendoza, R. Adipose Tissue as an Endocrine Organ. Cell. Endocrinol. Heal. Dis.**89,** 229–237 (2014).

34. Moreno-navarrete, J. M. & Fernández-real, J. M. Adipose Tissue Biology. 17–39 (2012). doi:10.1007/978-1-4614-0965-6

35. Stoker, H. S. General, Organic, and Biological Chemistry. 1056 (Cengage Learning, 2012).

36. Sethi, J. K. & Vidal-Puig, A. J. Thematic review series: adipocyte biology. Adipose tissue function and plasticity orchestrate nutritional adaptation. J. Lipid Res.**48,** 1253–62 (2007).

37. Women and Health. **23,** 1282 (Elsevier Science, 1999).

38. Hassan, M., Latif, N. & Yacoub, M. Adipose tissue: friend or foe? Nat. Rev. Cardiol.**9,** 689–702 (2012).

39. Saely, C. H., Geiger, K. & Drexel, H. Brown versus white adipose tissue: A mini-review. Gerontology**58,** 15–23 (2011).

40. Wu, J., Cohen, P. & Spiegelman, B. M. Adaptive thermogenesis in adipocytes: Is beige the new brown? Genes Dev.**27,** 234–250 (2013).

41. Wu, J. et al. Beige adipocytes are a distinct type of thermogenic fat cell in mouse and human. Cell**150,** 366–376 (2012).

42. Harms, M. & Seale, P. Brown and beige fat: development, function and therapeutic potential. Nat. Med.**19,** 1252–1263 (2013).

43. Esko, J. D., Kimata, K. & Lindahl, U. Proteoglycans and Sulfated Glycosaminoglycans. (2009).

44. Jackson, R. L., Busch, S. J. & Cardin, A. D. Glycosaminoglycans: molecular properties, protein interactions, and role in physiological processes. Physiol Rev**71,** 481–539 (1991).

45. Abueva, C. D. G. & Lee, B.-T. Poly(vinylphosphonic acid) immobilized on chitosan: a glycosaminoglycan-inspired matrix for bone regeneration. Int. J. Biol. Macromol.**64,** 294–301 (2014).

46. Grigoreas, G. H. a, Anagnostides, S. T. & Vynios, D. H. A solid-phase assay for the quantitative analysis of hyaluronic acid at the nanogram level. Anal. Biochem.**320,** 179–184 (2003).

47. Alberts, B. et al. The Extracellular Matrix of Animals. (2002).

48. Salbach, J. et al. Regenerative potential of glycosaminoglycans for skin and bone. J. Mol. Med. (Berl).**90,** 625–35 (2012).

49. Coombe, D. R. Biological implications of glycosaminoglycan interactions with haemopoietic cytokines. Immunol. Cell Biol.**86,** 598–607 (2008).

50. Glycobiology and Medicine. 292 (Springer Science & Business Media, 2012).

51. Extracellular Matrix: Pathobiology and Signaling. 938 (Walter de Gruyter, 2012).

52. Salbach, J. et al. The effect of the degree of sulfation of glycosaminoglycans on osteoclast function and signaling pathways. Biomaterials**33,** 8418–29 (2012).

53. Salbach-Hirsch, J. et al. Sulfated glycosaminoglycans support osteoblast functions and concurrently suppress osteoclasts. J. Cell. Biochem.**115,** 1101–11 (2014).

54. Gandhi, N. S. & Mancera, R. L. The structure of glycosaminoglycans and their interactions with proteins. Chem. Biol. Drug Des.**72,** 455–482 (2008).

55. Naik, P. Biochemistry. **30,** 684 (JP Medical Ltd, 2015).

56. Silva, T. H. et al. Materials of marine origin: a review on polymers and ceramics of biomedical interest. Int. Mater. Rev.**57,** 276–306 (2012).

57. Distribution and Biological Role: The Chemistry and Biology of Compounds Containing Amino Sugars. 620 (Elsevier Science, 2013).

58. Trowbridge, J. M. & Gallo, R. L. Dermatan sulfate: new functions from an old glycosaminoglycan. Glycobiology**12,** 117R–125R (2002).

59. Carbohydrate Chemistry, Biology and Medical Applications. 432 (Elsevier, 2011).

60. Lever, R. & Page, C. P. Novel drug development opportunities for heparin. Nat. Rev. Drug Discov.**1,** 140–8 (2002).

61. Raman, R., Sasisekharan, V. & Sasisekharan, R. Structural Insights into biological roles of protein-glycosaminoglycan interactions. Chem. Biol.**12,** 267–277 (2005).

62. Chemistry and Biology of Heparin and Heparan Sulfate. 792 (Elsevier, 2011).

63. Sasisekharan, R. & Venkataraman, G. Heparin and heparan sulfate: Biosynthesis, structure and function. Curr. Opin. Chem. Biol.**4,** 626–631 (2000).

64. Tumova, S., Woods, A. & Couchman, J. R. Heparan sulfate proteoglycans on the cell surface: Versatile coordinators of cellular functions. Int. J. Biochem. Cell Biol.**32,** 269–288 (2000).

65. Turnbull, J., Powell, A. & Guimond, S. Heparan sulfate: Decoding a dynamic multifunctional cell regulator. Trends Cell Biol.**11,** 75–82 (2001).

66. Funderburgh, J. L. Keratan sulfate: structure, biosynthesis, and function. Glycobiology**10,** 951–958 (2000).

67. Khabarov, V. N., Boykov, P. Y. & Selyanin, M. A. Hyaluronic Acid: Production, Properties, Application in Biology and Medicine. 216 (Wiley, 2014).

68. Necas, J., Bartosikova, L., Brauner, P. & Kolar, J. Hyaluronic acid (hyaluronan): A review. Vet. Med. (Praha).**53,** 397–411 (2008).

69. Day, A. J. & Prestwich, G. D. Hyaluronan-binding proteins: Tying up the giant. J. Biol. Chem.**277,** 4585–4588 (2002).

70. Mitrovic, D. The role of glycosaminoglycans (GAGs). (2004).

71. Bian, L., Guvendiren, M., Mauck, R. L. & Burdick, J. a. Hydrogels that mimic developmentally relevant matrix and N-cadherin interactions enhance MSC chondrogenesis. Proc. Natl. Acad. Sci. U. S. A.**110,** 10117–22 (2013).

72. Kim, I. L., Mauck, R. L. & Burdick, J. a. Hydrogel design for cartilage tissue engineering: a case study with hyaluronic acid. Biomaterials**32,** 8771–82 (2011).

73. Kiani, C., Chen, L., Wu, Y. J., Yee, A. J. & Yang, B. B. Structure and function of aggrecan. Cell Res.**12,** 19–32 (2002).

74. Iida, J. et al. A Role of Chondroitin Sulfate Glycosaminoglycan Binding Site in 4 1 Integrin-mediated Melanoma Cell Adhesion. J. Biol. Chem.**273,** 5955–5962 (1998).

75. Simon Davis, D. A. & Parish, C. R. Heparan sulfate: A ubiquitous glycosaminoglycan with multiple roles in immunity. Front. Immunol.**4,** 1–7 (2013).

76. Taylor, K. R. & Gallo, R. L. Glycosaminoglycans and their proteoglycans: host-associated molecular patterns for initiation and modulation of inflammation. FASEB J.**20,** 9–22 (2006).

77. Mathews, S., Mathew, S. A., Gupta, P. K., Bhonde, R. & Totey, S. Glycosaminoglycans enhance osteoblast differentiation of bone marrow derived human mesenchymal stem cells. 143–152 (2014). doi:10.1002/term

78. Bernstein, E. F., Underhill, C. B., Hahn, P. J., Brown, D. B. & Uitto, J. Chronic sun exposure alters both the content and distribution of dermal glycosaminoglycans. Br. J. Dermatol.**135,** 255–62 (1996).

79. Koistinen, P. & Heino, J. Integrins in Cancer Cell Invasion. (2013).

80. Hileman, R. E., Fromm, J. R., Weiler, J. M. & Linhardt, R. J. interactions : definition of consensus sites in glycosaminoglycan binding proteins. 156–167 (1998).

81. Effect of glycosaminoglycans on spinal cord regeneration . 1453

82. Shum, D. K. Y. & Chau, C. H. Changes in Glycosaminoglycans During Regeneration of Post-Crush Sciatic Nerves of Adult Guinea Pigs. **476,** (1996).

83. Moshiri, A. Tendon and Ligament Tissue Engineering, Healing and Regenerative Medicine. J. Sports Med. Doping Stud.**03,** (2013).

84. Divya, P. & Krishnan, L. K. Glycosaminoglycans restrained in a fibrin matrix improve ECM remodelling by endothelial cells grown for vascular tissue engineering. 377–388 (2009). doi:10.1002/term

85. Matsiko, A., Levingstone, T. J., O'Brien, F. J. & Gleeson, J. P. Addition of hyaluronic acid improves cellular infiltration and promotes early-stage chondrogenesis in a collagen-based scaffold for cartilage tissue engineering. J. Mech. Behav. Biomed. Mater.**11,** 41–52 (2012).

86. Dehsorkhi, A., Castelletto, V. & Hamley, I. W. Self-assembling amphiphilic peptides. J. Pept. Sci.**20,** 453–467 (2014).

87. Hamley, I. W. Lipopeptides: from self-assembly to bioactivity. Chem. Commun. (2015). doi:10.1039/C5CC01535A

88. Cui, H., Webber, M. J. & Stupp, S. I. Self-assembly of peptide amphiphiles: from molecules to nanostructures to biomaterials. Biopolymers**94,** 1–18 (2010).

89. Sardan, M., Kilinc, M., Genc, R., Tekinay, A. B. & Guler, M. O. Cell penetrating peptide amphiphile integrated liposomal systems for enhanced delivery of anticancer drugs to tumor cells. Faraday Discuss.**166,** 269 (2013).

90. Toksoz, S. & Guler, M. O. Self-assembled peptidic nanostructures. Nano Today**4,** 458–469 (2009).

91. Hartgerink, J. D., Beniash, E. & Stupp, S. I. Peptide-amphiphile nanofibers: a versatile scaffold for the preparation of self-assembling materials. Proc. Natl. Acad. Sci. U. S. A.**99,** 5133–5138 (2002).

92. Dehsorkhi, A., Castelletto, V., Hamley, I. W., Adamcik, J. & Mezzenga, R. The effect of pH on the self-assembly of a collagen derived peptide amphiphile. Soft Matter**9,** 6033 (2013).

93. Black, M. et al. Self-assembled peptide amphiphile micelles containing a cytotoxic T-cell epitope promote a protective immune response in vivo. Adv. Mater.**24,** 3845–9 (2012).

94. Sever, M., Mammadov, B., Guler, M. O. & Tekinay, A. B. Tenascin-C mimetic peptide nanofibers direct stem cell differentiat. 1–5

95. Ustun, S., Tombuloglu, A., Kilinc, M., Guler, M. O. & Tekinay, A. B. Growth and differentiation of prechondrogenic cells on bioactive self-assembled peptide nanofibers. Biomacromolecules**14,** 17–26 (2013).

96. Gulseren, G. et al. Alkaline Phosphatase-Mimicking Peptide Nanofibers for Osteogenic Differentiation. Biomacromolecules 150616140246003 (2015). doi:10.1021/acs.biomac.5b00593

97. Scott, C. M., Forster, C. L. & Kokkoli, E. 3D Cell Entrapment as a Function of the Weight Percent of Peptide-Amphiphile Hydrogels. Langmuir 150513155506007 (2015). doi:10.1021/acs.langmuir.5b00196

98. HYALGAN®: Mechanism Of Action. at <http://www.hyalgan.com/hcp/mechanism_of_action>

99. Greenfield, N. J. Using circular dichroism spectra to estimate protein secondary structure. Nat. Protoc.**1,** 2876–2890 (2006).

100. Sigma Aldrich. In vitro toxicology assay kit MTT based. Sigma Aldrich 3–4 (2012).

101. Uygun, B. E., Stojsih, S. E. & Matthew, H. W. T. Effects of immobilized glycosaminoglycans on the proliferation and differentiation of mesenchymal stem cells. Tissue Eng. Part A**15,** 3499–512 (2009).

102. Ragni, E., Viganò, M., Rebulla, P., Giordano, R. & Lazzari, L. What is beyond a qRT-PCR study on mesenchymal stem cell differentiation properties: how to choose the most reliable housekeeping genes. J. Cell. Mol. Med.**17,** 168–180 (2013).

103. Ceylan, H., Tekinay, A. B. & Guler, M. O. Selective adhesion and growth of vascular endothelial cells on bioactive peptide nanofiber functionalized stainless steel surface. Biomaterials**32,** 8797–805 (2011).

104. Schneider-Poetsch, T. et al. Inhibition of eukaryotic translation elongation by cycloheximide and lactimidomycin. Nat. Chem. Biol.**6,** 209–217 (2010).

105. Tsuchiya, K., Chen, G., Ushida, T., Matsuno, T. & Tateishi, T. The effect of coculture of chondrocytes with mesenchymal stem cells on their cartilaginous phenotype in vitro. Mater. Sci. Eng. C**24,** 391–396 (2004).

106. Shah, R. N. et al. Supramolecular design of self-assembling nanofibers for cartilage regeneration. Proc. Natl. Acad. Sci. U. S. A.**107,** 3293–3298 (2010).

107. Caldwell, K. L. & Wang, J. Cell-based articular cartilage repair: the link between development and regeneration. Osteoarthritis Cartilage**23,** 351–362 (2014).

108. Toh, W. S., Lim, T. C., Kurisawa, M. & Spector, M. Modulation of mesenchymal stem cell chondrogenesis in a tunable hyaluronic acid hydrogel microenvironment. Biomaterials**33,** 3835–45 (2012).

109. Kulterer, B. et al. Gene expression profiling of human mesenchymal stem cells derived from bone marrow during expansion and osteoblast differentiation. BMC Genomics**8,** 70 (2007).

110. Mwale, F., Stachura, D., Roughley, P. & Antoniou, J. Limitations of using aggrecan and type X collagen as markers of chondrogenesis in mesenchymal stem cell differentiation. J. Orthop. Res.**24,** 1791–8 (2006).

111. Agar, G. et al. The Chondrogenic Potential of Mesenchymal Cells and Chondrocytes from Osteoarthritic Subjects: A Comparative Analysis. Cartilage**2,** 40–9 (2011).

112. Stendahl, J. C., Rao, M. S., Guler, M. O. & Stupp, S. I. Intermolecular forces in the self-assembly of peptide amphiphile nanofibers. Adv. Funct. Mater.**16,** 499–508 (2006).

113. Shum, L. C., White, N. S., Mills, B. N., de Mesy Bentley, K. L. & Eliseev, R. a. Energy Metabolism in Mesenchymal Stem Cells During Osteogenic Differentiation. Stem Cells Dev.**25,** 114–122 (2016).

114. Macqueen, L., Sun, Y. & Simmons, C. A. Mesenchymal stem cell mechanobiology and emerging experimental platforms. (2013).

115. Endoh, T. & Ohtsuki, T. Cellular siRNA delivery using cell-penetrating peptides modified for endosomal escape. Adv. Drug Deliv. Rev.**61,** 704–709 (2009).

116. Yavin, E. et al. Attachment and Culture of Dissociated Cells From Rat Embryo Cerebral Hemispheres on Poly Lysine-Coated Surface. J. Cell Biol.**62,** 540–546 (1974).

117. Cooper, G. M. Cell Proliferation in Development and Differentiation. (2000).

118. Minoo, P. et al. Loss of proliferative potential during terminal differentiation coincides with the decreased abundance of a subset of heterogeneous ribonuclear proteins. J. Cell Biol.**109,** 1937–1946 (1989).

119. Deans, R. J. & Moseley, A. B. Mesenchymal stem cells. Exp. Hematol.**28,** 875–884 (2000).

120. Baumann, M. K. et al. Understanding Self-Assembled Amphiphilic Peptide Supramolecular Structures from Primary Structure Helix Propensity Understanding Self-Assembled Amphiphilic Peptide Supramolecular Structures from Primary Structure Helix Propensity. **75,** 7645–7647 (2008).

121. Makagiansar, I. T., Avery, M., Hu, Y., Audus, K. L. & Siahaan, T. J. Improving the selectivity of HAV-peptides in modulating E-cadherin-E-cadherin interactions in the intercellular junction of MDCK cell monolayers. Pharm. Res.**18,** 446–53 (2001).

122. Nemerow, G. R. & Stewart, P. L. Role of alpha(v) integrins in adenovirus cell entry and gene delivery. Microbiol. Mol. Biol. Rev.**63,** 725–734 (1999).

123. Bertram, J. P. et al. Synthetic Platelets : Nanotechnology to Halt Bleeding. **1,** 1–17 (2010).

124. An Introduction to Biomaterials. 576 (CRC Press, 2005).

125. Toksoz, S., Mammadov, R., Tekinay, A. B. & Guler, M. O. Electrostatic effects on nanofiber formation of self-assembling peptide amphiphiles. J. Colloid Interface Sci.**356,** 131–137 (2011).

126. Sreerama, N. & Woody, R. W. Computation and analysis of protein circular dichroism spectra. Methods Enzymol.**383,** 318–51 (2004).

127. Mehlem, A., Hagberg, C. E., Muhl, L., Eriksson, U. & Falkevall, A. Imaging of neutral lipids by oil red O for analyzing the metabolic status in health and disease. Nat. Protoc.**8,** 1149–1154 (2013).

128. Histochemistry. 493–497 (1992).

129. Moisan, A. et al. White-to-brown metabolic conversion of human adipocytes by JAK inhibition. Nat. Cell Biol.**17,** 57–67 (2014).

130. Manju C, Pillips SA, Theodore C, H. R. Adiponectin: More Than Just Another Fat Cell Hormone. Diabetes Care**26,** 2442–2450 (2003).

131. Pajvani, U. B. & Scherer, P. E. Adiponectin: systemic contributor to insulin sensitivity. Curr. Diab. Rep.**3,** 207–213 (2003).

132. Kiess, W. et al. Adipocytes and adipose tissue. Best Pract. Res. Clin. Endocrinol. Metab.**22,** 135–153 (2008).

133. Valan Arasu, M. et al. In Vitro and In Vivo Enhancement of Adipogenesis by Italian Ryegrass (Lolium multiflorum) in 3T3-L1 Cells and Mice. PLoS One**9,** e85297 (2014).

134. Hotamisligil, G. S. & Bernlohr, D. a. Metabolic functions of FABPs—mechanisms and therapeutic implications. Nat. Rev. Endocrinol.**11,** 592–605 (2015).

135. Lowe, C. E., O'Rahilly, S. & Rochford, J. J. Adipogenesis at a glance. J. Cell Sci.**124,** 2681–2686 (2011).

136. Urs, S. et al. Gene Expression Profiling in Human Preadipocytes and Adipocytes by Microarray Analysis. J. Nutr.**134,** 762–770 (2004).

137. Cristancho, A. G. & Lazar, M. a. Forming functional fat: a growing understanding of adipocyte differentiation. Nat. Rev. Mol. Cell Biol.**12,** 722–34 (2011).

138. Morganstein, D. L. et al. Human fetal mesenchymal stem cells differentiate into brown and white adipocytes: a role for ERRalpha in human UCP1 expression. Cell Res.**20,** 434–444 (2010).

139. Sharp, L. Z. et al. Human BAT Possesses Molecular Signatures That Resemble Beige/Brite Cells. PLoS One**7,** (2012).

140. Ahfeldt, T. et al. Programming human pluripotent stem cells into white and brown adipocytes. Nat. Cell Biol.**14,** 209–219 (2012).

141. Schulz, T. J. et al. Identification of inducible brown adipocyte progenitors residing in skeletal muscle and white fat. Proc. Natl. Acad. Sci. U. S. A.**108,** 143–8 (2011).

142. Enerbäck, S. Human Brown Adipose Tissue. Cell Metab.**11,** 248–252 (2010).

143. Yu, J. et al. Lipid droplet remodeling and interaction with mitochondria in mouse brown adipose tissue during cold treatment. Biochim. Biophys. Acta - Mol. Cell Res.**1853,** 918–928 (2015).

144. Blesneac, I. et al. Production of UCP1 a membrane protein from the inner mitochondrial membrane using the cell free expression system in the presence of a fluorinated surfactant. Biochim. Biophys. Acta - Biomembr.**1818,** 798–805 (2012).

145. Ando, T. & Yonamoto, Y. In Situ EPR Detection of Reactive Oxygen Species in Adherent Cells Using Polylysine-Coated Glass Plate. Appl. Magn. Reson. (2015). doi:10.1007/s00723-015-0688-x

146. July, P. Published July 1, 1975. **66,** 198–200 (1975).

147. Vivès, E., Schmidt, J. & Pèlegrin, A. Cell-penetrating and cell-targeting peptides in drug delivery. Biochim. Biophys. Acta**1786,** 126–38 (2008).

148. Madani, F., Lindberg, S., Langel, U., Futaki, S. & Gräslund, A. Mechanisms of cellular uptake of cell-penetrating peptides. J. Biophys.**2011,** 414729 (2011).

149. Adipose Stem Cells and Regenerative Medicine. 278 (Springer Science & Business Media, 2011).

150. Fisher, P. B. Mechanisms of Differentiation, Volume 1. 176 (CRC Press, 1990).

151. Augello, A. & De Bari, C. The regulation of differentiation in mesenchymal stem cells. Hum. Gene Ther.**21,** 1226–1238 (2010).

152. Wolf,G. Adiponectin: A regulator of energy homeostasis. Nutrition Reviews, Volume 61. No 8. 10.131/nr.2003.aug.290-292.

153. Scherer, P. E., Williams, S., Fogliano, M., Baldini, G. & Lodish, H. F. to C1q , Produced Exclusively in Adipocytes *. 26746–26749 (1995).

154. Liang, P. AdipoQ Is a Novel Adipose-specific Gene Dysregulated in Obesity *. **271,** 10697–10703 (1996).

155. Nakano, Y., Tobe, T., Choi-Miura, N.-H., Mazda, T. & Tomita, M. Isolation and characterization of GBP28, a novel gelatin-binding protein purified from human plasma. J. Biochem.**120,** 803–812 (1996).

156. Martella, E. et al. Secreted adiponectin as a marker to evaluate in vitro the adipogenic differentiation of human mesenchymal stromal cells. Cytotherapy**16,** 1476–1485 (2014).

157. Schaedlich, K., Knelangen, J. M., Santos, A. N., Fischer, B. & Santos, A. N. A simple method to sort ESC-derived adipocytes. Cytom. Part A**77,** 990–995 (2010).

158. Su, S.-H. et al. Caffeine inhibits adipogenic differentiation of primary adipose-derived stem cells and bone marrow stromal cells. Toxicol. In Vitro**27,** 1830–7 (2013).

159. Spiegelmans, B. M. & Green, H. Specific Protein Biosynthesis during the Adipose Conversion of. J. Biol. Chem.**255,** 8811–8818 (1980).